Norwegian University
of Life Sciences

Master's Thesis 2024 60 ECTS
Faculty of Chemistry, Biotechnology and Food Science (KBM)

Deciphering ADA2 Deficiency: Creating an ADA2 deficiency model using CRISPR/Cas genome editing

Sanne Iversen Lurås
Biotechnology

Deciphering ADA2 Deficiency: Creating an ADA2 deficiency model using CRISPR/Cas genome editing

Sanne Iversen Lurås

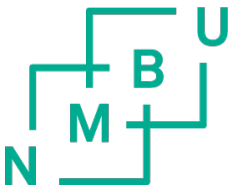

Norwegian University of Life Sciences

Supervisors:
Prof. Janna Saija Saarela
Dr. Monika Szymanska
Prof. Siv Kjølsrud Bøhn

University of Oslo,
Centre for Molecular Medicine Norway
and
The Norwegian University of Life Sciences,
Faculty of Chemistry, Biotechnology and Food Sciences

May 2024

Deciphering ADA2 Deficiency: Creating an ADA2 deficiency model using CRISPR/Cas genome editing
https://nmbu.brage.unit.no

Table of content

I Acknowledgment

This thesis was carried out at the Centre for Molecular Medicine Norway (NCMM), University of Oslo (UiO), as part of the Norwegian University of Life Sciences (NMBU) Master program in Biotechnology, at the Faculty of Chemistry, Biotechnology and Food Science (KBM). The work was performed from August 2023 to May 2024 under the supervision of Prof. Janna Saija Saarela, Dr. Monika Szymanska, and Prof. Siv Kjølsrud Bøhn.

I am thankful to my supervisor, Prof. Janna Saija Saarela, for the opportunity to be a part of her research group and for allowing me invaluable insight into this interesting scientific field. Furthermore, thank you to my supervisor at NMBU, Prof. Siv Kjølsrud Bøhn, for her support and guidance.

My deepest appreciation to Dr. Monika Szymanska, who stepped in as my supervisor. She has been a constant support, generously dedicating her time and sharing her knowledge, which has been priceless throughout this thesis. Over the past year, I have learned and experienced far beyond my expectations, for which I am sincerely grateful. I would like to thank all the amazing people at the Saarela group who have contributed tremendously to this: Johanna Lehtonen, Pu Chen, Weiwei Li, and especially Ragnhild Selvig Braathen. You have all been so welcoming, thank you for your camaraderie, insights, and always lending a helping hand.

I would like to express my gratitude to my friends at NMBU for making these past five years a special time I will always treasure. To my family and significant other, thank you for your love and understanding throughout my studies and especially for your encouragement and help this year.

Ås, May 2024

Sanne Iversen Lurås

II Abstract

Deficiency of adenosine deaminase 2 (DADA2) is a rare autoinflammatory disorder caused by biallelic mutations in the adenosine deaminase 2 (*ADA2*) gene. Patients with DADA2 display a broad spectrum of clinical manifestations, and the condition can be life-threatening. The disease mechanisms of DADA2 are largely unknown. To enhance the current knowledge, this study aimed to create DADA2 cell models and study the effect of *ADA2* knockout (KO) on two central immune cell mechanisms: monocyte proliferation and macrophage polarization.

To gene edit *ADA2*, guide RNA (gRNA) and CRISPR-associated protein 9 (Cas9) were inserted into THP-1 cells using electroporation. The edited cells were further sorted using the fluorescence-activated cell sorting (FACS) method, in which four out of the selected clones showed a homozygous deletion in the *ADA2* gene expected to cause a frameshift in the messenger RNA (mRNA).

A proliferation analysis using Incucyte S3 on *ADA2*-edited, non-sorted cells found that the edited cells had a significantly lower proliferation rate compared to the control cells. The effect of DADA2 on macrophage polarization was tested on sorted *ADA2*-edited cells and assessed with specific markers using quantitative PCR (qPCR). The cells were first differentiated to M0 and then polarized into M1 and M2a macrophages. The results indicated that DADA2 cell models had a favored polarization towards M1 macrophages. Experimental limitations were encountered, and further testing must be completed in order to draw reliable conclusions.

III Sammendrag

Mangel på adenosindeaminase 2 (DADA2) er en sjelden autoinflammatorisk lidelse forårsaket av bialleliske mutasjoner i adenosindeaminase 2 (*ADA2*) genet. Pasienter med DADA2 viser et bredt spekter av kliniske manifestasjoner, og tilstanden kan være livstruende. Sykdomsmekanismene til DADA2 er i stor grad ukjente og for å øke kunnskapen i dette feltet, hadde denne studien som mål å lage DADA2-cellemodeller og studere effekten av nedslått *ADA2* genuttrykk på to sentrale immune celle mekanismer: proliferasjon av monocytter og makrofagpolarisering.

For å gen redigere *ADA2* ble guide RNA (gRNA) og CRISPR-assosiert protein 9 (Cas9) introdusert inn i THP-1 celler ved bruk av elektroporering. De gen redigerte cellene ble videre sortert ved bruk av fluorescensaktivert cellesortering (FACS), hvor til slutt fire av de utvalgte klonene viste en homozygot delesjon i *ADA2*-genet som er forventet å forårsake en leseramme forskyvning i budbringer-RNA (mRNA).

En proliferasjon analyse som ble utført på *ADA2*-redigerte, ikke-sorterte celler ved bruk av Incucyte S3 viste at de redigerte cellene hadde en signifikant lavere proliferasjon sammenlignet med kontroll celler. Effekten av DADA2 på makrofagpolarisering ble testet på sorterte *ADA2*-redigerte celler og evaluert med spesifikke markører ved hjelp av kvantitativ PCR (qPCR). Cellene ble først differensiert til M0 og deretter polarisert til M1 og M2a makrofager. Resultatene indikerte at DADA2-cellemodeller viste en favorisert polarisering mot M1 makrofager. Eksperimentelle begrensninger oppsto, og ytterligere testing må gjøres for å trekke pålitelige konklusjoner.

IV Abbreviations

ADA	Adenosine deaminase
ADA1	Adenosine deaminase 1
ADA2	Adenosine deaminase 2
ADA3	Adenosine deaminase 3
ADGF	Adenosine deaminase-related growth factor
ALOX15	Arachidonate 15-lipoxygenase
ANOVA	Analysis of variance
ATCC	American Type Culture Collection
BCA	Bicinchoninic acid
BLAST	Basic local alignment search tool
BSA	Bovine serum albumin
cAMP	Cyclic adenosine monophosphate
Cas9	CRISPR-associated protein 9
cat	Catalog
cDNA	Complementary DNA
CECR1	Cat eye syndrome chromosome region, candidate 1
CRISPR	Clustered regulatory interspaced short palindromic repeats
crRNA	CRISPR RNA
CXCL9	CXC motif chemokine ligand 9
CXCL10	CXC motif chemokine ligand 10
DADA2	Deficiency of adenosine deaminase 2
DC	Dendritic cells
ddNTP	Dideoxynucleotide triphosphates
DEPC	Diethyl pyrocarbonate
DMSO	Dimethyl sulfoxide
DNA	Deoxyribonucleic acid
DNase	Deoxyribonuclease
dNTP	Deoxynucleotide triphosphates
DSB	Double stranded break
dsDNA	Double stranded DNA
EDTA	Ethylenediamine tetraacetic acid
EMQN	European Molecular Genetics Quality Network

FACS	Fluorescence-activated cell sorting
FBS	Fetal bovine serum
FVD	Fixable viability dye
FWD	Forward
gDNA	Genomic DNA
GFP	Green fluorescent protein
gRNA	Guide RNA
HDR	Homology-directed repair
HEK	Human embryonic kidney
HGMD	Human Gene Mutation Database
HRP	Horseradish peroxidase
HSCT	Hematopoietic stem cell transplantation
IC	Immune complex
IDT	Integrated DNA Technologies
IFN	Interferon
IgG	Immunoglobulin G
IL	Interleukin
IL10	Interleukin-10
iPSC	Induced pluripotent stem cell
KO	Knockout
LAF	Laminar flow cabinet
LF	Low fluorescence
LPS	Lipopolysaccharides
2-ME	2-mercaptoethanol
MEM	Minimum essential medium
MEM NEAA	Minimum essential medium non-essential amino acid
MHC	Major histocompatibility complex
MPS	Mononuclear phagocyte system
MRC1	Mannose receptor C-type 1
mRNA	Messenger RNA
N/A	Non applicable
NCBI	National Center for Biotechnology Information
NHEJ	Non-homologous end joining

NK	Natural killer
nTPM	Normalized transcript per million
PAM	Protospacer adjacent motif
PAMP	Pathogen-associated molecular pattern
PAN	Polyarteritis nodosa
PBMC	Peripheral blood mononuclear cell
PBS	Phosphate buffered saline
PCR	Polymerase chain reaction
PID	Primary immunodeficiency disease
pLDDT	Predicted local distance difference test
PLO	Poly-L-ornithine
PMA	Phorbol-12-myristate-13-acetate
PO	Polyolefin
PP	Polypropylene
PRR	Pathogen recognition receptor
P/S	Penicillin-Streptomycin
PVDF	Polyvinylidene difluoride
qPCR	quantitative PCR
REV	Reverse
RIPA	Radio-immunoprecipitation assay
RNA	Ribonucleic acid
RNase	Ribonuclease
RNA18SN1	RNA 18S ribosomal N1
RNP	Ribonucleoprotein
RPL37A	Ribosomal protein L37a
RPMI	Roswell Park Memorial Institute
RT	Room temperature
RT-PCR	Real-time PCR
SD	Standard deviation
SDS	Sodium dodecyl sulfate
SEM	Standard error of the mean
SF	Serum-free
TBS	Tris-buffered saline

TC	Tissue culture
TLR	Toll-like receptor
TNF	Tumor necrosis factor
tracrRNA	Trans-activating CRISPR RNA

V List of figures

VI List of tables

1 Introduction

1.1 The immune system

The human body´s immune system consists of an intricate network of organs, immune cells, and signaling molecules that cooperate with the aim of protecting the host. The immune system specializes in eliminating internally generated threats like cancer and invading pathogens while preserving host cells. The immune system can broadly be divided into the innate and the adaptive immune systems. The two systems are, among others, differentiated by cell composition, response speed, and recognition of pathogen specificity (Parkin & Cohen, 2001). While simultaneously being interconnected, as shown in **Figure 1** and explained further in sections 1.1.1 and 1.1.2.

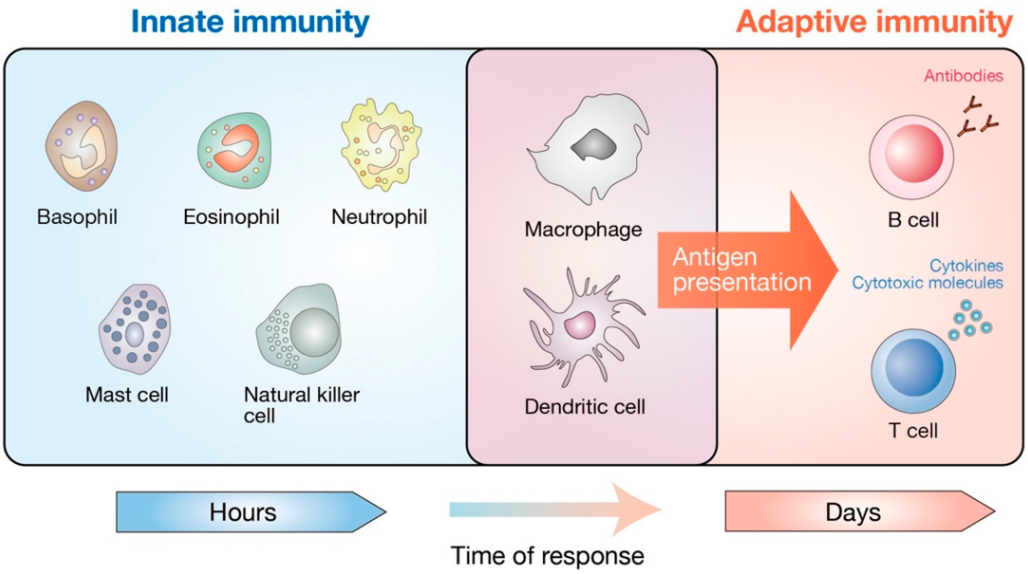

Figure 1. The immune system´s cellular components and relation. Innate and adaptive immunity constitute the immune system. The first is carried out by basophils, eosinophils, neutrophils, mast cells, NK cells, macrophages, and DCs. Through antigen presentation, macrophages and DCs bridge innate immunity with the adaptive immune system. The adaptive immune system is comprised of B cells and T cells, which produce antibodies, cytokines, and cytotoxic molecules to combat intracellular pathogens. Abbreviations: DCs, dendritic cells; NK, natural killer. The figure is retrieved with permission from Yamauchi & Moroishi (2019).

1.1.1 The innate response

The innate system is the first line of defense against pathogens and foreign substances (Delves & Roitt, 2000). It includes cells derived from either hematopoietic or non-hematopoietic origin. Hematopoietic cells originate in the bone marrow and are further divided into the lymphoid and myeloid lineage. An overview of the differentiation process is given in **Figure 2**. The innate response is carried out by cells from both lineages and includes inflammatory-releasing, phagocytic, and natural killer (NK) cells. Moreover, nonhematopoietic skin and epithelial cells circulating in respiratory, gastrointestinal, and genitourinary tracts are crucial in the defense mechanisms as well (Turvey & Broide, 2010).

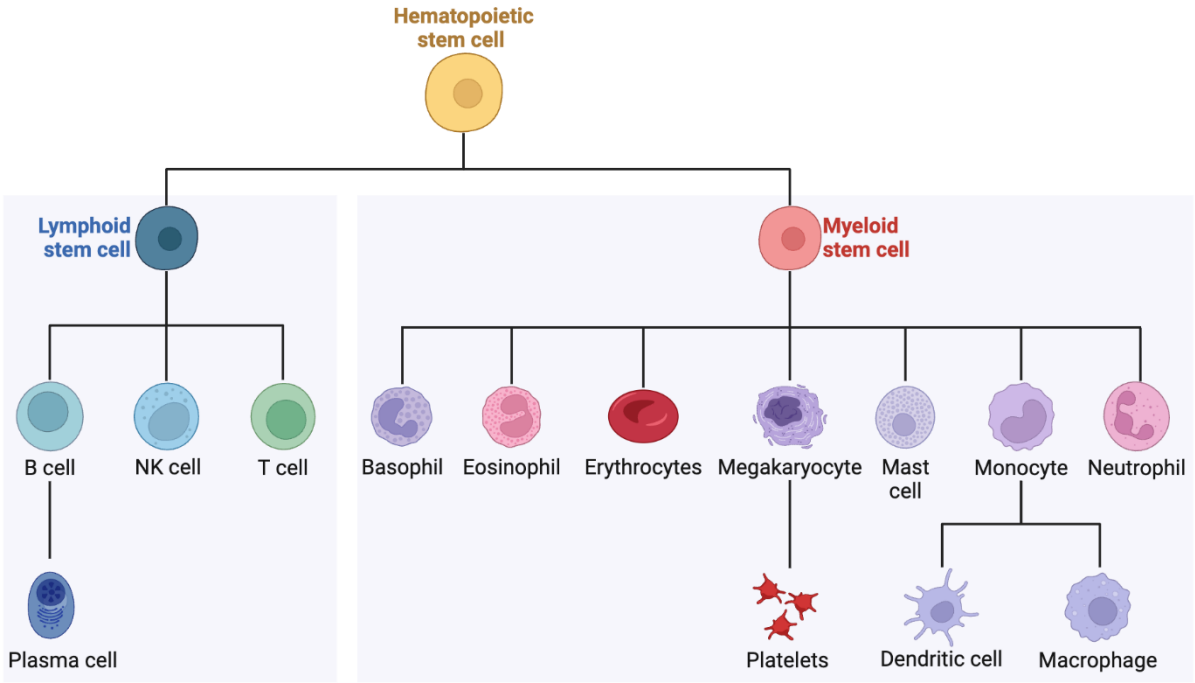

Figure 2. Multipotent stem cell differentiation. A hematopoietic stem cell can differentiate into cells belonging to the lymphoid or myeloid lineage. A lymphoid stem cell can differentiate into B cells, NK cells, or T cells. The myeloid lineage constitutes basophils, eosinophils, erythrocytes, megakaryocytes, mast cells, monocytes, and neutrophils. Abbreviations: NK, natural killer. The figure was created with BioRender.com with inspiration from Raza et al. (2021).

The innate immune cells respond to infections, neutralizing pathogens by recognizing conserved pathogenic molecular patterns through their pattern recognition receptors (PRR) (Akira et al., 2006). The innate response is rapid yet non-specific and remains unaltered despite repeated antigen encounters (Delves & Roitt, 2000). Although innate cells lack antigen-specific receptors, the cells are capable of differentiating between host cells and intruders (Akira et al., 2006).

The response against pathogen entry is complex, and the first barrier includes physical and chemical defenses, thanks to skin, mucosal surfaces, gastric acid, and enzymes in tears and saliva (Aristizábal & González, 2013). Next is the inflammatory-releasing cells. Upon encountering external antigens, mast cells and basophils secrete histamine, as well as other substances (Stone et al., 2010). Histamine temporarily increases endothelial tissue permeability, allowing immune cells and plasma components to infiltrate the site of infection. This, along with increased blood circulation and temperature, results in inflammation (Ashina et al., 2015).

Phagocytic cells, such as neutrophils, macrophages, and dendritic cells (DC), are activated by inflammatory mediators and can further trigger inflammatory responses by secreting their own mediators (Aderem, 2003; Savina & Amigorena, 2007). Phagocytic cells digest foreign cells by extending their outer membrane to engulf the target cell in a phagosome. The phagosome vesicle will then fuse with a lysosome to degrade the target (Richards & Endres, 2014). After digestion of target cells, they produce peptides from the target´s antigen. These peptides are presented on major histocompatibility complex (MHC) class I and II molecules. Among the phagocytic cells, DCs are the most potent antigen-presenting cells. Thus, connects the innate and adaptive immune systems by displaying antigens to T cells (Savina & Amigorena, 2007).

NK cells are another essential cell type in the immune system. The NK cells degrade target cells, which are recognized by their absence of MHC proteins or alternatively, immunoglobulin receptors present in NK cells bind to target cells coated with antibodies (Parkin & Cohen, 2001).

1.1.2 The adaptive response

The second line of defense is the adaptive immune system (Marshall et al., 2018). Unlike the innate immune response, it is antigen-specific, identifying pathogens by their distinct structures. The process of developing adaptive immunity is relatively slow, yet leads to the formation of immunological memory (Delves & Roitt, 2000).

The adaptive response is executed by B and T cells, and their mechanisms of action are visualized in **Figure 3**. The B cells execute the humoral immune response. When activated, the B cells differentiate into plasma cells, which release antibodies called immunoglobulins. The antibodies are proteins circulating through the bloodstream and lymphatic system to scavenge foreign antigens. Upon contact, the antibody can occupy the host cell´s receptors, inhibiting the

antigen from attaching causing pathogen deactivation. Additionally, antibody binding will label the pathogens for elimination, primarily executed by phagocytic cells of the innate immune system. B cells also evolve into memory cells essential for immunological memory (Hoffman et al., 2016).

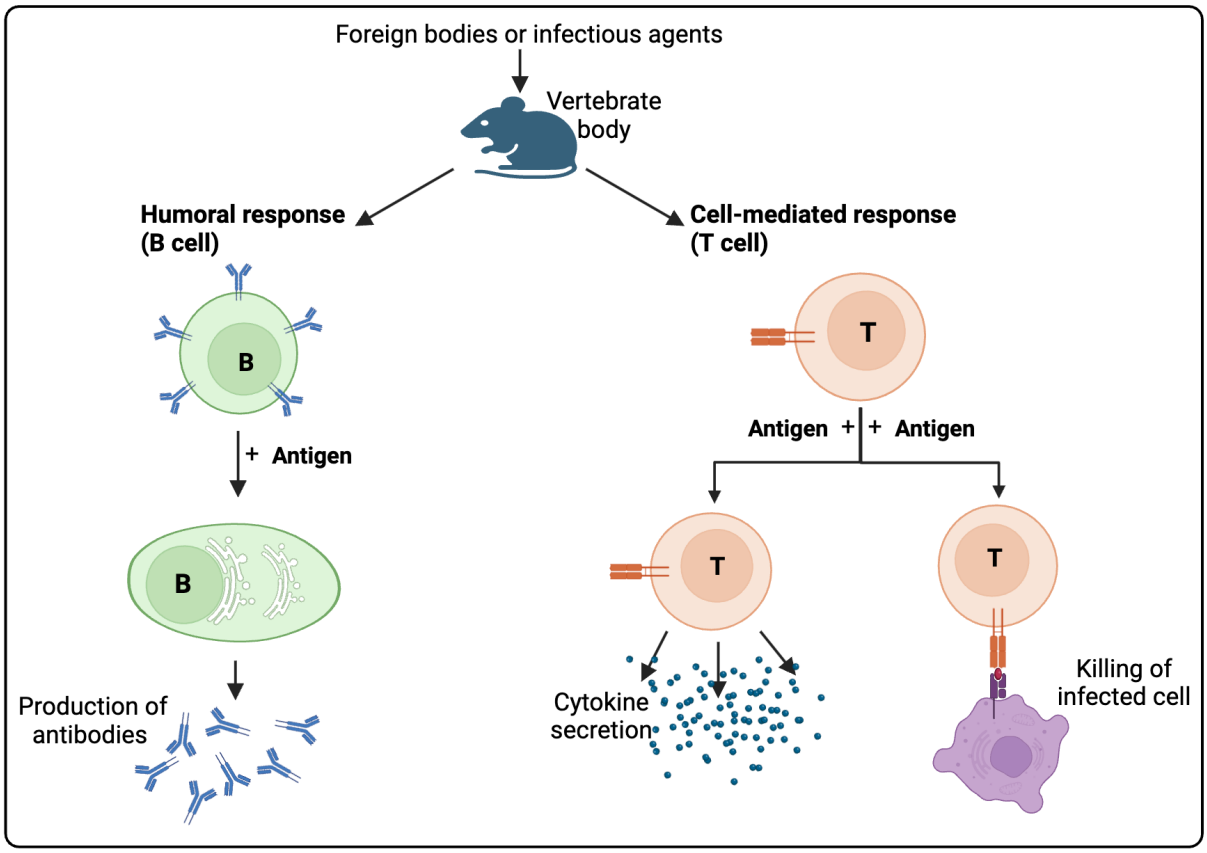

Figure 3. Defense mechanisms in adaptive immunity. B cells and T cells mediate adaptive immunity. Upon antigen activation, B cells execute a humoral response. The cells differentiate into antibody-producing cells. The secreted antibodies bind to target antigens, aiding the elimination of the foreign agent. The cell-mediated response is carried out by T cells, and their differentiation from naïve T cells to effector cells is initiated by antigens. The effector cells will either produce cytokines or directly lyse the target cells. Adapted from "An Outline for the Humoral and Cell-Mediated (Cellular) Branches of the Immune System" by BioRender.com (2023). Retrieved from https://app.biorender.com/biorender-templates.

T cells are responsible for the cell-mediated immune response. As shown in Figure 3, naïve T cells can mature into effector cells upon antigen exposure. Effectors have the ability to perform direct lysis or secrete cytokines that either have toxic effects on target cells or further activate B cells and macrophages. In addition to effector cells, memory cells are developed. Memory T offers long-term immunity, allowing rapid immune response upon reinfection (Broere & Van Eden, 2019).

1.1.3 Immune cells

The human body contains multiple immune cells. However, the work conducted in this master´s thesis focuses on monocytes and macrophages. Consequently, sections 1.1.3.1 and 1.1.3.2 will specifically address details related to these two immune cells, respectively.

1.1.3.1 Monocytes

Peripheral blood mononuclear cell (PBMC) is a collective term constituting peripheral blood cells with a single round nucleus. PBMCs include three main subtypes: monocytes, DCs, and lymphocytes. Lymphocytes are further divided into B cells, T cells, and NK cells. The frequencies of these populations in humans vary widely (Shaikh et al., 2019). However, PBMCs typically consist of 70-90% lymphocytes, 1-2% DCs, and 10-20% monocytes (Verhoeckx et al., 2015).

Monocytes are a type of PBMC with a distinct morphology, characterized by a two-bodied nuclei center often presented as a kidney-shaped nucleus (Skinner & Johnson, 2017). The cells are classified as circulating blood cells that, after birth, are generated in the bone marrow with a hematopoietic origin and are subsequently released into the blood flow or the lymphatic system (Yona & Jung, 2010). In humans, circulating monocytes have a half-life of approximately three days (Whitelaw, 1972), and can be divided into three subsets due to the differential expression of CD14 and CD16 surface markers. The classical monocytes, also known as $\mathrm{CD14^{+}CD16^{-}}$ monocytes, solely express CD14 and constitute approximately 80-90% of human monocytes. Intermediate and non-classical monocytes make up the remaining monocyte pool. Intermediate monocytes, $\mathrm{CD14^{+}CD16^{+}}$, express both the markers, while non-classical monocytes, $\mathrm{CD14^{Low}CD16^{+}}$, express CD16 and a limited level of CD14 (Guilliams et al., 2018; Passlick et al., 1989). CD14 is a PRR and has signaling capacities that are activated by pathogen-associated molecular pattern (PAMP) encounters, mainly lipopolysaccharides (LPS), commonly found in bacterial cell walls (Wu et al., 2019). CD16 is a receptor that binds immunoglobulin G (IgG), thereby provoking antibody-mediated functions (Lee et al., 2020).

Monocytes are crucial in the immune system. The cells have the ability to eliminate dead cells and pathogens through phagocytosis, activate adaptive immune responses, and replenish DC and macrophage populations (Boyette et al., 2017). Monocytes, along with macrophages and DCs, make up the mononuclear phagocyte system (MPS) (Hettinger et al., 2013). Monocytes

migrate constitutively from the bloodstream into noninflamed tissues while maintaining their monocytic character. A study showed minimal monocytic differentiation when the cells surveyed antigens under steady-state conditions (Jakubzick et al., 2013). However, during inflammation, the rate of migration is increased. After crossing the endothelium, local growth factors, cytokines, and microbial products can trigger their differentiation (Shi & Pamer, 2011). An *in vitro* study concluded that all three monocyte subsets can give rise to macrophages, yet classical monocytes are the primary source of monocyte-derived DC (Boyette et al., 2017).

1.1.3.2 Macrophages

Macrophages are present in most tissues of adult mammals and represent a heterogeneous population with tissue-specific functions. Tissue macrophages either have a monocytic or embryonic origin (self-renewing embryo-derived populations) (Davies et al., 2013).

Macrophage polarization is the activation of macrophages, which gives them specific functional phenotypes (Italiani & Boraschi, 2014). Prior to polarization, the cells are unpolarized and referred to as M0 macrophages. The activation is initiated by environmental changes leading to the subsequent development of various macrophage subtypes, including M1, M2a, M2b, M2c, and M2d (**Figure 4**) (Hourani et al., 2023). M1 polarization is typically stimulated by interferon (IFN)-γ and LPS. After exposure, M1 macrophages induce inflammatory responses by producing cytokines with proinflammatory roles (Martinez et al., 2008). M2 subsets have different roles, cell markers, and stimulating factors (Gharavi et al., 2022). M2a polarization can be activated by interleukin (IL)-4 or IL-13 (Martinez et al., 2008). This subtype plays a role in cell growth and tissue repair. The remaining M2b, M2c, and M2d subsets are active in inflammation, phagocytosis, and tumor progression, respectively (Gharavi et al., 2022).

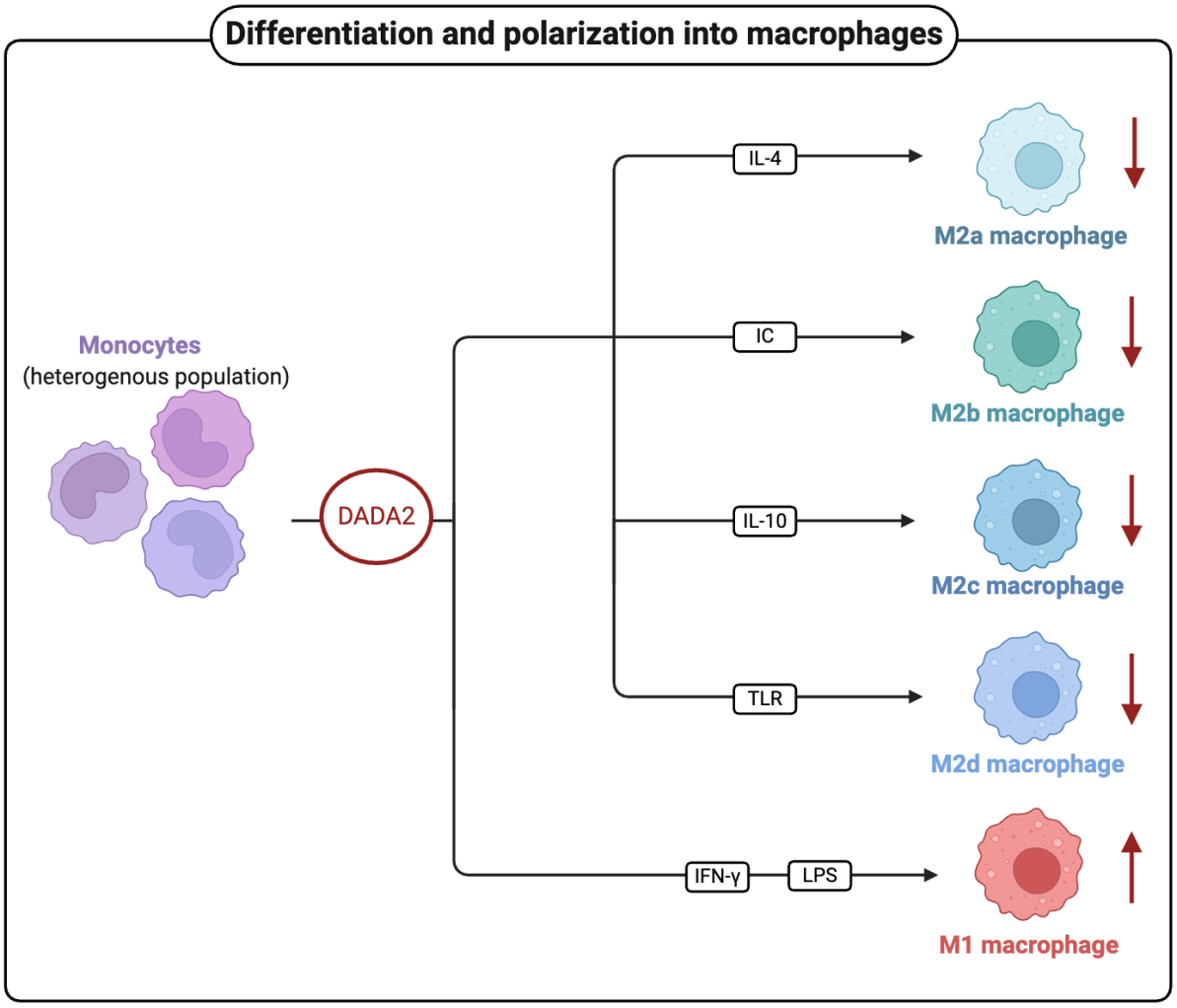

Figure 4. Differentiation and polarization of monocytes into macrophages. The differentiation process of monocytes into macrophages and further polarization into M1 or M2 macrophages activated by different stimulators. M2 macrophages are divided into M2a, M2b, M2c or M2d subtypes. DADA2 affects the polarization and moves it towards M1, increasing M1 and decreasing M2 polarization. Abbreviations: DADA2, deficiency of adenosine deaminase 2; IC, immune complex; IFN, interferon; IL, interleukin; LPS, lipopolysaccharides; TLR, toll-like receptor. The figure was created with BioRender.com with inspiration from Orekhov et al. (2019).

Macrophage polarization is a dynamic process that is capable of being reversed. An imbalance in macrophage subtypes can lead to the development of several diseases (Gharavi et al., 2022). The adenosine deaminase 2 (ADA2) enzyme is reported to be an essential regulator in preserving the M1 and M2 balance. In deficiency of adenosine deaminase 2 (DADA2) patients, macrophages tend to polarize towards M1 (Zhou et al., 2014). While M1 macrophages are pro-inflammatory, M2 secrete anti-inflammatory mediators. Balance is, therefore, crucial for optimal immune system function and resolution of inflammation (Gharavi et al., 2022).

1.2 Primary Immunodeficiency Diseases (PIDs)

Immunodeficiency is defined as a compromised or absent immune system and is either categorized as primary or secondary immunodeficiency (**Figure 5**). The latter are acquired and attributed to environmental factors, for instance, malnutrition and chemotherapy. PIDs constitute a diverse cluster of hereditary diseases that arise due to mutations in specific genes (Rezaei et al., 2017). PIDs can also be monogenic, i.e. arising from defects in one single gene, such as ADA2 deficiency (Wang et al., 2020) which is further described in section 1.3.

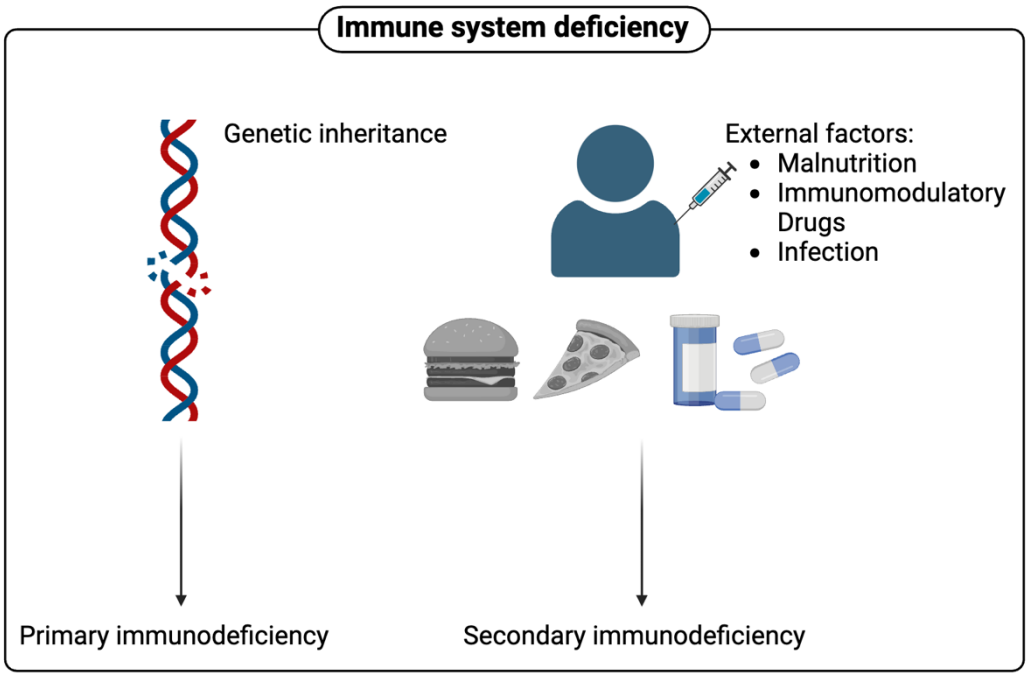

Figure 5. Immunodeficiency classification. There are two main types of immunodeficiencies: primary, which is caused by genetic inheritance, and secondary, which is acquired through external factors. The figure was created with BioRender.com.

PIDs commonly manifest as enhanced vulnerability to infections, autoimmune disorders, and an elevated likelihood of malignancy development (Picard et al., 2015). By estimation, a substantial proportion of individuals suffering from PIDs are likely to be underdiagnosed or diagnosed late after onset as a result of inadequate knowledge (Rezaei et al., 2017). This contributes to an increased mortality and morbidity rate within the affected population. It has been documented over 300 distinct types of PIDs (Picard et al., 2015). Insight derived from PID research offers a pivotal role in comprehending the immune system and helps develop novel therapeutic strategies. Increased medical knowledge may also improve the precision of diagnosis and lead to early intervention and effective care.

1.3 ADA2

As mentioned in the previous section, defects in *ADA2* lead to impaired immune defense mechanisms, which are characterized by multiple immunodeficiency symptoms. The human ADA2 protein of 59-kDa is encoded by the *ADA2* gene (formerly known as the cat eye syndrome chromosome region candidate 1, *CECR1*) positioned on chromosome 22 (Meyts & Aksentijevich, 2018). There are 30 splice variants of *ADA2*, and the most conserved and highly expressed transcript has a size of approximately 41 kb and consists of 10 exons (Martin et al., 2023). The protein structure is shown in **Figure 6**.

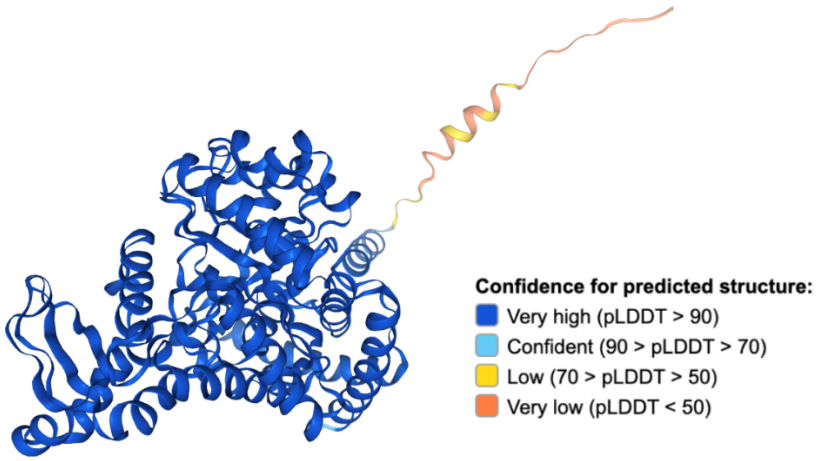

Figure 6. Predicted protein structure of the ADA2 protein. The confidence level for the predicted figure is illustrated with colors ranging from dark blue to orange. Dark blue represents high confidence, and orange denotes low. Abbreviations: ADA2, adenosine deaminase 2; pLDDT, predicted local distance difference test. Image credit: Human Protein Atlas (Uhlen et al., 2015). Image available at the following URL: v23.proteinatlas.org/ENSG00000093072-ADA2/structure.

ADA2 is one of three isoenzymes found in humans. Both ADA1 and ADA2 exhibit ADA activity, catalyzing the deamination of adenosine and 2′-deoxyadenosine to inosine and deoxyinosine. However, the functionality of ADA3 is largely unknown (Zavialov et al., 2010). Since both adenosine and 2′-deoxyadenosine influence human cells, it is vital to preserve their homeostasis (Gakis, 1996).

Despite the fact that ADA activity is demonstrated in both ADA1 and ADA2, one protein cannot compensate for the absence of the other, indicating individual functions of these proteins (Kaljas et al., 2017), which is consistent with their different catalytic and biochemical properties (Zavialov et al., 2010). ADA1 is ubiquitously expressed predominantly as an intracellular enzyme in monomeric form. While ADA2 is secreted as a dimeric protein and is primarily

expressed by myeloid cells. As shown in **Figure 7**, the *ADA2* gene is abundantly expressed by macrophages, monocytes, and DCs (Caorsi et al., 2016). In addition, the two proteins bind to distinct immune cell subsets expressing specific receptors for ADA1 and ADA2 (Kaljas et al., 2017) and have differential substrate affinity. ADA1 has a similar affinity to adenosine and 2′-deoxyadenosine, whilst ADA2 has a significantly weaker affinity for 2′-deoxyadenosine compared to adenosine (Gakis, 1996).

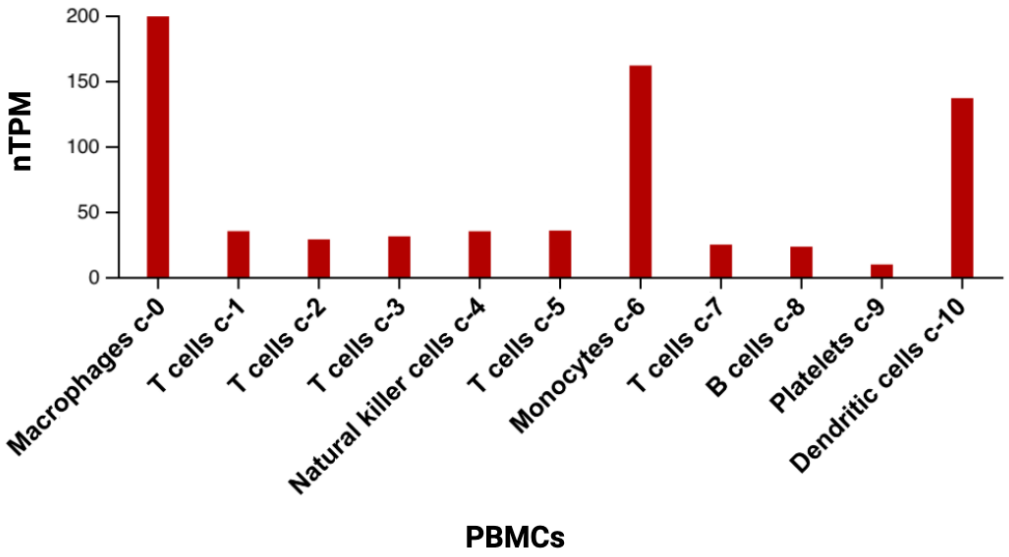

Figure 7. The mRNA level of *ADA2* in PBMCs. The expression of *ADA2* is measured on a single-cell level. A selection of PBMCs is listed along the x-axis. The cluster number is given after the cell type. The mRNA expression is measured in nTPM and shown on the y-axis. Abbreviations: ADA2, adenosine deaminase 2; mRNA, messenger RNA; nTPM, normalized transcript per million; PBMC, peripheral blood mononuclear cell; RNA, ribonucleic acid. Image credit: Human Protein Atlas (Uhlen et al., 2015). Image available at the following URL: v23.proteinatlas.org/ENSG00000093072-ADA2/single+cell+type.

Adenosine, a small endogenous purine nucleoside, is an extracellular molecule used for signaling. The adenosine concentration is low under physiological conditions. However, upon inflammation or tissue damage, the local concentration quickly accumulates (Hasko & Cronstein, 2004). The accumulation arises when the body either releases a significant quantity of ATP that is subsequently catabolized or transports adenosine over the cell membrane following the equilibrium gradient (Kaljas et al., 2017). ADA2 regulates the immune system by degrading the adenosine in the extracellular space (**Figure 8**) (Zavialov et al., 2010). The protein is also more stable at low pH and high temperature and subsequently exerts its effect at a higher level under hypoxia, tumor growth, and inflammation fitting the adenosine accumulation (Zavialov & Engstrom, 2005).

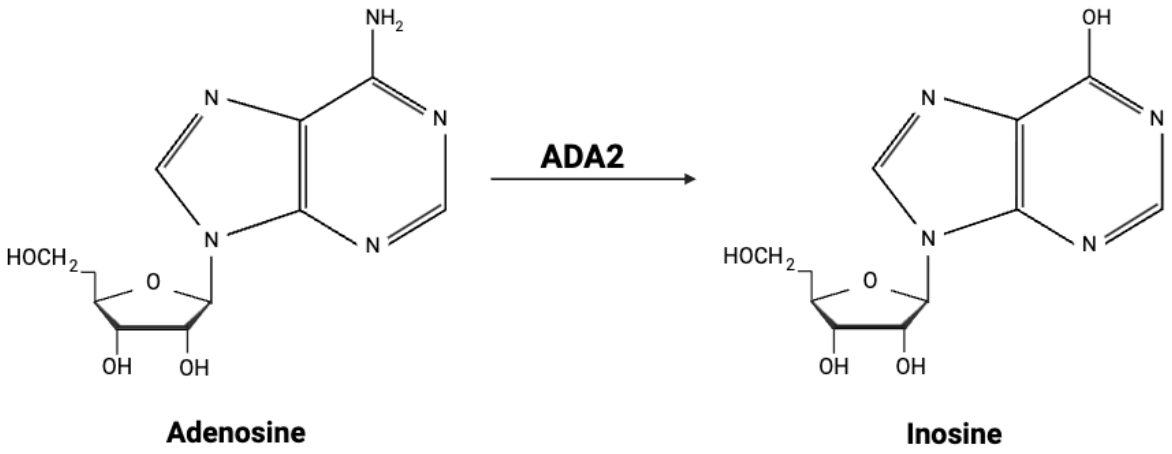

Figure 8. Adenosine deamination. ADA2 catalyzes the deamination of adenosine to inosine. Abbreviations: ADA2, adenosine deaminase 2. The figure was created with BioRender.com.

Adenosine is a crucial mediator that can either activate or suppress cellular functions by modulating the level of cyclic adenosine monophosphate (cAMP) via adenylyl cyclase. Adenosine performs its function by activating A_1, A_{2A}, A_{2B}, and A_3, which are G-protein-coupled adenosine receptors. The activation of A_{2A} and A_{2B} receptors stimulate the adenylyl cyclase, subsequently increasing the cAMP level. While the remaining receptors inhibit the adenylyl cyclase (Jacobson & Gao, 2006). The four receptors are expressed abundantly on immune cells, including monocytes and macrophages (Hasko et al., 2008).

In addition to the enzymatic activity, ADA2 has high sequence similarity to adenosine deaminase-related growth factors (ADGFs). In correspondence, findings suggest the protein has growth factor ability, binding to receptors and triggering signaling pathways (Zavialov & Engstrom, 2005). ADA2 promotes the differentiation of monocytes into macrophages and further induces macrophage proliferation as well as monocyte-activated T-cells (Zavialov et al., 2010).

1.3.1 ADA2 deficiency

In May 2024, the Human Gene Mutation Database (HGMD) reported 186 mutations in *ADA2*, of which 157 were disease-causing. The majority, 65%, were missense mutations where one single nucleotide is replaced, causing the incorporation of a different amino acid in the protein translation. While 28% resulted in indels, either insertions or deletions, and the remaining mutations led to splicing substitutions (HGMD® Professional 2024.1).

Biallelic mutations in *ADA2* were first reported as a cause of early-onset stroke in 2014 (Navon Elkan et al., 2014; Zhou et al., 2014). Biallelic mutations refer to both alleles being altered. However, the alteration does not have to be homozygote (Meyts & Aksentijevich, 2018). DADA2 is classified as a rare disease, and the disease prevalence is estimated to be 1 per 222 000 individuals. Over 30 000 individuals are predicted to be affected by DADA2 worldwide (Jee et al., 2022). The disease typically has an early onset. In 77% of DADA2 disease cases, the onset occurs before the age of 10 years (Meyts & Aksentijevich, 2018). However, late-onset cases have been increasingly reported. A potential cause could be misdiagnosis due to different symptom presentations in adults (Fayand et al., 2021).

DADA2 is characterized by multiple phenotypes: stroke, autoinflammation, immunodeficiency, vasculopathy, immune cytopenias, lymphoproliferation, and bone marrow failure (Hashem et al., 2021). The typical clinical presentation is characterized by chronic or recurrent systemic inflammation, accompanied by fever, elevation of acute phase reactants, and skin manifestations. The disease can be mild and limited to skin symptoms (**Figure 9**), while others may have a severe, potentially life-threatening disease that involves multiple organs (Caorsi et al., 2016). Studies have correlated greater severity to lower enzyme activity (Lee et al., 2020; Van Montfrans et al., 2016). The mortality rate for patients below the age of 30 is approximately 8% (Sahin et al., 2020).

Figure 9. Various skin manifestations in DADA2 patients. Pictures of patients exhibiting DADA2 skin symptoms. A) Skin discoloration in irregular pattern, a symptom of livedo racemosa. B) PAN, a type of systemic vasculitis affecting arteries. C) Decreased blood flow to the extremities, a sign of Raynaud's phenomenon. D) Blue discoloration of the extremities and open skin wounds, which are symptoms of acral cyanosis and cutaneous ulcer. E) Verruca vulgaris, commonly known as warts. Abbreviations: DADA2, deficiency of adenosine deaminase 2; PAN, polyarteritis nodosa. The figure is retrieved with permission from Barron et al. (2022).

1.3.1.1 DADA2 treatment

A common treatment choice for DADA2 is tumor necrosis factor (TNF) inhibitors, which effectively control inflammation and vascular integrity. However, they are unable to treat bone marrow failure and reverse cytopenias, conditions associated with low blood cell counts. Hematopoietic stem cell transplantation (HSCT) is an effective treatment method since ADA2 is mainly produced by myeloid cells (Hashem et al., 2021). The treatment replaces dysfunctional hematopoietic stem cells with healthy cells obtained from a compatible human leukocyte antigen-matched donor. Before the procedure, the patient is required to carry out immunosuppressive chemotherapy to avert rejection of the transplant and bone marrow depletion (Aschan, 2007).

Studies have shown that HSCT has been successful in restoring ADA2 activity and reversing refractory cytopenia, immunodeficiency, and vasculopathy (Hashem et al., 2021; Van Eyck et al., 2015; van Montfrans et al., 2014). However, due to the high risk of treatment complications, it could be argued that it should be reserved for severe disease cases only (Van Eyck et al., 2015). Employing gene therapy to develop personalized medicines for DADA2 patients is

heavily studied and needed, especially when compatible donors are not available. Gene therapy can be used to correct the disease-causing mutations in the patient's stem cells *in vitro,* which then can be reintroduced into the patient (Staal et al., 2019).

1.4 Gene therapy using CRISPR/Cas9 gene editing

The discovery of clustered regularly interspaced short palindromic repeats (CRISPR) sequences dates back to the late 1980s and early 1990s when researchers first observed these repetitive deoxyribonucleic acid (DNA) sequences in the genomes of bacteria and archaea (Ishino et al., 1987; Mojica et al., 1993). Later the CRISPR/ CRISPR-associated protein 9 (Cas9) system was identified as a defense mechanism used by bacteria and archaea to protect themselves from viruses and plasmids by recognizing and destroying foreign nucleic acids by targeting specific sequences within them (Barrangou et al., 2007; Makarova et al., 2006). The CRISPR/Cas system also serves as an immunological memory as it is used to insert foreign DNA elements into their own CRISPR "DNA database" within a DNA area termed CRISPR arrays. When under attack, the procaryote will express the ribonucleic acid (RNA) from the array, and after cleaving the RNA into mature CRISPR RNAs (crRNAs), the crRNA will bind to the invading DNA and interfere with the intruder's proliferation cycle (Brouns et al., 2008; Hille & Charpentier, 2016).

Groundbreaking studies by the laboratories of Emmanuelle Charpentier, George Church, Jennifer Doudna, and Feng Zhang demonstrated that the CRISPR/Cas9 system could be adapted for programmable genome editing in eukaryotic cells (Cong et al., 2013; Jinek et al., 2012; Jinek et al., 2013; Mali et al., 2013) Since then, the use of CRISPR/Cas9 has allowed researchers to make precise changes to the DNA sequence of a cell's genome by targeting specific locations and introducing modifications such as insertions, deletions, or substitutions. Gene therapy using CRISPR/Cas9 has shown significant progress in the medical field. In 2016, the first clinical trial of CRISPR/Cas9 was performed on humans with lung cancer in which gene-edited cells were injected into the patients (Lu et al., 2020), and in 2023, a CRISPR/Cas9 therapy for sickle cell disease and transfusion-dependent β-thalassemia was approved (Hoy, 2024). Nevertheless, to broaden therapeutic employment, more research is needed to reduce off-target effects, specifically unintended genome editing, and ethical concerns.

The CRISPR system used to modify the genome in eukaryote organisms in research has mainly evolved from mechanisms found in *Streptococcus pyogenes* (Mojica & Montoliu, 2016). The CRISPR/Cas9 mechanisms are displayed in **Figure 10**.

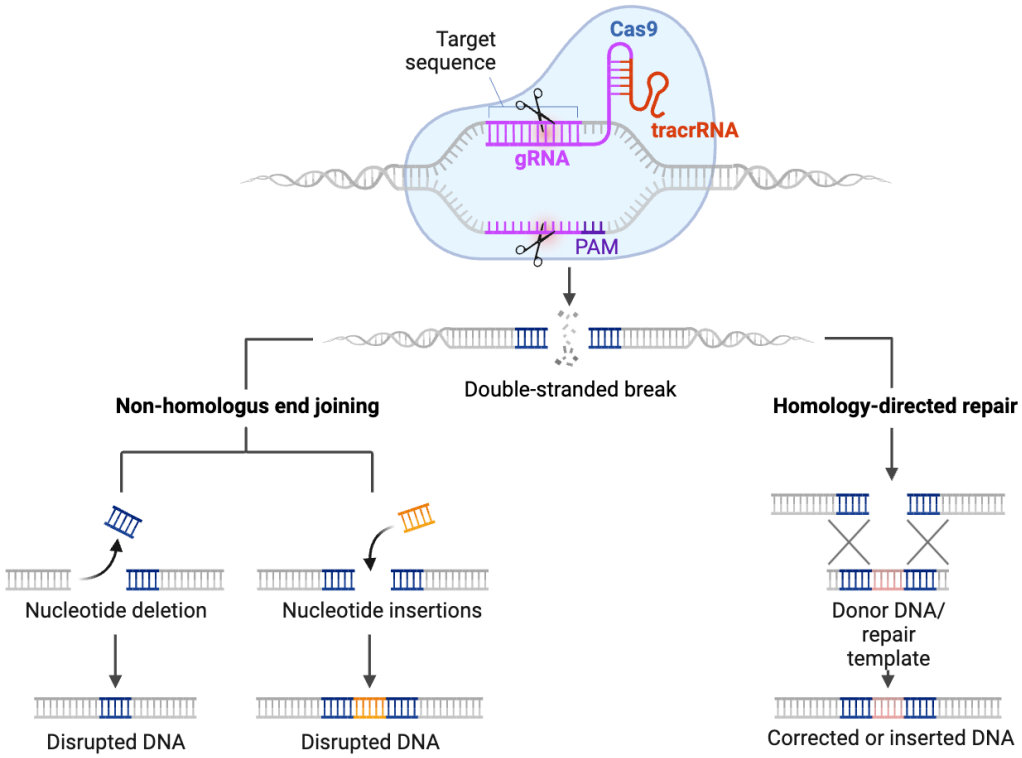

Figure 10. The CRISPR/Cas9 gene editing mechanism followed by DNA repair pathways. Cas9 is guided by gRNA to the target sequence, where it creates a double-stranded cut. The cut is repaired by one of the two DNA repair pathways. NHEJ (on the left) ligates the DNA ends without a template. HDR (on the right) uses a homologous DNA template to mend the DNA ends. Abbreviations: Cas9, CRISPR-associated protein 9; CRISPR, clustered regulatory interspaced short palindromic repeats; DNA, deoxyribonucleic acid; gRNA, guide RNA; HDR, homology-directed repair; NHEJ, non-homologous end joining; PAM, protospacer adjacent motif; RNA, ribonucleic acid; tracrRNA, trans-activating CRISPR RNA. Adapted from "CRISPR/Cas9 Gene Editing" by BioRender.com (2020). Retrieved from https://app.biorender.com/biorender-templates.

Two fundamental components of the CRISPR/Cas9 system are Cas9 and guide RNA (gRNA). Cas9 is a DNA endonuclease that cleaves target DNA and creates a double-stranded break (DSB) (Jinek et al., 2012). The gRNA recognizes and guides Cas9 to the desired target sequence. It comprises crRNA and trans-activating CRISPR RNA (tracrRNA), which hybridize and form a duplex. The tracrRNA recruits Cas9, whereas crRNA directs the enzyme to the target sequence (Doudna & Charpentier, 2014). In the absence of gRNA, Cas9 is inactive (Asmamaw & Zawdie, 2021).

The protospacer adjacent motif (PAM) sequence is a conserved DNA sequence located downstream of the cut site. With the help of gRNA, Cas9 recognizes the PAM sequence. Once

Cas9 hybridizes to PAM, a conformational change is triggered, and the local DNA unwinds. Cas9 cuts the target sequence approximately three base pairs upstream of PAM (Le Rhun et al., 2019). The DSB created by Cas9 is repaired either by a homology-directed repair (HDR) or a non-homologous end joining (NHEJ) mechanism. HDR is most active during the late S and G2 phases of the cell cycle, and repairs DSBs using a homologous DNA template. In CRISPR/Cas9 gene editing, many exogenous DNA templates containing the desired sequence are required. Thus, controllable insertions or deletions can be achieved. In the absence of homologous DNA, the repair is facilitated through NHEJ. NHEJ is active throughout the cell cycle and connects the DNA fragments via an enzymatic process. NHEJ is error-prone, resulting in random insertions and deletions (Asmamaw & Zawdie, 2021).

1.5 Knowledge gaps

There is limited understanding of how specific mutations in the *ADA2* gene correlate with the wide range of clinical manifestations observed in DADA2 patients. Different patients with the same mutation can exhibit different symptoms. Furthermore, while it is known that ADA2 is involved in the differentiation and function of certain immune cells and in modulating inflammation, the exact mechanisms by which ADA2 deficiency leads to the diverse clinical manifestations of the disease are not fully understood. It also indicates that the severity and manifestations of the disease are greatly affected by environmental and epigenetic factors (Nanthapisal et al., 2016; van Montfrans et al., 2016).

Multiple species express the ADA2 protein abundantly. However, rodents lack orthologues of the human gene (Footz et al., 2001). The lack of a suitable animal model may account for some of the knowledge gaps regarding the protein. Since much of ADA2 functionality in different cell types remains undiscovered, particularly in aspects of DADA2, it is imperative to acquire more knowledge on the underlying mechanisms of how ADA2 malfunction contributes to disturbances in cellular biochemical pathways.

2 Aims

Expanding our knowledge of ADA2´s role within the immune system is essential to improve targeted therapies for DADA2. It is, therefore, advantageous to create cellular disease models to study immune diseases, enabling analysis in a controlled environment. Thus, the main objectives of this thesis were 1) to create ADA2 deficient cell models using CRISPR/Cas9 and 2) to test the functionality of the CRISPR/Cas9-edited cells. The specific sub-aims are listed below. The genome editing was conducted in the THP-1 monocyte cell line, known to express ADA2 abundantly.

The specific project aims were as follows:

1. Knockout (KO) the *ADA2* gene in THP-1 monocytes by CRISPR/Cas9 technology.
    a. Evaluate the KO efficiency using polymerase chain reaction (PCR) and qPCR (quantitative PCR).
    b. Sort CRISPR/Cas9-edited cells to create single-cell clones.
2. Test functional characterizations of the CRISPR/Cas9-edited cells.
    a. Assess the proliferation of the CRISPR/Cas9-edited cells compared with non-edited control cells.
    b. Differentiate and polarize the CRISPR/Cas9-edited cells from monocytes into M1 and M2a macrophages and compare the outcome to non-edited control cells.

3 Materials and methods

A list of the software, kits, materials, equipment, and instruments employed in this master´s thesis is available in **Appendix A Tables A1-A4**, respectively. **Figure 11** schematizes an overview of the practical lab work conducted.

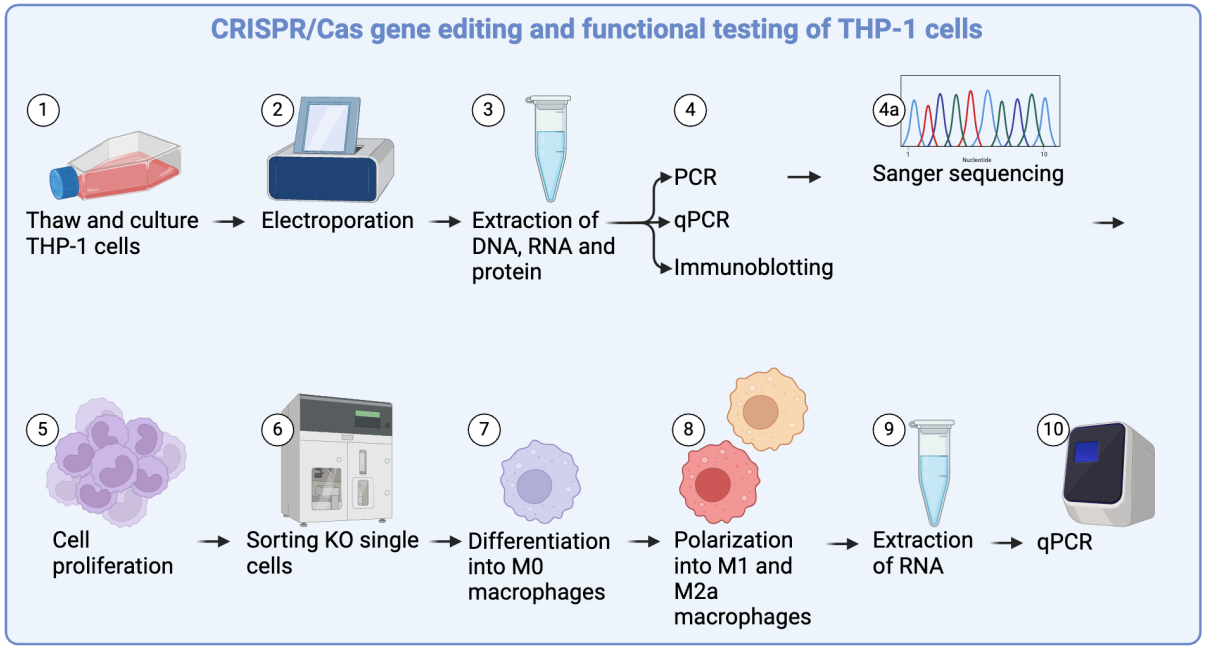

Figure 11. Flow chart of the CRISPR/Cas9-mediated KO of *ADA2* and functional testing performed on THP-1 cells. THP-1 cells were thawed and expanded prior to electroporation, where an RNP complex targeting *ADA2* was introduced into the cells. After electroporation, DNA, RNA, and protein were extracted. DNA was amplified with PCR and sent for Sanger sequencing. RNA was used to synthesize cDNA, and transcript levels were assessed by qPCR. Expression of ADA2 protein was detected using immunoblotting. The proliferation abilities of *ADA2*-edited cells were analyzed with Incucyte S3. The edited cells were sorted with the FACS method to obtain single-cell clones. The sorted cells were differentiated into M0 macrophages and polarized into M1 and M2a subtypes. To validate the polarization, RNA was extracted to measure the relative mRNA level of M1 and M2a markers. Abbreviations: ADA2, adenosine deaminase 2; Cas9, CRISPR-associated protein 9; cDNA, complementary DNA; CRISPR, clustered regulatory interspaced short palindromic repeats; DNA, deoxyribonucleic acid; FACS, fluorescence-activated cell sorting; KO, knockout; mRNA, messenger RNA; PCR, polymerase chain reaction; qPCR, quantitative PCR; RNA, ribonucleic acid; RNP, ribonucleoprotein. The figure was created with BioRender.com.

3.1 Cell line

To create a cell model to study the effect of *ADA2* KO, CRISPR/Cas9 editing was conducted in the THP-1 cell line obtained from American Type Culture Collection (ATCC). The THP-1 cell line is a widely used human cell line derived from a male patient with acute monocytic leukemia (Tsuchiya et al., 1980). The cell line is known for efficient transfection and high expression of the ADA2 protein and was, therefore, a suitable model for this study. In 2022, a vial of THP-1 cells was expanded and cryopreserved at passage three prior to project start.

3.2 Cell culture and maintenance

THP-1 cells were cultured in Roswell Park Memorial Institute (RPMI) 1640 Medium (ATCC modification, Gibco) supplemented with 10% fetal bovine serum (FBS, Gibco), 1% Penicillin-Streptomycin (P/S, Gibco), 0.05 mM 2-mercaptoethanol (2-ME, Thermo Scientific), and 1X minimum essential medium non-essential amino acid (MEM NEAA, Gibco) solution. **Table 1** contains the components for all the mediums employed.

Table 1. Medium compositions. The components for each medium used to maintain THP-1 cells.

Medium	Ingredients
Culture medium	RPMI supplemented with 10% FBS, 1% P/S, 0.05 mM 2-ME, and 1X MEM NEAA
Thawing medium	RPMI supplemented with 10% FBS, 0.05 mM 2-ME, and 1X MEM NEAA
Recovery medium	RPMI supplemented with 10% FBS, 0.05 mM 2-ME, and 1X MEM NEAA
Freezing medium	90% FBS and 10% DMSO

Abbreviations: DMSO, dimethyl sulfoxide; FBS, fetal bovine serum; 2-ME, 2-mercaptoethanol; MEM NEAA, minimum essential medium non-essential amino acid; P/S, Penicillin-Streptomycin; RPMI, Roswell Park Memorial Institute.

FBS contains growth factors, amino acids, proteins, hormones, antibodies, inorganic salts, and vitamins, which are all components essential for growth and proliferation. P/S was included to prevent bacterial contamination. Due to the sensitivity of THP-1 cells, 2-ME was added to reduce oxidative stress. Lastly, the culture medium was supplemented with MEM NEAA to promote cellular function and viability.

Unless otherwise stated, cells were cultivated in an incubator at 37°C and 5 % CO_2, pelleted by centrifugation at 300 *x* g for 5 min at room temperature (RT), and prior to use the culture medium was preheated to 37°C in a bead bath.

Laboratory work related to THP-1 cells was carried out inside a Laminar Flow Cabinet (LAF) with continuous ventilation. To prevent contamination, aseptic techniques were always applied. The workstation inside the LAF, equipment, and gloves entering the hood were disinfected with 70% ethanol.

3.2.1 Thawing

Previously expanded cryovials of THP-1 cells were transferred from -150°C onto dry ice. The vials were thawed in a water bath set to 37°C prior to adding 1 ml of RT thawing medium (Table 1). The total content of each vial was transferred to a 15 ml tube containing 9 ml of RT thawing medium. The remaining cells were washed out by transferring 1 ml of thawing medium back into the vial. After centrifugation, 1 ml of pre-warmed cell culture medium was used to resuspend the pellet. An aliquot of the cell suspension was used to count the cells. Based on the cell count, an appropriate amount of culture medium was added to the cells and transferred to a suitable size of non-treated T-flask. The cell culture flask was thereafter placed in the incubator.

3.2.2 Medium renewal

Cell cultures received fresh medium every two to three days, either through medium replacement or passaging. The medium replacement was conducted by pipetting a cell suspension up and down 3-5 times to loosen the cells from the vessel. Afterward, the suspension was transferred to a 50 ml tube and centrifuged. Half of the supernatant was replaced with fresh pre-warmed culture medium. The pellet was resuspended, and the solution was transferred back to the T-flask. Alternatively, the cell culture was passaged by dividing the cell suspension into an appropriate number and size of non-treated T-flasks, and fresh pre-warmed culture medium was added to achieve a density of $2 - 4 * 10^5$ cells/ml per flask. The flasks were transferred back to the incubator.

Medium renewal of single-cell cultures in 96-well plates was executed in a similar matter, with the exception that the cells remained in the plates during the centrifugation step.

3.2.3 Cryopreservation

Cryopreservation is the process of freezing live cells or other biological materials to maintain their structural integrity and viability for usage after an extended time. To cryopreserve THP-1 cells, cell suspensions were made homogeneous by pipetting, transferred to 50 ml tubes, and centrifuged. The resulting cell pellets were resuspended in 1 ml of freezing medium before the desired volume was added to the solution to obtain a concentration of $5 - 10 * 10^6$ cells/ml. The freezing medium consisted of 90% FBS and 10% dimethyl sulfoxide (DMSO, Merck). DMSO is a cryoprotective agent that reduces the medium's freezing point and enables a slower

cooling rate, thereby decreasing the likelihood of forming ice crystals, which can induce cellular death. Cell suspension of 1 ml was quickly distributed into each cryovial. The vials were placed in a CoolCell container and stored at -80°C for 24h to ensure a cooling rate of approximately -1°C/min before the vials were transferred to -150°C for long-term storage.

3.2.4 Cell counting

Throughout the experimental procedures, THP-1 cells were assessed using the Countess II™ Automated Cell Counter (Invitrogen) to determine cell density and viability. An aliquot of cell suspension was mixed with Trypan Blue Stain (Invitrogen) in a 1:1 ratio. The dye stains dead cells blue by penetrating their impaired plasma membrane. Viable cells have intact membranes and remain unstained. The mix was loaded into a counting chamber slide, which was subsequently placed into Countess II. Each cell sample was measured twice, and the average number of cells was calculated.

3.3 CRISPR/Cas9 editing

Electroporation is an effective delivery method used to introduce CRISPR/Cas components into a wide range of cell types (Potter, 1988). High-voltage pulses are applied to create pores in the cell membrane. Reversible and transient pores will form using a voltage surpassing the cellular membrane barrier. Through the pores, exogenous molecules can be inserted into the target cells (Gehl, 2003). Nucleofection is an enhanced electroporation technology that, in addition to creating pores in the cell membrane, forms pores in the nuclear membrane. Nucleofection enables the direct introduction of ribonucleoprotein (RNP) complexes, which consist of Cas9 and gRNA, into the cell´s nuclei while maintaining high levels of cell viability. Nucleofection causes less cellular stress, leading to more effective transfection of hard-to-transfect cells (Maasho et al., 2004). Hence, nucleofection was used to deliver RNP complexes into the THP-1 cell line.

3.3.1 CRISPR/Cas9 editing procedure

Three days prior to transfection, cells were subcultured at $1 * 10^5$ cells/ml. On the day of, the RNP complex was prepared by mixing gRNA (Integrated DNA Technologies, IDT) and Cas9, (Karolinska Institutet). The complex was quickly spun down, incubated for 15 minutes at RT, and then placed on ice. Prior to use, gRNA was dissolved in duplex buffer (IDT) to a final concentration of 100 µM. The two gRNAs used, named LC1 and RC2, were gifted by Judith Staerk and are listed in **Appendix A Table A6**. Cells were electroporated with either exclusively the LC1 gRNA or a combination of LC1 and RC2 gRNAs. The total gRNA amount was equal in both conditions, with a 1:1 LC1 and RC2 ratio when used together.

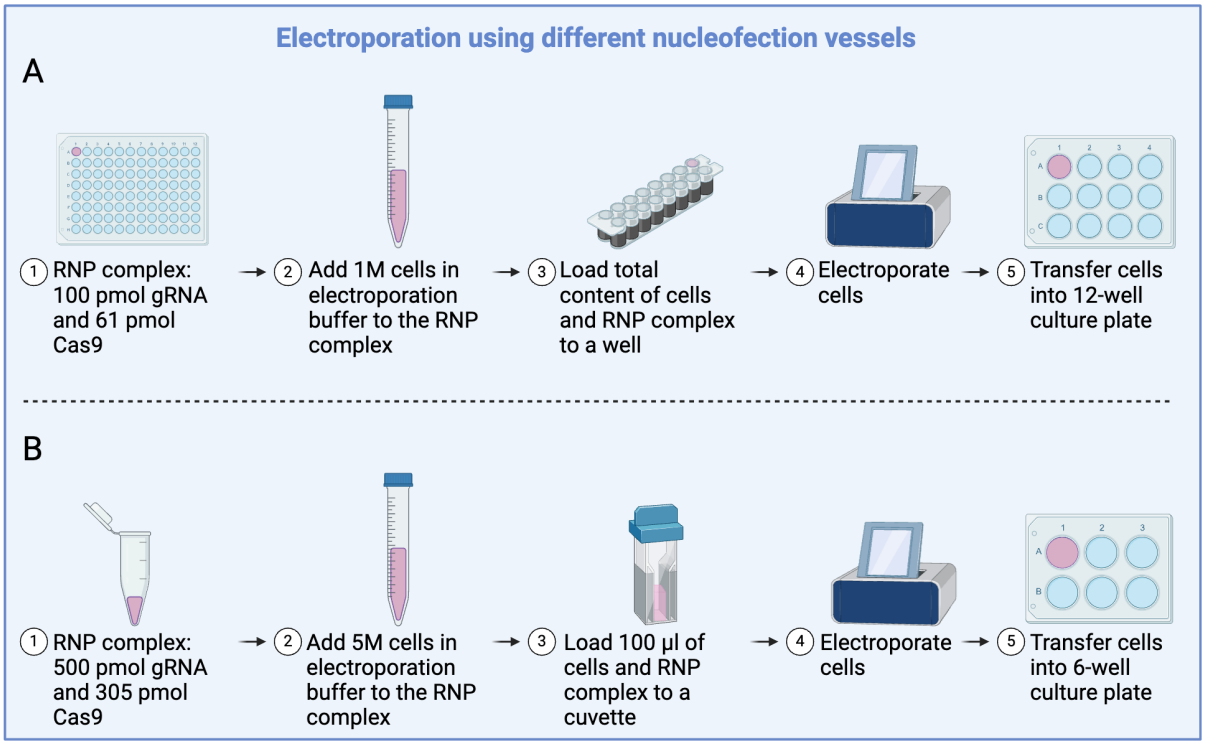

Figure 12. Flow chart of electroporation performed in strip and cuvette. A) RNP complex was prepared in a 96-well plate prior to adding cells resuspended in electroporation buffer. The content in each well was loaded into the electroporation strip, which was inserted into the Lonza machine. Following electroporation, the transfected cells were cultured in a 12-well plate. B) RNP complex was mixed in a 1.5 ml tube, cells in electroporation buffer were added, and 100 µl of the suspension was transferred into an electroporation cuvette. Cells were electroporated and cultivated in a 6-well plate. Abbreviations: Cas9, CRISPR-associated protein 9; CRISPR, clustered regulatory interspaced short palindromic repeats; gRNA, guide RNA; RNA, ribonucleic acid; RNP, ribonucleoprotein. The figure was created with BioRender.com.

As shown in **Figure 12**, the electroporation procedure varied depending on which vessel it was performed in. For electroporation conducted in the Nucleofector™ electroporation strip (Lonza), 100 pmol gRNA and 61 pmol Cas9 were added to each well in a 96-well plate. One well equaled one sample. The required number of cells per sample was $1 * 10^6$. The cell suspension needed to obtain the wanted number of cells was pelleted and washed with pre-warmed 1X phosphate buffered saline (PBS, Medicago). After centrifugation, the pellet was carefully resuspended with 20 µl of electroporation buffer per sample. Next, 20 µl of cell suspension was dispensed into each well containing the RNP complex. Finally, the resulting solution was added to a well in the electroporation strip. The control samples constituted 20 µl of cells resuspended only in electroporation buffer.

The desired number of cells per sample for electroporation in a Nucleofector ™ electroporation cuvette (Lonza) was $5 * 10^6$. Therefore, 500 pmol gRNA and 305 pmol Cas9 were mixed in a 1.5 ml tube per sample. The washed cell pellet was resuspended with 100 µl of electroporation

buffer per sample, and 100µl of the mixture was transferred to each tube containing prepared RNP complex. Solely 100 µl of the mixture was loaded into a cuvette. The control samples constituted 20 µl of cells resuspended only in electroporation buffer.

The presence of air bubbles can create errors during electroporation. Visible air bubbles were removed with a 100 µl pipette tip. To ensure no solution was left on the vessel walls and to remove remaining air bubbles, the electroporation vessels were gently taped against the benchtop prior to being placed into the 4D Nucleofector System (Lonza) for electroporation. "SG cell line" was set as the electroporation solution and "DV-100" as the pulse code.

Immediately after transfection, pre-warmed recovery medium, consisting of culture medium without P/S (Table 1), was added to the cells. In the strips, 100 µl of recovery medium was added, and the total content of each well was transferred to a non-treated 12-well plate containing 1 ml of pre-warmed recovery medium. Following the transfer, 100 µl of the recovery medium was transferred back into the well to wash out the remaining cells. During the wash step, the medium was pipetted up and down gently 2-3 times. The cells were evenly distributed in their plates by rocking the plate back and forth, then subsequently placed in the incubator. The same procedure was applied to electroporation in cuvettes with minor exceptions. Following electroporation, 500 µl of pre-warmed recovery medium was added to the cuvettes. The cuvette content was transferred to a non-treated 6-well plate with 2 ml pre-warmed recovery medium. To wash out the remaining cells, 500 µl of recovery medium was transferred back into the cuvette.

After 24h, culture medium was added to the cells to reach a density of $5 * 10^5$ cells/ml. Following every second or third day, the cells either received a medium renewal or were passaged to a density of $2 - 4 * 10^5$ cells/ml. DNA, RNA, and protein were extracted 2-8 days post-electroporation. Electroporated cells were functionally examined and single-cell sorted.

3.4 Optimization of electroporation using a GFP vector

Flow cytometry is a commonly used method to analyze cells in solution. A single cell passes through one or multiple laser beams at a time. The light dispersed is read by detectors, which generate electronic signals. The signals are analyzed by the software to describe the cell's physical or chemical characteristics (McKinnon, 2018). In this experiment, a GFP (green fluorescent protein) vector was electroporated into target cells, and their GFP expression was detected using flow cytometry.

Prior to electroporating THP-1 cells with an RNP complex targeting *ADA2*, the electroporation procedure was optimized with a pmaxGFP™ Vector (Lonza). The electroporation was conducted in the Nucleofector ™ electroporation strip and followed the same procedure as described in section 3.3.1, with the exception that the RNP complex (Cas9 and gRNA) was replaced with 1 µl of pmaxGFP™ Vector. Following electroporation, the cells were placed in the incubator. After overnight incubation, electroporated cells were made homogeneous by pipetting and placed in a 15 ml tube. The cells were pelleted and washed twice with 1X PBS. The washed pellets were resuspended in 1 ml of 1X PBS to obtain approximately $1 * 10^6$ cells/ml. To stain the cells for viability, 1 µl of fixable viability dye (FVD, Invitrogen) was added to the cell suspensions. FVD irreversibly labels cells with compromised cell membranes and was utilized in this study to exclude dead cells from the analysis.

Immediately after the dye was added, the tubes were vortexed and incubated at 4°C protected from light for 30 min. Cells were washed twice and then resuspended in 500 µl of 1X PBS supplemented with 2% FBS and 2 mM ethylenediamine tetraacetic acid (EDTA, Invitrogen). Cell suspensions were placed on ice and vortexed immediately before analysis using SH800S Cell Sorter (Sony). Cells were gated as single live and GFP-positive cells. Data analysis was completed in FlowJo v10 (Becton Dickinson), and the general gating strategy is shown in **Appendix D Figure A3**.

3.5 Proliferation analysis

A proliferation analysis was conducted on electroporated bulk, non-sorted cells using Incucyte S3 Live Cell Analysis Instrument (Sartorius). The control sample consisted of non-edited cells that were electroporated without an RNP complex. THP-1 cells are suspension cells. Therefore, to allow the cells to attach, culture-treated 96-well plates were coated with 50 µl of 0.01% poly-L-ornithine solution (PLO, Merck) for 1 hour at RT and left for an additional hour to air dry. Cells were seeded in culture medium at a density of $5 * 10^3$ cells/ml. For each condition, eight technical replicates were made consisting of 100 µl of cells suspension. The plates were incubated in Incucyte S3, which was placed in an incubator to maintain a 37°C and 5 % CO_2 condition. The Incucyte scanned the plates with a 10X objective every three hours. Three days later, the cells had reached a confluency of approximately 15% and received 100 µl of pre-warmed culture medium. Plates were transferred back into Incucyte S3, and the data of each well was normalized to this time point, defined as time zero. To mask the THP-1 cells, the minimum area was set to 200 μm^2 and the maximum eccentricity to 0.955. The masking is visualized in one random well in **Appendix F Figure A9**.

3.6 Single-cell sorting

To create single-cell clones that stably do not express the *ADA2* gene, electroporated cells were sorted with the fluorescence-activated cell sorting (FACS) method into 96-well plates. The cells were electroporated with either LC1 or LC1 and RC2 gRNAs. The electroporation protocol is described in section 3.3.1. Prior to sorting, cells were pipetted up and down in their respective T-flasks. An aliquot consisting of $5 * 10^6$ cells was centrifuged, and the resulting pellet was washed twice with pre-warmed 1X PBS. Following centrifugation, the pellet was resuspended in flow cytometry staining buffer. The buffer consisted of 1X PBS supplemented with 2% FBS and 2 mM EDTA. The samples were placed on ice until the SH800S Cell Sorter was ready. Immediately before sorting, the cells were passed through a 40 μm filter to separate the cells and then vortexed.

Due to the size of monocytes, the sorting program "Single Cells (3 drops)" was employed. The sample pressure was held at 4, and the cells were gated based on size and as single cells. The general gating strategy is shown in **Appendix D Figure A7**. Cells were sorted into pre-prepared 96-well plates consisting of 100 μl pre-warmed culture medium. Prior to cell sorting, a mock test was conducted with an identical, sealed 96-well plate to visualize where in the wells the droplets landed.

Immediately after sorting, the plates were spun down at 300 *x* g for 1 min to ensure the cells were in the medium. Cell density was monitored daily, and the medium was changed every 2-3 days. Following 27 days of cultivation, 10 single-cell clones were chosen from each gRNA condition and further cultured in non-treated 12-well plates. The next day, the cells were transferred to suitable non-treated T-flasks and received a medium renewal or were passaged every 2-3 days.

3.7 Differentiation and polarization of THP-1 cells into macrophages

To explore the effect of DADA2 on macrophage polarization and the potential shift towards M1, sorted cells were differentiated and polarized to M1 and M2a macrophages. **Figure 13** shows a schematic illustration of the optimized procedure.

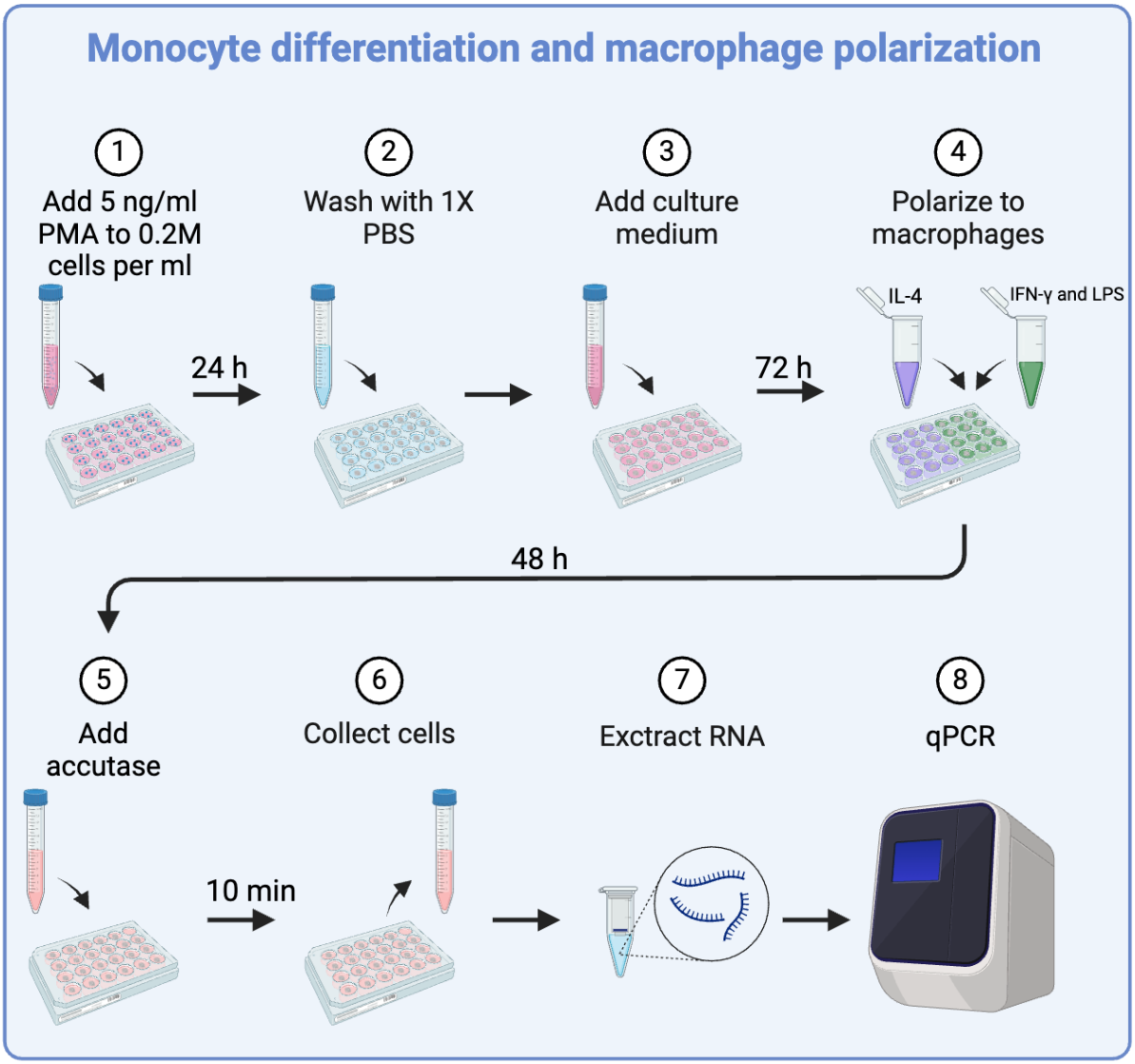

Figure 13. The optimized monocyte differentiation and macrophage polarization procedure. THP-1 cells were stimulated with PMA. After 24h, the stimulation was discarded, and PBS was added to remove residual PMA. Following 72h of rest, the cells were polarized to either M1 or M2a macrophages for 48h. Accutase was used to detach the cells. RNA from the collected cells was extracted, and synthesized cDNA was analyzed with qPCR. Abbreviations: cDNA, complementary DNA; DNA, deoxyribonucleic acid; IFN, interferon; IL, interleukin; LPS, lipopolysaccharides; PBS, phosphate buffered saline; PCR, polymerase chain reaction; PMA, phorbol-12-myristate-13-acetate; qPCR, quantitative polymerase chain reaction; RNA, ribonucleic acid. The figure was created with BioRender.com.

Sorted electroporated cells were mixed by pipetting prior to being seeded in pre-warmed culture medium to a cell concentration of $2 * 10^5$ cells/ml. To differentiate the monocytes into M0 macrophages, the cell suspensions were supplemented with 5 ng/ml phorbol-12-myristate-13-acetate (PMA, Merck). Subsequently, 500 µl of the mixture was distributed into 24-well culture-treated plates.

Plates were stimulated with PMA for 24h in the incubator. After stimulation, the medium was removed, and each well was washed with 1X PBS before 750 µl of pre-warmed culture medium was added. The plates were placed in the incubator for 72h to rest. Upon completion, the medium was replaced with 500 µl of pre-warmed culture medium supplemented with polarization stimuli. Three replicas of each condition were polarized to M1 with 20 ng/ml IFN-γ (Gibco) and 50 ng/ml LPS (Invitrogen). The remaining three replicas were polarized to M2a with the use of 30 ng/ml IL-4 (Gibco). Three replicates consisting of control cells, which were electroporated without an RNP complex, were either left untreated, unpolarized, or polarized to M1 and M2a. After 48h in the incubator, the macrophages were detached by replacing the medium with 500 µl of accutase (Thermo Scientific). The following cell harvest and RNA extraction are described in section 3.8.

3.8 DNA and RNA extraction

Before DNA and RNA extraction, a homogeneous solution of monocytes was washed twice with cold 1X PBS and pelleted. To harvest the derived macrophages, the culture medium was removed before 500 µl of accutase was added to detach the cells. Following 10 min in the incubator, the enzyme was neutralized with 500 µl of culture medium. Pipetting was employed to loosen the cells from the culture plate. The detached cells were collected and washed twice with cold 1X PBS. After the harvest, monocyte and macrophage pellets were either placed in dry ice and stored temporarily at -80°C, or the nucleic acids were immediately extracted.

Four days post electroporation, a proportion of electroporated bulk cells were harvested for DNA and RNA extraction using AllPrep DNA/RNA mini kit (Qiagen), according to the manufacturer's protocol. Cell pellets were homogenized by centrifugation (2 min, full speed) using QIAshredder spin column (Qiagen). Before RNA extraction, the work area and equipment were sprayed with RNase-Away (Thermo Scientific) to eliminate RNA degrading enzymes. To eliminate residual DNA from the RNeasy® spin column, the RNase-Free DNase Set (Qiagen) was used following the guidelines provided by the manufacturer.

Total RNA Purification Kit (Norgen Biotek) was used to isolate and purify RNA from: 1) electroporated bulk cells 2-7 days post-electroporation to conduct a time analysis, 2) sorted cells, and 3) M1 and M2a macrophages. The provided manual was followed. To remove the remaining DNA RNase-Free DNase I Kit (Norgen Biotek) was applied according to the producent's protocol.

Eluted genomic DNA (gDNA) was quantified using Qubit dsDNA HS Assay Kit (Thermo Scientific) according to the provided guidelines. Measurements were conducted with the Qubit™ 4 Fluorometer (Invitrogen) instrument. Concentrations and RNA purity were estimated using Nanodrop® 2000 (Thermo Scientific). A 260/280 absorbance ratio of 2 ± 0.2 was deemed satisfactory. The DNA and RNA samples were stored at -80°C prior to downstream applications.

3.9 Sanger sequencing

Sanger sequencing is a first-generation method used to determine nucleotide sequences. Target DNA is combined with a primer, DNA polymerase, deoxynucleotide triphosphates (dNTPs), and fluorescently labeled dideoxynucleotide triphosphates (ddNTPs). The incorporation of ddNTP terminates the elongation step in DNA replication, creating DNA fragments of varying lengths. The fragments are separated, and the fluorescent signal from each fragment is detected (Sanger & Coulson, 1975). To validate *ADA2* KO on a genomic level, extracted gDNA was sent to Eurofins for Sanger sequencing. Prior to sequencing, the gDNA had to be amplified and purified, which are steps described in sections 3.9.1 – 3.9.3.

3.9.1 PCR

Extracted gDNA was amplified by PCR using Phusion Plus PCR Master Mix (Thermo Scientific) according to the manufacturer´s protocol. For each reaction, 40 ng DNA template was added. Judith Staerk kindly gifted the primer pair used for Sanger sequencing, labeled "LC1-RC2" (IDT). The primer sequences and PCR cycling parameters are shown in **Appendix B Table A9** and **Table A11**, respectively.

3.9.2 Electrophoresis

To visualize the amplified PCR products, agarose gel electrophoresis was performed. The products were run on a 2% agarose gel (Invitrogen), and SYBR Safe DNA (Invitrogen) was utilized to visualize the DNA. 6X DNA loading dye (Thermo Scientific) was pipetted into the PCR products in a 1:5 ratio. The ladders used were ZipRulerExpress DNA 1 (Thermo Scientific). The electrophoresis was run at 80V for 45 min. ChemiDoc Imaging System (Bio-Rad) was used to assess and image the gel.

3.9.3 Purification of PCR product

Purification of PCR products ahead of sequencing was carried out according to the ExoSAP-IT™ *Express* PCR Product Cleanup Reagent kit (Thermo Scientific). After purification, the samples were diluted with nuclease-free water (Invitrogen) to a final concentration of 1.5 ng/µl due to the product length size. The DNA concentration was measured using Qubit dsDNA HS Assay Kit together with the Qubit™ 4 Fluorometer. Sanger sequencing was performed at Eurofins Genomics. The primer pair was synthesized and stored in Eurofins Genomics, so the

samples were not premixed in advance. The Sequencher software (Gene Codes Corporation) was used to examine the sequencing results.

The Monarch DNA Gel Extraction Kit (New England Biolabs) was employed according to the manufacturer's protocol to purify PCR products providing two band sizes on the agarose gel. The bands were cut out of the gel and placed into separate pre-weighed 1.5 ml tubes.

3.10 Evaluation of gene expression

qPCR was employed to quantify the relative amount of gene expression. Throughout a qPCR reaction, the increase in amplification amount is monitored in real-time (Peirson & Butler, 2007). The obtained C_q-value represents the number of cycles needed for the fluorescent signal from the amplified DNA or complementary DNA (cDNA) to reach a certain threshold. The value correlates to the DNA or cDNA amount in the initial sample (Haimes & Kelley, 2015). In this study, SYBR Green was used as the fluorescent dye. The steps performed to enable the evaluation of gene expression are described in sections 3.10.1 – 3.10.3.

3.10.1 cDNA synthesis

RNA was synthesized to cDNA using the iScript™ Advanced cDNA Synthesis Kit (Bio-Rad). The protocol was carried out according to the manufacturer's instructions. The PCR parameters are found in **Appendix B Table A12**. To verify *ADA2* KO, the RNA input was 500 ng, and to analyze macrophage markers, the input was 150 ng RNA.

3.10.2 qPCR primers

qPCR primers targeting *ADA2* and macrophage markers were designed in NCBI Primer BLAST. The GC content of the PCR product was between 40-60%. The allele frequencies for the potential SNP were kept under 1%, and the resulting PCR length was between 70 to 200 bp. The tools used to assess this are given in Appendix A Table A1. All the tested qPCR primers were obtained commercially from IDT, and their sequences are presented in **Appendix B Table A10**. The two qPCR primer pairs used to evaluate *ADA2* KO were gifted from a researcher in the Saarela group. The pair targeting *ADA2* binds to exons 4 and 5 and is, therefore, labeled "exon 4-5". The other pair targets the reference gene RNA 18S ribosomal N1 (*RNA18SN1*). The primer locations are shown in **Appendix B Figure A1**.

The qPCR primers were efficiency tested by diluting cDNA collected from non-edited cells electroporated without an RNP complex. To assess the accuracy of primers targeting genes in THP-1 cells, cDNA was made from RNA extracted from THP-1 cells. To test the primer pairs used on M1 and M2a macrophages, cDNA was synthesized from RNA extracted from derived M1 and M2a macrophages, respectively. The obtained cDNA was diluted in a 10-fold dilution series ranging from stock concentration to 1:10000 dilution. Nuclease-free water was the diluent in all the efficiency tests.

The raw data was collected with the CFX Maestro software (Bio-Rad). The average Cq-value, calculated based on three replicates, for each dilution was utilized to create a standard curve. Any replication that varied over 0.5 cycles was removed from the analysis. The standard curve was used to calculate the primer efficiency according to the following equation (equation 3).

$$\text{Primer efficiency} = (10^{\frac{-1}{\text{slope}}}) - 1) * 100 \quad (3)$$

3.10.3 qPCR

PowerTrack™ SYBR Green Master Mix (Thermo Scientific) was used to analyze the messenger RNA (mRNA) level of all the target genes. The qPCR procedure given by the manufacturer was implemented with minor exceptions. The PowerTrack SYBR Green Master Mix, forward and reverse primer, and nuclease-free water were first combined in a master mix and distributed to the relevant wells in a PCR plate. Diluted cDNA was mixed with Yellow Sample Buffer and then added to the relevant wells containing the master mix, resulting in a total volume of 10 µl. Three technical replicas were made for each condition. The qPCR was run using CFX Opus 96 Real-time PCR system (Bio-Rad). The negative control samples consisted of nuclease-free water instead of cDNA and Yellow Sample Buffer. The cycling parameters are listed in **Appendix B Table A13**.

To validate the *ADA2* KO efficiency, cDNA was diluted 1:10 with nuclease-free water to prevent inhibitory effects from the cDNA synthesis reagents. Given the low RNA yield extracted from the macrophages, the cDNA was diluted 1:5.

3.10.3.1 ΔΔCq method

The ΔΔCq method was used to estimate the relative gene expression of *ADA2*, CXC motif chemokine ligand 9 (*CXCL9*), CXC motif chemokine ligand 10 (*CXCL10*), arachidonate 15-

lipoxygenase (*ALOX15*), and mannose receptor C-type 1 (*MRC1*). To do so, the expression level of the target genes was normalized to an endogenous reference. The reference gene was *RNA18SN1* for THP-1 cells and ribosomal Protein L37a (*RPL37A)* for M1 and M2a macrophages. The reference genes had unchanged expression upon treatment exposure. To assess whether the expression levels of the target genes were changed, the equations listed below were used (equations 2-3). Replicas differing over 0.5 cycles from the remaining replicates were excluded.

$$\Delta\mathrm{Cq} = \mathrm{Cq}\,(\text{target gene}) - \mathrm{Cq}\,(\text{reference gene}) \quad (2)$$

$$\Delta\Delta\mathrm{Cq} = 2^{\Delta\mathrm{Cq}\,(\text{treatment}) - \Delta\mathrm{Cq}\,(\text{control})} \quad (3)$$

3.11 Protein detection method

3.11.1 Protein extraction

Proteins were extracted from electroporated bulk cells. From each suspension, $10 * 10^6$ cells were pelleted and washed twice with cold 1X PBS. The two first centrifugation steps were carried out at 500 *x* g for 5 min at RT, and the last wash step at 500 *x* g for 5 min at 4°C. The supernatant was discharged, and 250 µl of radio-immunoprecipitation assay (RIPA) buffer (Thermo Scientific) supplemented with 1X Halt™ Protease Inhibitor Cocktail (Thermo Scientific) was added to resuspend the cell pellet. Cells in RIPA mixture were shaken at 4°C for 15 min prior to being pelleted by centrifugation at 14 000 *x* g for 15 min at 4°C. The samples were homogenized by centrifugation at full speed for 2 min at 4°C using QIAshredder spin column.

Pierce BCA Protein assay kit (Thermo Scientific) was applied to measure the total protein concentration in the obtained cell lysates. The standard protocol described by the manufacturer was carried out. The sole exception was that the extracted protein was diluted at both 1:8 and 1:10 to ensure good reading. Infinite 200 Pro microplate reader (Tecan) was used to measure the absorbance of the standards and samples at 570 nm. Standards and samples were measured in triplicates, and the average absorbance was calculated. The average absorbance measured from the blank standard was subtracted from the remaining standards and samples. A standard curve was created by plotting the average absorbance for each bovine serum albumin (BSA) standard against its concentration. The curve was used to measure the protein concentration of the unknown samples. Protein samples were aliquoted and stored at -80°C until further use in immunoblot analysis.

3.11.2 Immunoblotting

Immunoblotting is a technique for detecting proteins. The proteins are separated by size using gel electrophoresis, transferred to a membrane, and probed with targeting antibodies. By conjugating secondary antibodies to horseradish peroxidase (HRP), quantification and identification of desired proteins can be chemiluminescent detected. To assess the *ADA2* KO on protein level, immunoblotting was performed. An overview of the main steps is shown in **Figure 14**.

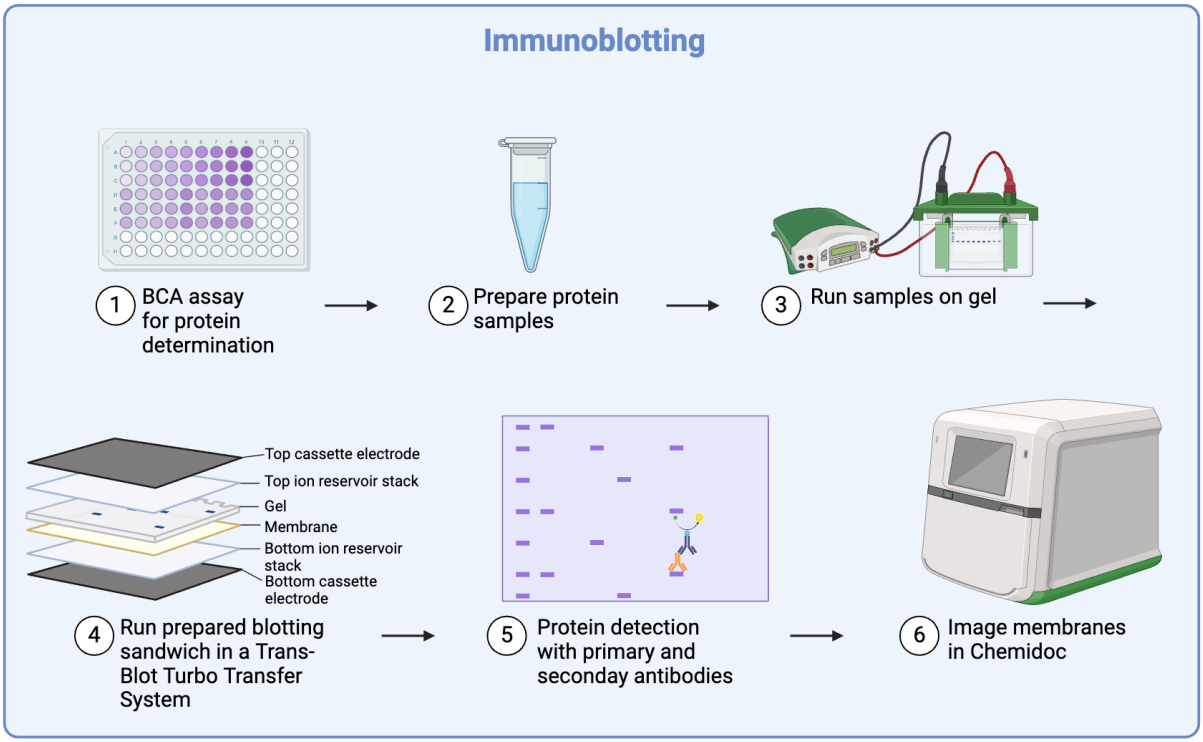

Figure 14. Flow chart of the immunoblotting procedure. First, the total protein content in the samples were calculated. Thereafter, the protein samples were prepared before being loaded onto the gel. Proteins were separated by gel electrophoresis and transferred to a membrane with the use of a blotting sandwich. The membrane was probed with a primary antibody, followed by a secondary antibody conjugated with HRP. To visualize the protein expression, the membrane was imaged by the Chemidoc Imaging System. Abbreviations: BCA, bicinchoninic acid; HRP, horseradish peroxidase. The figure was created with BioRender.com.

The total protein level, calculated with the use of the BCA assay (explained in section 3.11.1), was used to normalize the sample concentrations. Ten µg of protein was loaded onto the gel. Proteins were separated on 4–20% Mini-PROTEAN® TGX™ Precast Protein gels (Bio-Rad) in accordance with the manual with one exception: the gels were run at 80°C for the first 30 min and at 150V for the remaining 50 min. The Precision Plus Protein™ All Blue Prestained Protein Standards (Bio-Rad) were added in the relevant lanes. When completed, Trans-Blot

Turbo Mini 0.45 µm LF PVDF Transfer Kit (Bio-Rad) was used to blot the gels onto membranes according to the provided protocol.

The blotting was run using the Trans-blot Turbo Transfer System (Bio-Rad). The program used was "Mixed MW". No-Stain Protein Labeling Reagent (Thermo Scientific) was used to label the membranes following the instructions provided by the manufacturer. After the labeling process, the membranes were incubated in 5% blotting grade blocker nonfat dry milk (Bio-Rad) diluted in 0.1% TBST which consisted of 1X tris-buffered saline (TBS, Medicago) and 0.1% Tween® Detergent (Merck). After 1 hour of incubation at RT on a plate rotator, the solution was replaced with primary antibody diluted in a solution consisting of 5% blotting grade blocker non-fat dry milk diluted in 0.1% TBST. The three primary antibodies tested were labeled ADA2 TH (Invitrogen), ADA2 AN (Abnova), and ADA2 LB (Lifespan Biosciences). **Appendix A Table A7** presents information about the antibodies and their dilution factors.

The membranes were incubated with primary antibodies overnight at 4°C on a plate rotator. The next day, the membranes were washed: 1X with 0.1% TBST, followed by 4X with 0.2% TBST (1X tris-buffered saline, 0.2% Tween® Detergent), and lastly 2X with 0.1% TBST. The membranes were blocked for 1 hour with a secondary antibody (Cell Signaling Technology) diluted in 5% blotting grade blocker nonfat dry milk in 0.1% TBST on a plate rotator at RT. Information and the dilution ratios of the tested secondary antibodies are provided in Appendix A Table A7. Following the same three washing steps, the membranes were quickly rinsed and then stored in 1X TBS at 4°C until imaging was carried out with the ChemiDoc Imaging System.

The total protein staining was first imaged using fluorescence. Thereafter, the membranes were incubated in SuperSignal™ West Dura Extended Duration Substrate (Thermo Scientific) according to the provided protocol. The ladder was imaged using colorimetry and the samples with chemiluminescence.

3.12 Statistical analysis

Statistical analysis was done using GraphPad Prism 10 (GraphPad Software). The statistical significance of CRISPR/Cas9 editing was calculated using one-way analysis of variance (ANOVA), and the effect of proliferation and macrophage polarization of *ADA2*-edited cells were determined with two-way ANOVA. A $P<0.05$ was considered statistically significant.

4 Results

4.1 Creating ADA2 deficiency models using CRISPR/Cas9

Multiple reagents and conditions were tested to find the most efficient method for CRISPR/Cas9 gene editing in THP-1 cells prior to creating DADA2 cell models. First, the optimal proliferation condition and PCR primers were assessed, and then the editing was optimized regarding the electroporation buffer, culture medium, pulse code, and post-electroporation time point for KO efficiency analysis.

4.1.1 Optimizing the THP-1 cell proliferation condition

To study the effect of culture media and select the condition yielding the highest cell number and viability, THP-1 cells were cultured in three different media compositions. Condition 1) solely consisted of RPMI 1640 Medium supplemented with 10% FBS and 1% P/S. Condition 2) consisted of 1) and 0.05 mM 2-ME, and condition 3) of 2) and 1X MEM NEAA. THP-1 cells are highly sensitive and can undergo apoptosis or differentiation if exposed to oxidative stress. 2-ME is associated with reduced oxidative stress, hence supplemented into conditions 2 and 3. MEM NEAA was added in condition 3 to provide the cells with additional nutrients that can facilitate increased viability and proliferation. The cell viability and the total number of viable cells were recorded in a period of eight days.

Table 2. Monitoring of THP-1 cell proliferation. The cell number and viability obtained from three different culture media over an eight-day period.

	Condition 1		Condition 2		Condition 3	
	Cell number	Viability	Cell number	Viability	Cell number	Viability
Day 1	2.25 M	N/A	2.25 M	N/A	2.25 M	N/A
Day 4	5.28 M	89.5%	5.60 M	93.5%	8.49 M	93.0%
Day 6	11.6 M	95.0%	11.94 M	93.0%	19.06 M	96.0%
Day 8	25.26 M	98.5%	25.74 M	97.0%	38.25 M	96.0%

M, millions; N/A, non applicable (equivalent to data not provided).

As presented in **Table 2**, the three conditions provided sufficient cell proliferation and viability. The average viability was 94.3%, 94.5%, and 95.0% for condition 1, 2, and 3, respectively. Condition 3 resulted in the highest viable cell number. Given similar viability across the conditions, condition 3 was deemed the most productive and optimal based on the final cell

number. Consequently, condition 3 was used as the standard culture medium for the remaining experiments.

4.1.2 Identifying the optimal annealing temperature for PCR amplification

The optimal annealing temperature in the PCR amplification was investigated to later enable verification of the CRISPR/Cas9 edit at the genomic level. Correct annealing temperature achieves specific binding between the PCR primer pair and target DNA, resulting in the amplification of target DNA. The two gRNAs used in the CRISPR/Cas9 experiments were LC1 and RC2. To amplify the gDNA region complementary to the two guides, the "LC1-RC2" primer pair was utilized. A suitable annealing temperature was determined with a gradient PCR program ranging from 58°C to 72°C. Based on the gel electrophoresis, the optimal annealing temperature for the "LC1-RC2" primer pair was 66.4°C due to producing a single band implying specific binding between the primer pair and unedited target DNA. The PCR reaction resulted in a band size that corresponded to the distance (246 bp) between the forward and reverse primer (**Figure 15**). Due to PCR restrictions, the annealing temperature was set at 66°C for the following PCR amplifications conducted prior to Sanger sequencing, which still yielded a single band on the agarose gel (data not shown). Based on the gel electrophoresis, the "LC1-RC2" primer pair was determined successful in amplifying the desired gDNA region and hence used for Sanger sequencing.

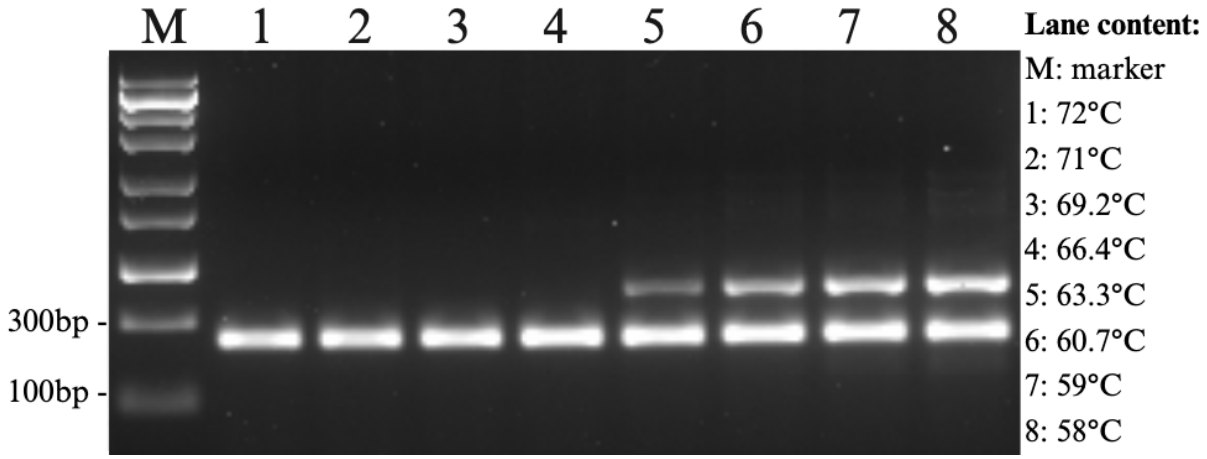

Figure 15. Gel electrophoresis to find the optimal annealing temperature for the "LC1-RC2" primer pair targeting *ADA2*. Non-edited gDNA was subjected to a gradient PCR program ranging from 58°C to 72°C. The lanes contain gDNA amplified at different annealing temperatures: lane 1) at 72°C, 2) 71°C, 3) 69.2°C, 4) 66.4°C, 5) 63.3°C, 6) 60.7°C, 7) 59°C, and 8) 58°C. The marker used was ZipRulerExpress DNA 1. Abbreviations: ADA2, adenosine deaminase 2; DNA, deoxyribonucleic acid; gDNA, genomic DNA; PCR, polymerase chain reaction.

4.1.3 Identifying the optimal qPCR primers for amplifying the *ADA2* gene

The KO efficiency of *ADA2* on the mRNA level was evaluated using qPCR. Consequently, multiple qPCR primers targeting the *ADA2* gene were designed and tested for their efficiency in targeting *ADA2* in non-edited THP-1. Solely one primer pair, referred to as "exon 4-5", showed an efficiency of 102%, which was within the wanted range of 95% to 105%. In addition, the primers amplified the gene with a C_q-value of approximately 26, and the melting peak analysis showed that the primer pair produced only a single peak. Based on the obtained data, the primer pair was concluded to be specific in measuring the mRNA level of *ADA2*.

However, to accurately evaluate the KO efficiency, the primer pair should flank the cut sites of the gRNAs. The reverse "exon 4-5" primer overlapped with the cut site for the LC1 guide and did not flank the RC2 guide, which is located downstream of the reverse primer, as shown in Appendix B Figure A1. The RC2 guide was exclusively used together with the LC1 guide. Consequently, the qPCR primers were used to detect the KOs generated by LC1. Given the aim of the study, a decision was made to compromise the accuracy of the qPCR results since the samples were further validated on DNA level and single-cell sorted.

RNA18SN1 was used as the reference gene to calculate the gene expression of *ADA2*. The primer pair targeting *RNA18SN1* showed constant gene expression in treated samples and controls, gave a single melting temperature peak, and was 98.2% efficient according to the efficiency test conducted. The C_q-value for *RNA18SN1* was, on average, 15 cycles lower than the value for *ADA2*. At the end of the thesis, we realized that the different C_q-values could interfere with the qPCR normalization. Due to time constraints, new primer pairs were not designed.

4.1.4 Optimizing the electroporation buffer for transfection efficiency

To study the effect of electroporation buffers and select the buffer yielding the highest transfection efficiency and cell viability, a GFP vector was inserted into THP-1 cells using electroporation. The electroporation buffer provided by the nucleofector kit, named SG cell line buffer, was compared to two more cost-beneficial buffers: NCMM´s "homemade" buffer (recipe is found in **Appendix A Table A8**) and Opti-minimal essential medium (MEM). Opti-MEM is not a standard electroporation buffer, it is a reduced serum medium. Among other components, the serum consists of poly-L-glutamate, which has been associated with improved electroporation results by increasing efficiency and reducing toxicity (Nicol et al., 2002). Thus, it was tested as an alternative to the other two buffers. A comparison of a viable GFP-positive and negative sample is shown in **Appendix D Figure A4**.

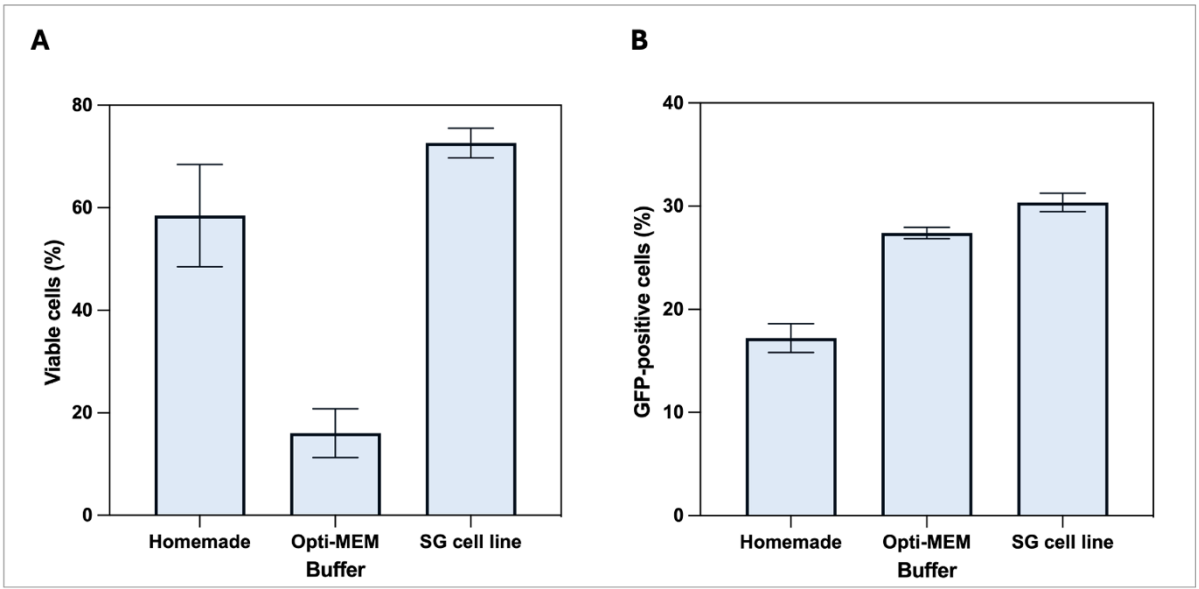

Figure 16. Effect of electroporation buffers on electroporation in THP-1 cells. Three electroporation buffers: "homemade", Opti-MEM, and SG cell line, were compared according to A) cell viability and B) GFP-positive cells. The amount of viable and viable GFP-positive cells is measured in percentage along the respective y-axis. The bar represents the mean (n=3) ±SD of technical replicates. Data was analyzed and gated according to the gating strategy in Appendix D Figure A3. Flow results of one replicate from each condition can be found in **Appendix D Figure A5-6**. Abbreviations: GFP, green fluorescent protein; MEM, minimal essential medium; SD, standard deviation.

The SG cell line buffer showed higher performance values, both in transfection efficiency and cell viability (**Figure 16**). In the SG cell line buffer, the GFP-positive cells constituted 30.4% of the viable cell population. Electroporation in Opti-MEM resulted in 27.4%, while the "homemade" buffer was ineffective with 17.2% of viable transfected cells. The measured

viability was 72.7%, 16.1%, and 58.5%, for the SG cell line, Opti-MEM, and “homemade” buffer conditions, respectively.

There was only a marginal difference between the SG cell line and Opti-MEM buffer regarding viable GFP-positive cells, indicating that the Lonza instrument does not exclusively need to be used with the provided buffer to achieve similar electroporation efficiency. However, since the Opti-MEM condition resulted in considerably low cell viability, it was not used further. The SG cell line buffer was found to be the most effective and was used in the remaining electroporation experiments.

The data presented in Figure 16 shows cell viability stained 24h after electroporation. The recorded viability was lower than expected. A new experiment was conducted with a plan to evaluate cell viability 48h after transfection. However, the cell viability dramatically declined from 24h to 48h post-electroporation, and the experiment was discontinued.

4.1.5 Assessing the effect of a culture medium supplement on transfection efficiency

The THP-1 manufacturer does not recommend adding MEM NEAA to the culture medium. However, as described in section 4.1.1, supplementing MEM NEAA to the culture medium increased the proliferation rate of THP-1 cells. Therefore, the potential impact of MEM NEAA on the electroporation performance was investigated. THP-1 cells were either cultivated with or without MEM NEAA prior to and after electroporation and compared with respect to viability and transfection efficiency (i.e. number of GFP-positive cells). The cells cultivated with MEM NEAA had a higher viability than the cells cultivated without MEM NEAA (61.9% versus 56.4%). The proportion of viable cells expressing GFP 24h post-electroporation was 19.8% and 22.5% with and without MEM NEAA, respectively (**Figure 17**). Thus, adding MEM NEAA to the medium gave better cell viability with little impact on transfection efficiency. Based on this data and the culture medium optimization (section 4.1.1), it was decided to continue supplementing MEM NEAA to the culture media for the following experiments, considering that the cells were to be cultivated as single-cells eventually.

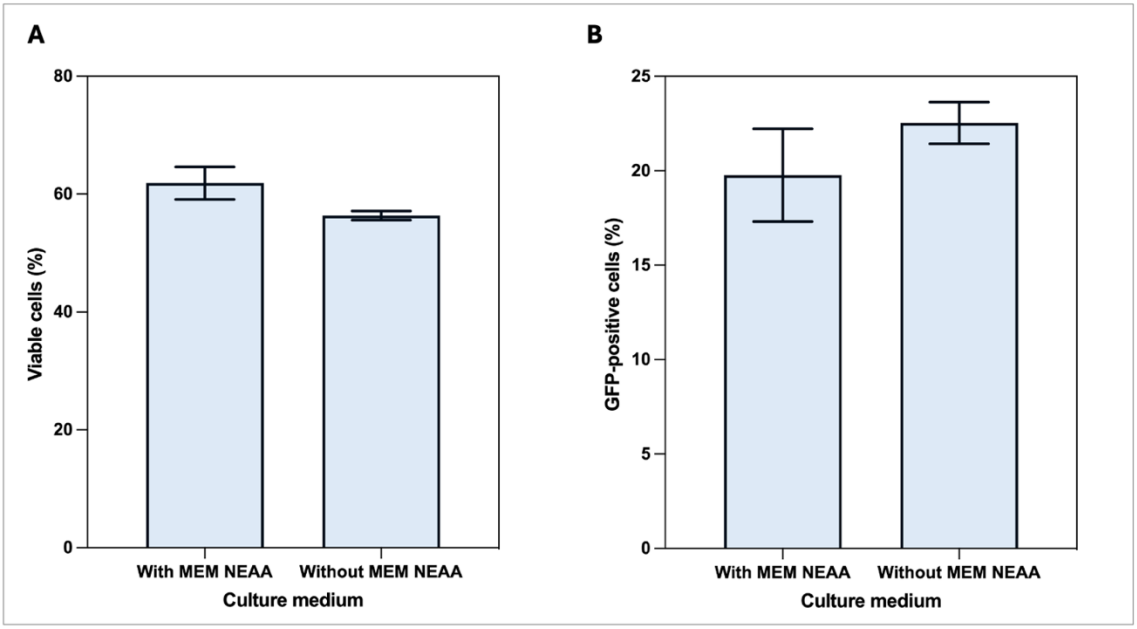

Figure 17. Effect of culture media on electroporation in THP-1 cells. THP-1 cells cultured in media with or without MEM NEAA were electroporated and compared according to A) cell viability and B) GFP-positive cells. The amount of viable and viable GFP-positive cells is measured in percentage along the respective y-axis. The bar represents the mean (n=3) ±SD of technical replicates. Data was analyzed and gated according to the gating strategy in Appendix D Figure A3. Abbreviations: GFP, green fluorescent protein; MEM NEAA, minimal essential medium; SD, standard deviation.

4.1.6 Optimizing the pulse code for *ADA2* KO efficiency

The Knowledge Center from Lonza, which is the manufacturer of the utilized nucleofector kit and instrument, recommends using pulse code FF-100 for electroporating THP-1 cells. However, it also reports that another pulse code, DV-100, can yield 22-28% higher electroporation efficiency and 3-17% more viable THP-1 cells compared to FF-100. Therefore, the two pulse codes were tested with regard to transfection efficiency by measuring relative *ADA2* mRNA expression. The *ADA2* gene was edited with two different gRNA conditions. In one condition, cells were electroporated exclusively with the LC1 guide, while in the other condition, cells were electroporated with the LC1 and RC2 guides (labeled LC1/RC2). The negative control constituted cells electroporated without an RNP complex. RNA was extracted four days post-electroporation. For both gRNA conditions, electroporation using the FF-100 pulse code was less efficient in producing *ADA2* KO as measured by a lower reduction in *ADA2* mRNA expression compared to cells electroporated with DV-100. DV-100 provided a KO efficiency of 77% (i.e. 77% reduction in *ADA2* mRNA expression) when cells were electroporated with LC1 compared to 52% using FF-100, and of 52% versus 38% for the LC1/RC2 cells (**Figure 18**). To conclude, DV-100 was superior to FF-100 because it achieved the highest KO efficiency. The results also indicated that the KO efficiency was higher when

the LC1 guide was used alone than together with RC2, particularly when applying the DV-100 pulse code. Consequently, DV-100 was used for the following experiments.

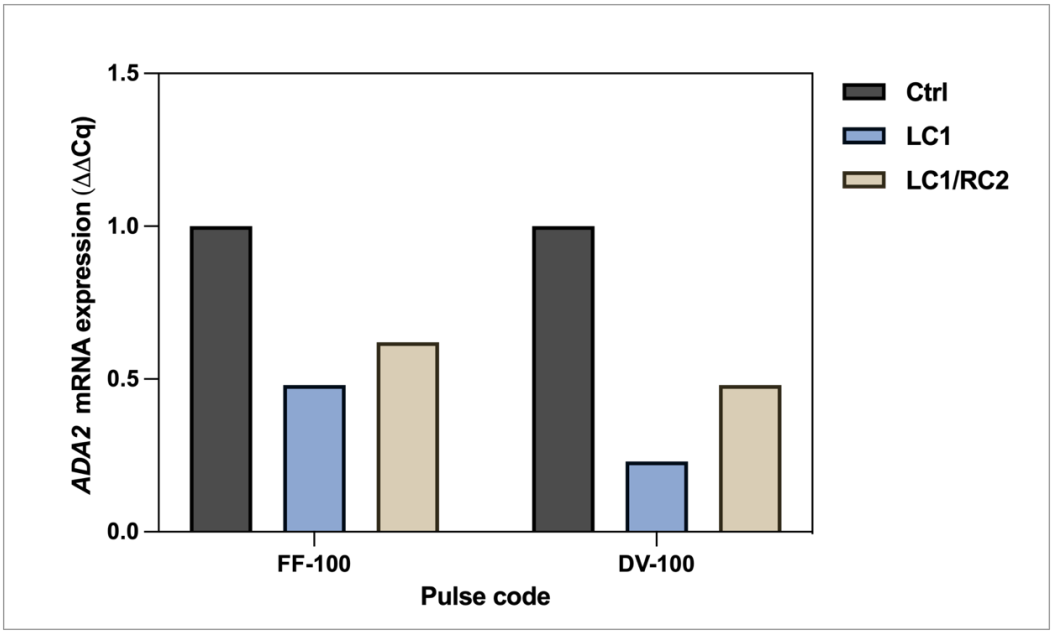

Figure 18. Effect of electroporation pulse codes on *ADA2* mRNA expression. THP-1 cells were electroporated with either LC1 or LC1/RC2 gRNAs at two different pulse codes. The pulse codes are shown along the x-axis, and the relative mRNA expression ($\Delta\Delta C_q$) of *ADA2* is shown along the y-axis. *RNA18SN1* was used as the reference gene to normalize *ADA2* expression. Cells from three technical replicates were combined during cell harvesting. Abbreviations: ADA2, adenosine deaminase 2; cDNA, complementary DNA; gRNA, guide RNA; mRNA, messenger RNA; RNA, ribonucleic acid; RNA18SN1, RNA 18S ribosomal N1.

4.1.7 Selection of incubation time post-electroporation

A time-course analysis was performed to select the optimal timing for RNA extraction post-electroporation. The optimal time represented the point when the relative mRNA expression of *ADA2* had stabilized following transfection. THP-1 cells were electroporated with either the LC1 or LC1/RC2 gRNAs, while the control cells were electroporated without an RNP complex. RNA was extracted day 2, 3, 4, and 7 after electroporation, and *ADA2* mRNA levels were measured to assess the proportion of *ADA2*-edited cells. Cells electroporated with the LC1 guide showed a time-dependent decrease in mRNA levels of *ADA2* with fold changes compared to negative control of 0.40, 0.28, 0.23, and 0.17 at day 2, 3, 4, and 7, respectively. The fold change for the LC1/RC2 sample was not as efficient as for LC1, providing decreases of 0.66, 0.50, 0.48, and 0.50 at the respective time points (**Figure 19**). For the LC1/RC2 sample, the difference in the KO efficiency from day 3 to 7 was marginal. The difference was greater for the LC1 sample, yet the mRNA expression levels were sufficiently similar on day 4 and 7 post-

electroporation. Due to time efficiency, it was decided to extract RNA four days after electroporation for the following experiments.

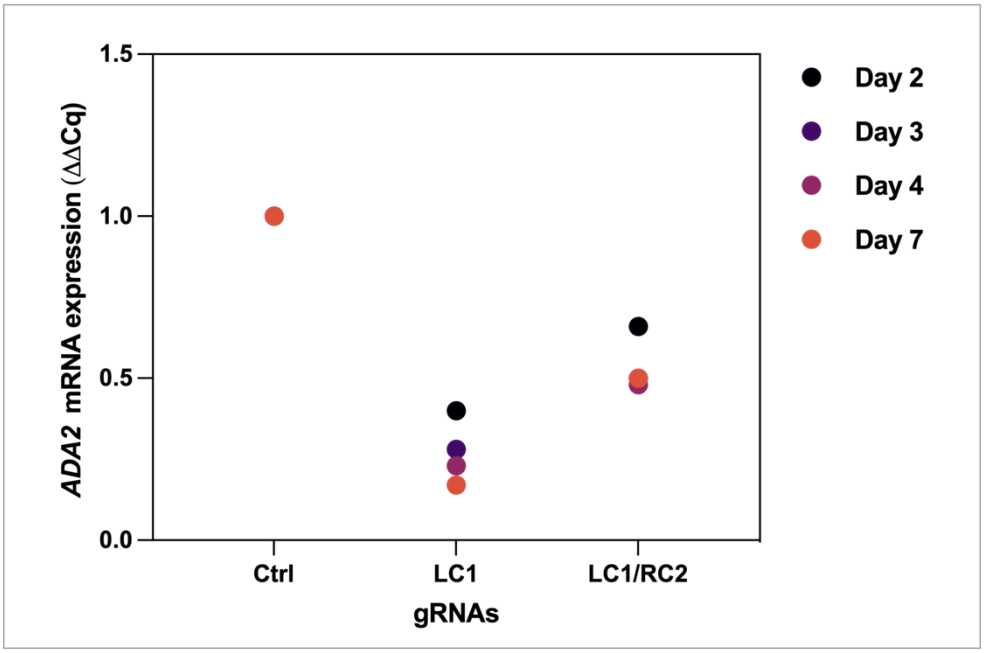

Figure 19. The relative mRNA expression of *ADA2* following electroporation. Total RNA from electroporated THP-1 cells was extracted 2, 3, 4, and 7 days after electroporation. The gRNA combinations are listed along the x-axis, and the relative mRNA expression ($\Delta\Delta C_q$) of *ADA2* is along the y-axis. *RNA18SN1* was used as the reference gene to normalize *ADA2* expression. Cells from three technical replicates were combined during cell harvesting. Abbreviations: ADA2, adenosine deaminase 2; cDNA, complementary DNA; gRNA, guide RNA; mRNA, messenger RNA; RNA, ribonucleic acid; RNA18SN1, RNA 18S ribosomal N1.

4.1.8 Evaluation of *ADA2* KO with optimized CRISPR/Cas9 conditions

With the optimized CRISPR/Cas9 conditions, defined by the SG cell line electroporation buffer and DV-100 pulse code, THP-1 cells were electroporated with either the LC1 or LC1/RC2 guides. The objective was to KO *ADA2* and further use the cells in a proliferation analysis and single-cell sorting. Four days after the RNP complex was inserted into the cells, DNA and RNA were extracted to assess the KO efficiency. According to the relative mRNA levels, both conditions resulted in a significant reduction of *ADA2* expression compared to the negative control, which consisted of cells electroporated without an RNP complex. The LC1 condition resulted in a mean KO efficiency of 69% compared to 54% in the LC1/RC2 condition. The difference between the two conditions was not significant (**Figure 20**).

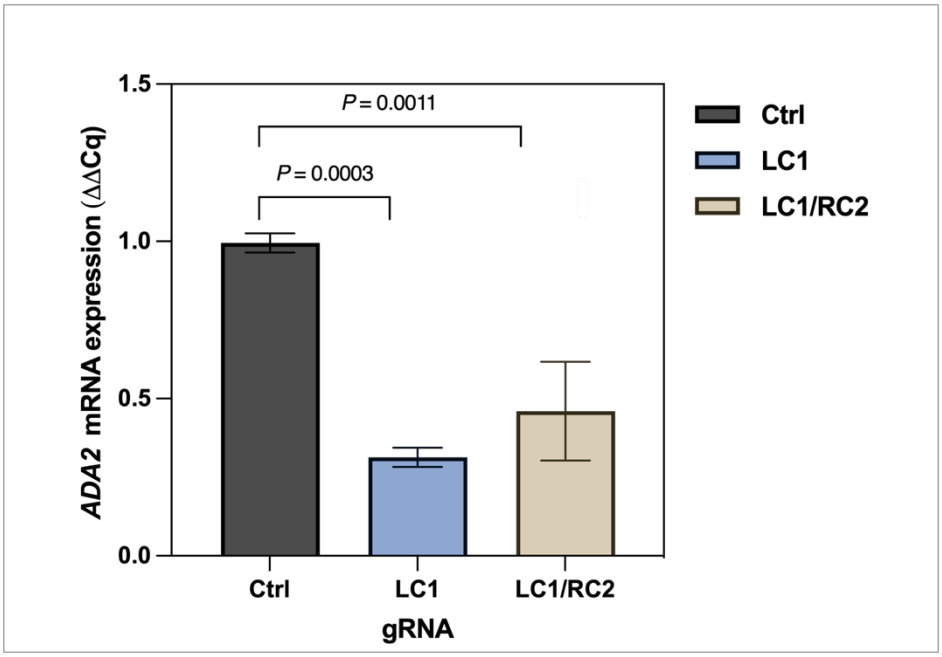

Figure 20. Effect of *ADA2* editing. THP-1 cells were electroporated with an optimized CRISPR/Cas9 protocol. The gRNA combinations are listed along the x-axis, and the relative mRNA expression ($\Delta\Delta C_q$) of *ADA2* is along the y-axis. *RNA18SN1* was used as the reference gene to normalize *ADA2* expression. The bar represents the mean (n=3) ±SD of biological replicates. Significant differences with *P*-values <0.05 are displayed. Abbreviations: ADA2, adenosine deaminase 2; Cas, CRISPR-associated protein 9; CRISPR, clustered regulatory interspaced short palindromic repeats; gRNA, guide RNA; mRNA, messenger RNA; RNA, ribonucleic acid; RNA18SN1, RNA 18S ribosomal N1; SD, standard deviation.

The LC1 and LC1/RC2 samples were sent for Sanger sequencing to confirm the gene edit. The presented Sanger sequencing results were obtained exclusively from the forward primer since the reverse "LC1/RC2" primer provided poor-quality sequences. It could be caused by a potential extra binding site shown in Appendix B Figure A1. A deletion of one adenine nucleotide was detected for both gRNA conditions. The effect of the RC2 guide on the LC1/RC2 samples was difficult to decipher due to the edit caused by the LC1 guide (**Figure 21**). Despite that, the LC1 guide proved efficient, and cells electroporated with both LC1 and LC1/RC2 were chosen for single-cell sorting and proliferation analysis.

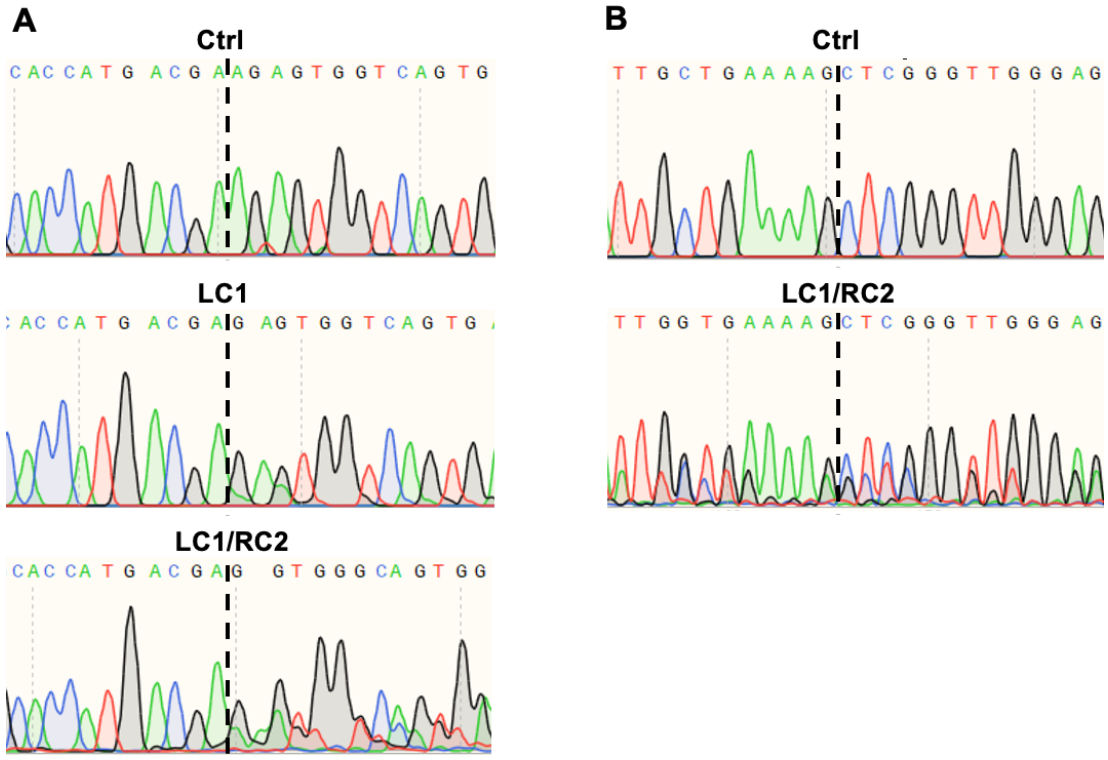

Figure 21. Sanger chromatogram of *ADA2*-edited bulk cells. The data shown represent results for one out of three biological replicates. The vertical dotted lines denote the gRNA cut site. A) The obtained sequences of cells electroporated with the LC1 and LC1/RC2 gRNAs at the LC1 cut site. B) The sequencing results of the LC1/RC2 electroporated cells at the RC2 cut site. Abbreviations: ADA2, adenosine deaminase 2; gRNA, guide RNA; RNA, ribonucleic acid.

4.1.8.1 Testing suboptimal ADA2 antibodies to assess the protein expression in *ADA2*-edited cells

Immunoblotting can be used to evaluate the protein level of ADA2 in the CRISPR/Cas9-edited cells to further evaluate the *ADA2* KO efficiency. Immunoblotting requires an antibody that is highly specific to the protein to be assessed. Unfortunately, none of the commercially available antibodies for ADA2 tested in the Saarela group have been found to be specific in previous tests. Despite this, three different primary antibodies, named ADA2 TH, ADA2 AN, and ADA2 LB, were examined for their ability to detect ADA2 in cell lysates. The *ADA2*-edited cells had been exposed to an RNP complex with either the LC1 or LC1/RC2 gRNAs. The positive control was cell lysate obtained from non-edited cells electroporated without an RNP complex.

The ADA2 protein is approximately 59-kDa in size. Therefore, with a specific antibody, it would be expected to see a strong band between 65 and 50 kDa for the control and a weaker band for the electroporated bulk cells as an indicator of reduced mRNA expression due to KO of *ADA2*. However, the immunoblotting results showed unspecific binding of all the tested

ADA2 antibodies. Multiple bands were stained by the tested antibodies, and no difference was observed between the control and the *ADA2*-edited cells (**Figure 22**). To conclude, the immunoblot analysis using the three ADA2 antibodies was not efficient in measuring the efficiency of *ADA2* KO. However, as the qPCR indicated significantly reduced *ADA2* expression in the edited cells (Figure 20) and the targeted genome sequencing showed a one base deletion (Figure 21), which is expected to change the reading frame and lead to premature stop codon, the electroporated cells were single-cell sorted.

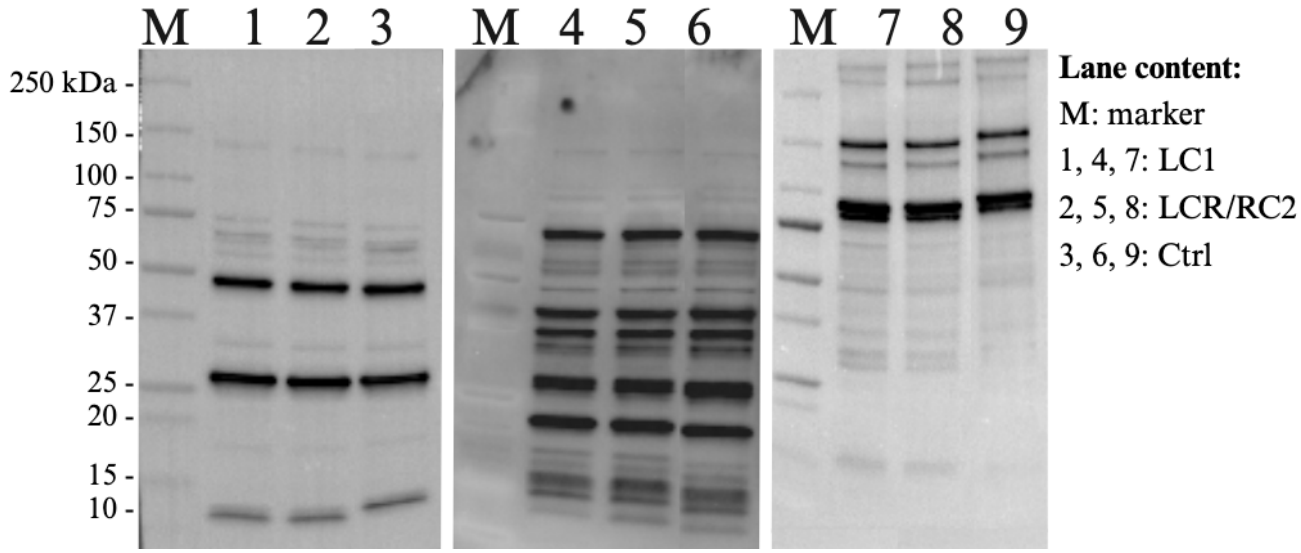

Figure 22. Immunoblotting for ADA2. The protein expression of ADA2 was examined in THP-1 cells electroporated with LC1 (lane 1, 4, 7), LC1/RC2 (lane 2, 5, 8), and cells electroporated without an RNP complex (lane 3, 6, 9). The primary antibodies tested were ADA2 TH (lane 1-3), ADA2 AN (lane 4-6), and ADA2 LB (lane 7-9). The marker used was Precision Plus Protein™ All Blue Prestained Protein Standards. Total protein was detected for all the samples and is presented in **Appendix E Figure A8**. Abbreviations: ADA2, adenosine deaminase 2; RNP, ribonucleoprotein.

4.1.9 Evaluation of *ADA2* KO in single-cell clones

To be certain that *ADA2* CRISPR/Cas9-edited THP-1 cells had reduced *ADA2* expression, the cells were sorted to create single-cell clones and then assessed using qPCR and Sanger sequencing. The goal of single-cell sorting was to produce ADA2 deficiency models. Given unknown off-target effects, cells electroporated with the LC1 guide with a 77% KO efficiency and LC1/RC2 guides with a 51% KO efficiency were sorted.

For optimization, each sample was sorted into three different 96-well plates: culture-treated flat-shape, non-treated flat-shape, and non-treated U-shape. Cells sorted in U-shape bottom plates were transferred to a non-treated flat-shape bottom plate when cell clusters were detected

under the light microscope. Cells plated in culture-treated flat bottom plates had substantially better proliferation rates than cells in the remaining plates. After one month of cultivation, cells in multiple wells reached a confluency of over 80%. In contrast, an equivalent cell confluency was only observed in three wells of the non-treated plates. Ten wells from each condition (LC1 and LC1/RC2 electroporated cells) were selected and subcultured into larger non-treated plates. The selection was not randomized due to the varying cell densities (**Figure 23**). Some wells displayed abundant cell cultures, other single-cell clones required a longer cultivation period, and in several wells, no cellular growth was observed.

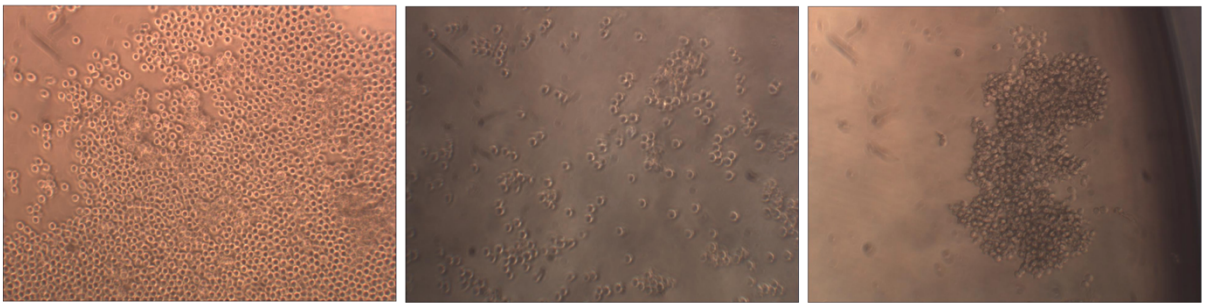

Figure 23. Sorted THP-1 cell cultures. Pictures of three wells in a 96-well plate consisting of sorted THP-1 cells. Pictures were taken 27 days after sorting with a GXCAM camera and GXCapture™ software in conjunction with a light microscope with 20X magnification.

The 20 subcultured clones were subjected to qPCR to assess whether the samples contained reduced *ADA2* mRNA levels. A mistake did occur, causing one clone to be overlooked. The clone measured no amplification for *ADA2,* yet the reference gene was amplified. It was assumed that something went wrong with the sample and that no C_q-value was recorded for both the target and reference gene. When the misconception was realized, the sample had been discharged. Apart from this sample, the other 19 clones showed a reduction in *ADA2* expression in relation to the negative control consisting of cells electroporated without an RNP complex. The qPCR results of the three clones from each condition with the lowest *ADA2* mRNA levels are presented in **Table 3**. The clones showed a 98-99% reduction in relative *ADA2* expression, indicating that a 1-2% expression persisted. The expressions for the remaining clones are attached in **Appendix C Table A14**.

Table 3. Reduced expression of *ADA2* in sorted THP-1 cells. The relative mRNA expression ($\Delta\Delta C_q$) and KO efficiency of *ADA2*. *RNA18SN1* was used as the reference gene to normalize *ADA2* expression.

Sample	$\Delta\Delta C_q$	KO efficiency
LC1 1	0,01	99 %
LC1 2	0,01	99 %
LC1 3	0,01	99 %
LC1/RC2 1	0,02	98 %
LC1/RC2 2	0,01	99 %
LC1/RC2 3	0,01	99 %

Abbreviations: ADA2, adenosine deaminase 2; KO, knockout; mRNA, messenger RNA; RNA, ribonucleic acid; RNA18SN1, RNA 18S ribosomal N1.

The six clones shown in Table 3 were sent for Sanger sequencing, and the results are displayed in **Figure 24**. Prior to sequencing, the target gDNA was amplified and visualized using an agarose gel. No difference in band size was detected in the samples apart from LC1/RC2 clone 1 (**Appendix C Figure A2**). The samples sent for sequencing were purified from the PCR reaction. In addition, the two bands created by LC1/RC2 clone 1 were extracted from the gel, purified, and sequenced. Regardless, the LC1 cut site could not be assessed for this clone, and no visible sequence alternations were produced by the RC2 guide (Figure 24). Indicating that LC1/RC2 clone 1 was edited in an unknown matter or that technical problems occurred in the sequencing.

All three LC1 edited clones had a verifiable homozygous deletion in the LC1 cut site, consisting of one adenine nucleotide, suggesting that the single clone selection had been successful. LC1/RC2 clone 2 showed the same homozygous deletion in the LC1 cut site combined with an additional alteration of the sequence in the other allele after the RC2 cut site. The chromatogram indicated that the second alteration was a deletion of 13 nucleotides. Based on the results LC1/RC2 clone 2 was either a single clone containing a homozygous deletion (LC1 site) and a heterozygous alteration (RC2) or two clones with both containing the deletion at LC1 and one containing the second alteration at RC2. The deletion in LC1/RC2 clone 3 caused an ambiguous sequence following the LC1 cut site, suggesting a heterozygous deletion in the LC1 cut site or multiple independent clones growing in the same well. Consequently, alternations caused by the RC2 guide could not be evaluated for this clone (Figure 24).

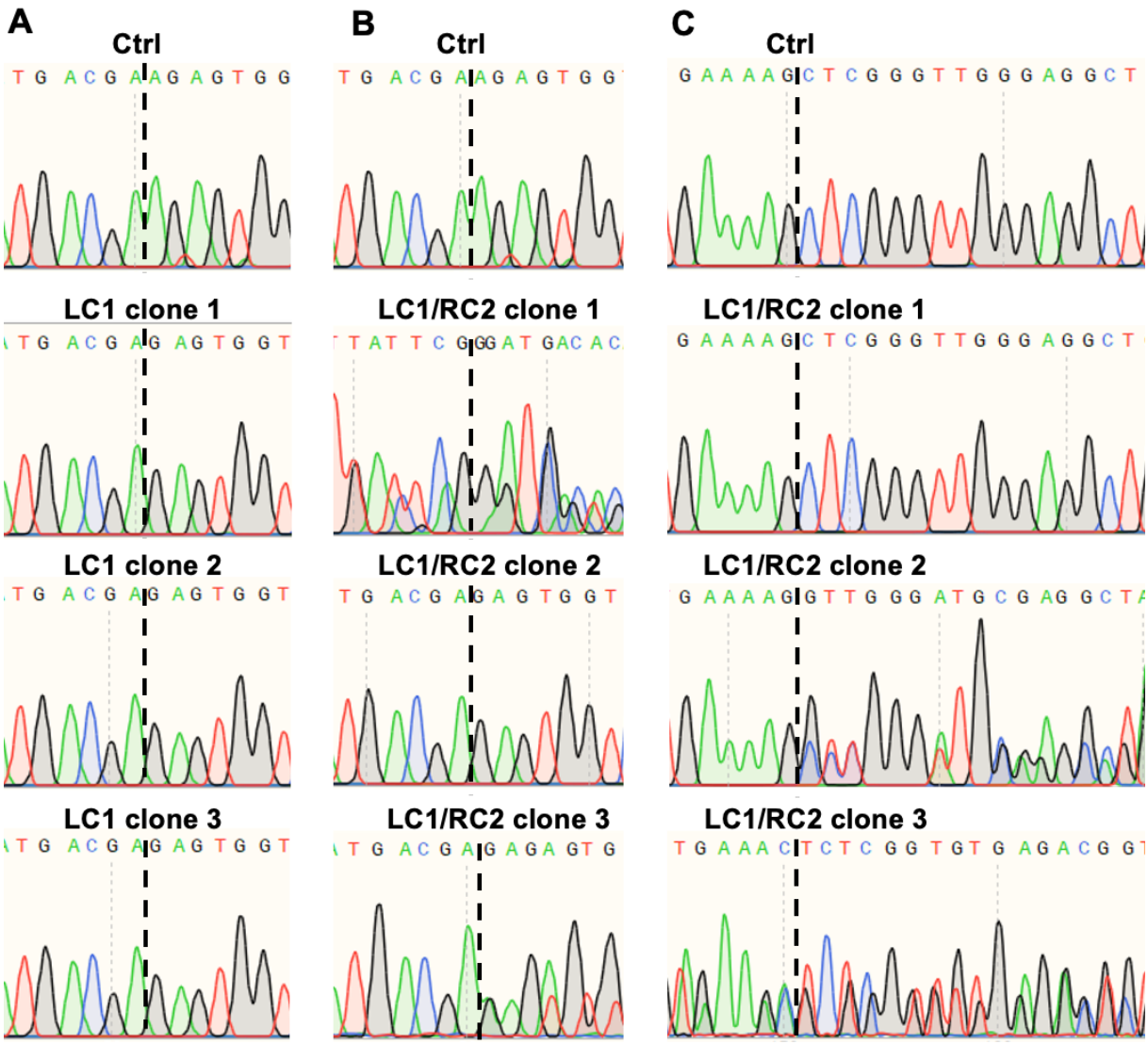

Figure 24. Sanger chromatogram of sorted *ADA2*-edited cells. The vertical dotted line presents the gRNA cut site A) The sequences obtained from sorted cells electroporated with the LC1 guide at the LC1 cut site B) The sequencing results of sorted cells electroporated with LC1/RC2 gRNAs at the LC1 cut site. C) The LC1/RC2 single-cell clone sequences at the RC2 cut site. Abbreviations: ADA2, adenosine deaminase 2; gRNA, guide RNA; RNA, ribonucleic acid.

4.2 Functionally assessing *ADA2* CRISPR/Cas9-edited THP-1 cells

The level of ADA2 may impact cellular function in various ways. To delve further into this, we conducted a study investigating the influence of reduced ADA2 levels on the degree of THP-1 proliferation and macrophage polarization.

4.2.1 Impact of *ADA2* KO on THP-1 proliferation

The rate of proliferation was analyzed on bulk, non-sorted *ADA2*-edited THP-1 cells. The experiment was performed to evaluate the effect of *ADA2* KO on monocytic cell proliferation. The cells analyzed were electroporated with LC1 or LC1/RC2 gRNAs and measured a mean KO efficiency of 69% and 54%, respectively, four days post-electroporation (section 4.1.8). For comparison, non-edited cells electroporated without an RNP complex were utilized as the negative control.

Prior to day 4 in the proliferation analysis, the cells transfected with LC1 had a similar proliferation rate as the control, while the LC1/RC2 had a slightly lower proliferation rate. Both electroporation conditions showed reduced cell proliferation compared to the control from day 4 to day 6.5, with a larger difference between the control and cells exposed to LC1 than LC1/RC2 (**Figure 25**). The total proliferation of the LC1 and LC1/RC2 electroporated cells was found to be significantly lower than the control (P=0.003 versus P=0.015).

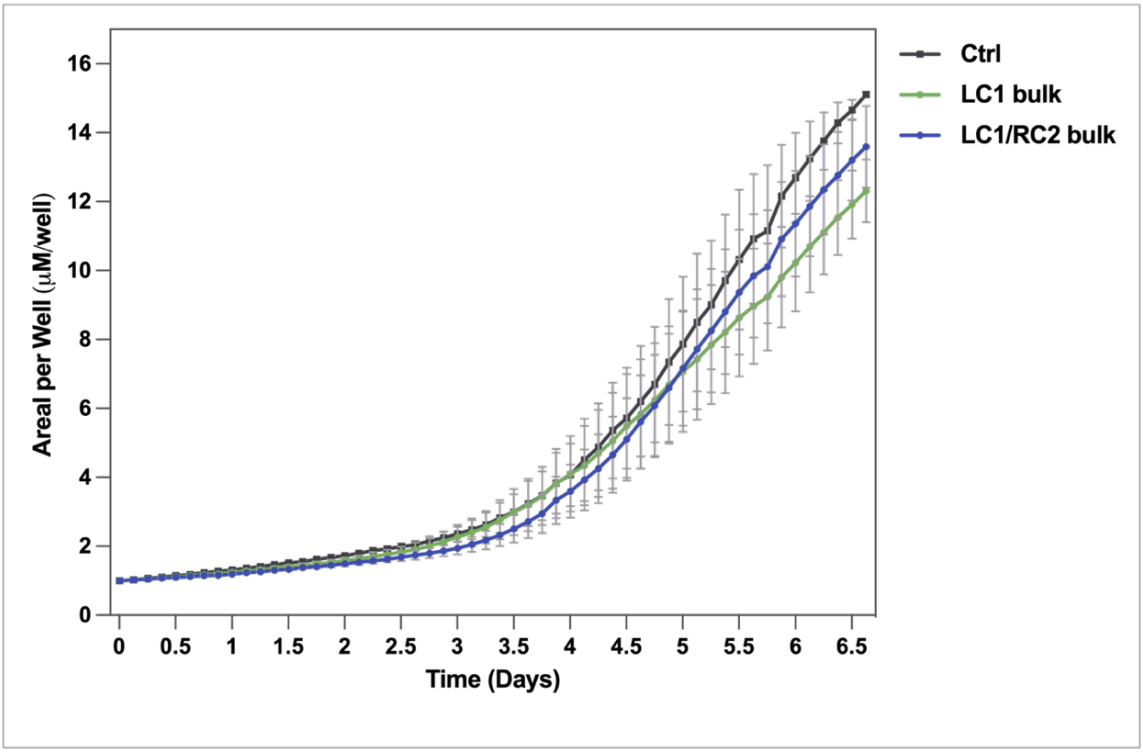

Figure 25. Proliferation of electroporated bulk cells. THP-1 cells electroporated with LC1 or LC1/RC2 gRNAs were incubated in Incucyte S3, where their proliferation rates were assessed and compared to non-edited control cells. The time is shown along the x-axis and the areal per well ratio along the y-axis. The graph represents the mean (n=3 except for the control where n=2) ±SEM of biological replicates. Abbreviations: gRNA, guide RNA; RNA, ribonucleic acid; SEM, standard error of the mean.

The analysis was conducted using three biological replicates, except for the negative control with n=2. **Appendix F Figure A10** contains figures of the individual biological replicates. It took three days for the cells to reach approximately 15% confluency, causing the wells to receive fresh medium prior to the analysis. Upon media transfer, the cells in the eight technical replicates for the control outlier were shifted toward one side of the well (**Appendix F Figure A11**). This interfered with the accuracy of the Incucyte measurements, which require equally distributed cells in the well to get precise data. Consequently, the data for this control replicate was removed from the proliferation analysis.

4.2.2 Optimizing the THP-1 differentiation into M0 macrophages and further polarization into M1 and M2a macrophages

Following single-cell sorting, the protocol for monocyte differentiation and macrophage polarization was optimized to enable functional assessment of *ADA2* KO on macrophage polarization. Together with a fellow researcher at the Saarela group, multiple conditions were investigated to yield the most efficient differentiation and polarization of monocytes into M1 and M2a macrophages. The most suitable conditions were determined based on light microscopy according to phenotypic morphology reported by Baxter et al. (2020). The M0 macrophages can be identified by their round morphology. M1 cells have flattened irregular cell shapes with cytoplasmic extensions, while M2a exhibits flattened round shapes.

PMA, which activates protein kinase C to initiate a series of signaling events that change the morphology and function of cells, was used to induce monocyte differentiation into macrophages. Different durations of PMA stimulations (24h and 48h) and resting time following PMA treatment (24h, 48h, and 72h) were assessed (data not shown). The selection landed on 24h PMA stimulation and 72h resting time. These durations yielded cells with M0 morphology, while M1 morphology was observed in the remaining conditions. This was unwanted, as cells should be unpolarized before exposure to polarization stimuli. The three cell densities tested were: $1.0 * 10^5$ cells/well, $2.5 * 10^5$ cells/well, and $5.0 * 10^5$ cells/well (data not shown). The confluency achieved with $1.0 * 10^5$ cells/well was too low, and with $2.5 * 10^5$ cells/well, floating cells were observed after PMA stimulation, implying that either the PMA concentration or cell number must increase or decrease, respectively. The five PMA concentrations tested were: 5ng/ml, 10ng/ml, 25ng/ml, 50ng/ml, and 100ng/ml. A morphology change from M0 to M1 macrophages was observed when the PMA concentration was equal to or higher than 10 ng/ml. **Figure 26** visualizes the morphology difference between 5 ng/ml and 100 ng/ml after 24h PMA stimulation and 72h rest. Consequently, it was determined that the PMA concentration was held at 5ng/ml and that the cell density was lowered to $2.0 * 10^5$ cells/well.

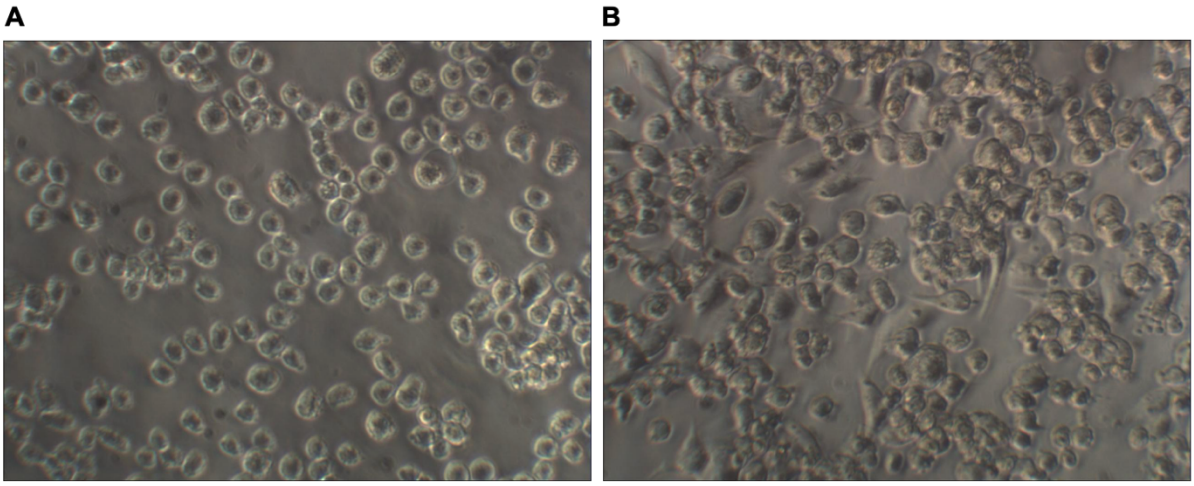

Figure 26. M0 macrophages derived from THP-1 cells. To obtain M0 macrophages THP-1 cells were stimulated with A) 5ng/ml or B) 100ng/ml of PMA for 24h. Pictures were taken after 72h resting time using a GXCAM camera and GXCapture™ software in conjunction with a light microscope with 20X magnification. Abbreviations: PMA, phorbol-12-myristate-13-acetate.

The choice of culture medium was determined by comparing ImmunoCult Macrophage Medium to the culture medium used to cultivate the THP-1 cells (data not shown). ImmunoCult Macrophage Medium is specifically designed to facilitate the differentiation process from human monocytes into macrophages. The specialized medium is costly. Hence, the differentiation effect was assessed and compared to the more cost-beneficial medium. After the cells had rested following PMA stimulation, both media resulted in successful M1 and M2a polarization. However, subjectively, it was observed that the more cost-beneficial medium yielded cells with more M1 and M2a morphology. Consequently, the medium used for THP-1 cultivation was utilized in macrophage differentiation and polarization.

To find the optimal polarization concentrations, different LPS and IL-4 concentrations were examined. To yield the most M1 macrophages, 20 ng/ml IFN-γ was tested together with either 50 ng/ml, 100 ng/ml, or 250 ng/ml LPS. The results suggested that 50 ng/ml LPS led to cells exhibiting the most M1 morphology with irregular cell shapes. Therefore, it was decided to proceed with 20 ng/ml IFN-γ and 50 ng/ml LPS for the remaining experiments (**Figure 27**).

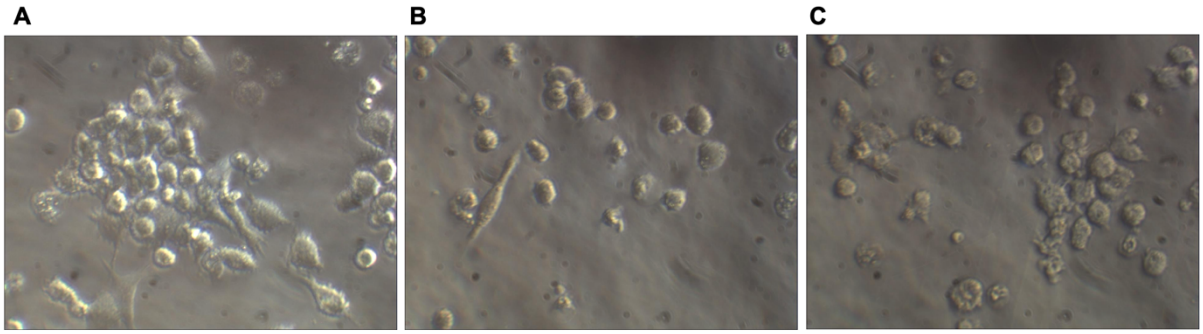

Figure 27. M1 macrophages derived from THP-1 cells. M1 macrophages were obtained by stimulating resting (M0) macrophages with 20 ng/ml IFN-γ and the following LPS concentrations: A) 50 ng/ml, B) 100 ng/ml and C) 250 ng/ml. Pictures were taken after 48h stimulation, using a GXCAM camera and GXCapture™ software in conjunction with a light microscope with 32X magnification. Abbreviations: IFN, interferon; LPS, lipopolysaccharides.

To polarize the resting macrophages to M2a macrophages, the cells were stimulated with either 20 ng/ml, 25 ng/ml, or 30 ng/ml IL-4. The highest concentration yielded more cells with a flattened round shape, more closely resembling the M2a morphology, and was thus selected for further experiments (**Figure 28**).

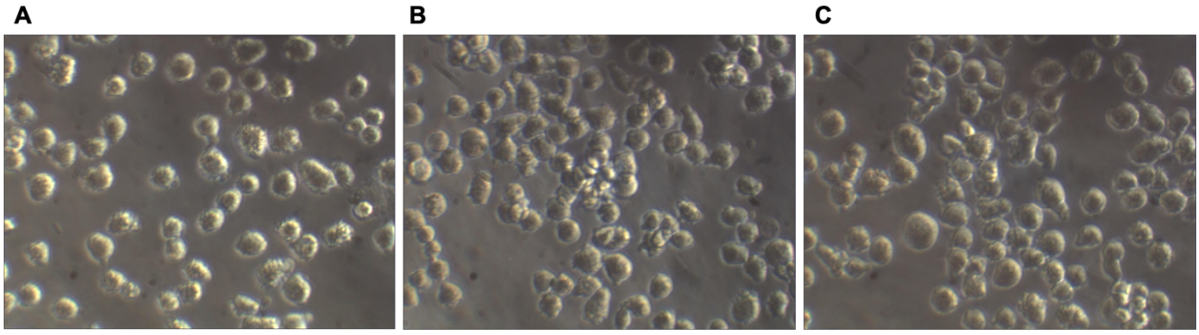

Figure 28. M2a macrophages derived from THP-1 cells. M2a macrophages were obtained by stimulating resting (M0) macrophages with the following IL-4 concentrations: A) 20 ng/ml, B) 25 ng/ml and C) 30 ng/ml. Pictures were taken after 48h stimulation, using a GXCAM camera and GXCapture™ software in conjunction with a light microscope with 32X magnification. Abbreviations: IL, interleukin.

4.2.3 Identifying the optimal qPCR primer pairs for amplifying macrophage markers

qPCR was implemented to examine the mRNA expression levels of macrophage markers following macrophage polarization of the sorted *ADA2*-edited cells. To find specific qPCR primers, two primer pairs were designed for each macrophage marker: the M1 markers were *CXCL9, CXCL10, TNF-α,* and the M2 markers were *ALOX15, MRC1,* and interleukin-10 (*IL10)*. All the markers had at least one primer pair within the wanted primer efficiency range, which was 95% to 105%, except for *IL10* and *TNF-α* (**Table 4**). These genes were, therefore, excluded as markers for the following experiments. Based on the efficiencies in Table 4, primer pair 1 for *MRC1* and primer pair 2 for *CXCL9* and *CXCL10* were within the desired range and were subsequently selected to measure the mRNA level of their respective genes. Both primer pairs for *ALOX15* had an efficiency between 95% and 105%. Primer pair 2 was closest to 100% and was therefore chosen for further analysis.

Table 4. Primer efficiency test for macrophage markers. Two primer pairs for each macrophage gene marker were efficiency tested on non-edited macrophages. The efficiency is given in percentage.

Gene	*CXCL9*		*CXCL10*		*TNF-α*		*ALOX15*		*MRC1*		*IL10*	
Primer pair	1	2	1	2	1	2	1	2	1	2	1	2
Efficiency (%)	107	103	106	100	68	77	98	101	96	92	126	137

Abbreviations: ALOX15, arachidonate 15-lipoxygenase; CXCL9, CXC motif chemokine ligand 9; CXCL10, CXC motif chemokine ligand 10; IL10, interleukin 10; MRC1, mannose receptor C-type 1; TNF, tumor necrosis factor.

RPL37A encodes a human ribosomal protein and was used as the reference gene to normalize target expression in macrophages. Ribosomes are essential for translating mRNA into proteins in all cells. Hence, *RPL37A* is often used to normalize gene expression. Two primer pairs targeting *RPL37A* were designed and tested (**Table 5**). Primer pair 2 achieved efficiency within 95-105% for both macrophage subtypes and was consequently selected for normalization.

Table 5. Primer efficiency test for the macrophage reference gene. Two primer pairs targeting *RPL37A* were efficiency tested on non-edited M1 and M2a macrophages. The efficiency is given in percentage.

Gene	*RPL37A*			
Macrophage subtype	M1		M2a	
Primer pair	1	2	1	2
Efficiency (%)	107	103	104	100

Abbreviations: RPL37A, ribosomal protein L37a.

4.2.4 The impact of sorted *ADA2*-edited cells on macrophage polarization

Next, we investigated whether the reduced ADA2 levels affected the polarization of M0 into M1 and M2a macrophages. Following the optimized experimental conditions sorted *ADA2* CRISPR/Ca9-edited THP-1 cells were differentiated, using PMA, and polarized, using IL-4 for M2a and LPS and IFN-γ for M1. The edited cells were the six clones electroporated with either LC1 or LC1/RC2 gRNAs, which exhibited the highest calculated *ADA2* KO efficiencies (Table 3). The macrophage polarization was assessed by measuring the mRNA levels of two typical M1-produced chemokines (*CXCL9* and *CXCL10*) and two M2a-associated biomarkers (*ALOX15* and *MRC1*). The mRNA expressions in *ADA2*-edited M1 and M2a macrophages were then compared to M1 and M2a derived from THP-1 cells electroporated without an RNP complex. In addition, untreated cells, which were not exposed to PMA nor a polarization agent, were included in the experiment, and they had substantially higher total RNA concentration than the treated samples (177.5 ng/µl RNA versus 29 ng/µl).

The resulting M1 macrophages were analyzed using primer pairs targeting *CXCL9* and *CXCL10* (**Figure 29**). The LC1/RC2 clones showed significantly increased expression of *CXCL9* and *CXCL10* compared to the control with a mean 2.56 and 2.61 fold change, respectively. The LC1 sorted cells also showed a mean increase in the relative mRNA levels of *CXCL9* (1.46 fold change) and *CXCL10* (2.10 fold change). However, the increase was not significant.

The clones polarized into M2a macrophages due to cultivation with IL-4 expressed the M2 markers, *ALOX15* and *MRC1*, at a lower level than the control (Figure 29). The LC1 clones had a mean 0.93 fold change in relative *ALOX15* expression and a 0.94 fold change in *MRC1* expression, neither difference being significant. The LC1/RC2 clones, on average, had a non-significant 0.89 and 0.74 fold change reduction of *ALOX15* and *MRC1* expression, respectively.

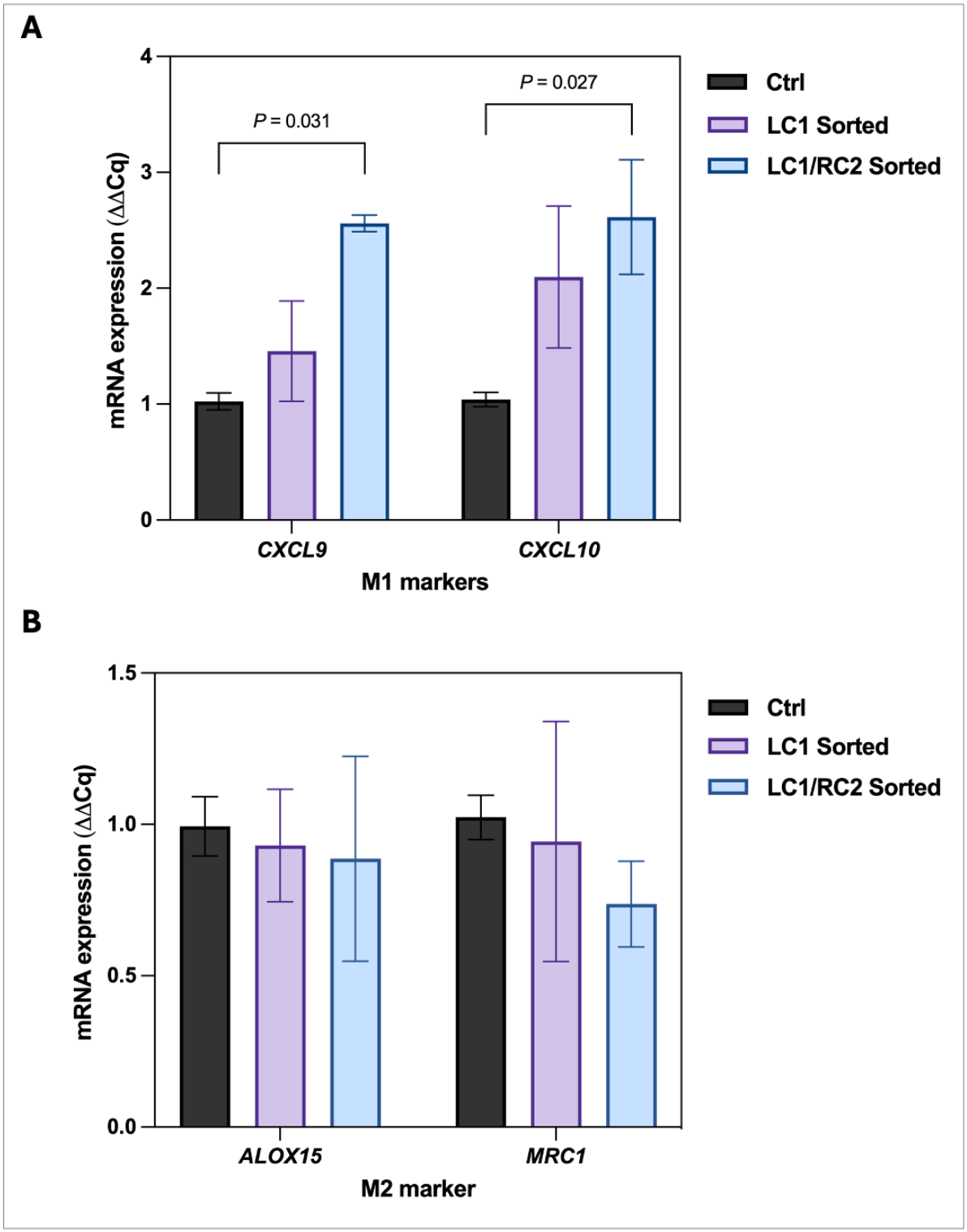

Figure 29. Relative mRNA expression of M1 and M2a macrophage markers in sorted cells. Sorted *ADA2*-edited THP-1 cells were incubated with PMA followed by polarization stimuli, either A) LPS and IFN-γ to generate M1 macrophages or B) IL-4 to generate M2a macrophages. The relative mRNA expression of M1 markers (*CXCL9* and *CXCL10*) and M2a markers (*ALOX15* and *MRC1*) are shown on the respective y-axis. *RPL37A* was used as the reference gene to normalize the expressions. The bar denotes the mean (n=3) ±SEM of biological replicates. Significant differences with *P*-values <0.05 are displayed. Abbreviations: ADA2, adenosine deaminase 2; ALOX15, arachidonate 15-lipoxygenase; CXCL9, CXC motif chemokine ligand 9; CXCL10, CXC motif chemokine ligand 10; IFN, interferon; IL, interleukin; LPS, lipopolysaccharides; MRC1, mannose receptor C-type 1; mRNA, messenger RNA; PMA, phorbol-12-myristate-13-acetate; RNA, ribonucleic acid; RPL37A, ribosomal protein L37a; SEM, standard error of the mean.

5 Discussion

DADA2 is a rare immune deficiency that can cause stroke, bone marrow failure, and, in the most serious of cases, mortality. One of the challenges with DADA2 is the lack of knowledge, particularly in aspects of how ADA2 deficiency affects cellular functions. By improving our understanding of how DADA2 impacts cellular functionalities, we can contribute towards a better comprehension of the disease mechanisms which is critical in the pursuit of more effective and targeted treatments.

This study aimed to create a DADA2 cell model using CRISPR/Cas9 technology within the THP-1 cell line and evaluate the effect of ADA2 deficiency in functional studies. While the experimental setup suffered from restraints, which will be addressed in the following sections, the work successfully resulted in selected sorted cells with altered *ADA2* gene sequences and a measured 98-99% reduction of relative *ADA2* mRNA expression. To our knowledge, studies on DADA2 cell models created with CRISPR/Cas9 and single-cell sorting have not been reported previously. Currently, research has dominantly been conducted on patient cells, and due to a lack of *ADA2* orthologues in rodents, animal studies have been limited. We hope DADA2 cell line models can help fill some knowledge gaps in the research field, given the ease and availability of human cell lines compared to primary cells.

Functionally, the *ADA2*-edited cells were found to have a lower proliferation rate than non-edited control cells. To the best of our understanding, direct investigation of monocytic proliferation in ADA2 deficient cells has not been reported. Further studies validating the statistical significance are needed and will be conducted in the future. The macrophage polarization analysis indicated that sorted *ADA2*-edited cells had affected M1 and M2a polarization with a shift towards M1 macrophages. The obtained results correlated with previous findings and were excepted due to DADA2´s association with inflammatory manifestations (Zhou et al., 2014).

5.1 Selection of cell material

Gene editing studies can be performed on primary cells and cell lines. Both approaches present challenges and advantages. Some advantages of cell lines are, among others, their minimal degree of phenotypical variability because of their homogeneous genetic background, accessibility, and ease of genetic modification. THP-1 is an immortalized cell line that does not have a limited survival period in a culture, contrary to primary cells (Qin, 2012). This was beneficial in this study, given the time-consuming process of creating DADA2 cell models. However, cell lines are genetically altered for continuous passaging, which can lead to genetic and phenotypic instability after prolonged culture (Gibas et al., 1984; van Steenbrugge et al., 1991). Caution should, therefore, be exercised when employing cell lines.

Compared to other monocytic cell lines, THP-1 cells exhibit a lower expression of the ADA2 protein despite being highly expressed. According to the Human Protein Atlas, the cell lines U937 and Mono Mac 6 have a much higher expression (Uhlen et al., 2015). Nevertheless, THP-1 cells differentiate into macrophages that behave more similarly to native monocyte-derived macrophages (Auwerx, 1991). Studies have also shown morphological and functional resemblance between THP-1 and primary monocytes. Thus, THP-1 cells are widely used to study monocytic function and regulation (Qin, 2012). Due to its abundant ADA2 expression and ability to differentiate into native-like macrophages, the THP-1 cell line is well-suited for this study and can provide cellular indications later validated in primary monocytes.

5.2 CRISPR/Cas9 used as a tool to create a disease cell model

5.2.1 Evaluation of CRISPR/Cas9 editing of *ADA2* in THP-1 cells

The THP-1 cell line had not previously been studied in the Saarela group. Thus, it was necessary to optimize the proliferation condition of THP-1 cells and genome editing conditions prior to single-cell sorting. Due to time constraints, the optimization was done as a screening experiment to select the most promising conditions. Therefore, the culture medium, electroporation buffer, and pulse code were assessed with a biological sample size of n=1. In order to draw significant conclusions, the experiments must be repeated to reach a biological sample size of n=3. The presented data gives a preliminary indication that the cells thrived in a culture medium supplemented with 2-ME and MEM NEAA, and that the SG cell line buffer and DV-100 pulse code provided the most efficient genome editing results.

A time-course analysis was conducted with the aim of identifying which day the KO efficiency had stabilized. It was investigated by extracting RNA from electroporated cells on day 2, 3, 4, and 7 after transfection (Figure 19). Cells electroporated with the LC1 guide showed a decrease in mRNA levels of *ADA2* at each time point. This may imply that the duration of the RNP complex activity and binding was still present at day 7 or that the *ADA2*-edited cells had a higher proliferation rate. The latter is more likely because the complex is susceptible to degradation by both protease and RNase, and a previous study reported that Cas9 activity was barely detectable after 48h when delivered in an RNP complex (Liang et al., 2015). Regardless, the time-dependent decline could be a coincident given the fact that a substantial decline in *ADA2* expression was not observed for cells electroporated with LC1/RC2 gRNAs following day 3.

An important observation from the time-course analysis was that the proportion of *ADA2*-edited cells was not stably decreasing after electroporation. However, in the case of LC1/RC2 cells, the measured *ADA2* expression was reduced by 2% from day 3 to day 4. Given the minimal difference, it is possible that the cell solution was not as homogeneous as desired before harvesting an aliquot. In total, the analysis indicated that the cells were not dying due to altered *ADA2* gene sequence. This made single-cell sorting plausible, given the long cultivation period required. In the future, the relative *ADA2* expression should be measured at later stages as well with multiple biological replicates to establish a definitive conclusion regarding the viability of *ADA2*-edited cells post-transfection.

After the optimization was complete, the data reproducibility was validated with a biological sample size of n=3 (Figure 20). The LC1 and LC1/RC2 gRNAs conditions gave significant KO efficiencies of *ADA2*. The cells electroporated exclusively with the LC1 gRNA resulted in the highest measured KO efficiency, exceeding all expectations, with a mean efficiency of 69%. Electroporation with nucleofection technology in the THP-1 cell line has been reported to be effective in previous work. Lonza, the manufacturer of the utilized nucleofector instrument and kit, achieved a transfection efficiency of roughly 65% in THP-1 cells using their optimized protocol. Martinet et al. (2003) received up to 80% transfection efficiency, which was 20% higher than what they obtained with standard electroporation (without nucleofection technology), suggesting that nucleofection is more efficient in THP-1 cells. The data collected from Lonza and Martinet et al. (2003) are based on the transfection of GFP in the form of a vector and mRNA, respectively. The results cannot directly be compared to the experiments performed in this study, where an RNP complex was introduced into the cells, removing the need for intracellular transcription and translation. However, the work published by Martinet et al. (2003) indicated that further optimization can result in a higher *ADA2* KO efficiency. The LC1/RC2 condition measured a lower KO efficiency (54%) than the LC1 condition. A plausible cause could be inadequate KO detection by the qPCR primer pair due to not flanking the RC2 guide. A new primer pair must be designed and validated to accurately detect the gene edit when both the LC1 and RC2 gRNAs are used.

5.2.2 Evaluation of the DADA2 cell models

ADA2 CRISPR/Cas9-edited THP-1 cells were single-cell sorted into multiple plates in order to identify DADA2 cell models. After examining the wells with microscopy, culture-treated flat plates were deemed the most efficient due to higher cell density. Given that the THP-1 cell line is suspension cells, the cells were expected to thrive better in non-treated plates. It could be that culture-treated plates provide a more favorable environment for single cells regardless of whether they are suspension or adherent cells. The advantage of culture-treated plates is that the hydrophilic surface facilitates attachment and cell spreading. This can promote cell-cell and cell-matrix interaction, which could benefit the viability and proliferation of cell cultures consisting of few cells.

Unexpectedly, six of the 20 selected single-cell clones, which constituted the largest cell cultures, measured ≥ 98% reduction in relative *ADA2* expression (Table 3). It was believed that the *ADA2*-edited cells would have a lower proliferation rate compared to the non-edited cells. However, THP-1 is a tumor cell line. ADA2 plays a crucial role in the immune system, and tumor tissues containing a high level of ADA2 are associated with a favorable prognosis (Gao et al., 2022), so lack of ADA2 could possibly facilitate the proliferation of cancerous cells. Another hypothetical reason why *ADA2*-edited cells constituted a relatively high proportion of the selected clones is that *ADA2*-edited cells could be more resilient. Single-cell sorting can induce stress, and if the edited cells are more resilient, they can recover and subsequently proliferate quickly. A third factor could be the gating used to sort the cells. The monocyte gating was quite strict, minimizing the risk of sorting THP-1 derived macrophages, yet it could be that the gating favored *ADA2*-edited cells as well (Appendix D Figure A7).

Based on the Sanger sequencing results, the LC1 guide surpassed all anticipations regarding specificity and created a KO consisting of one nucleotide deletion in five out of the six sorted clones (Figure 24). Four of them (LC1 clones 1-3 and LC1/RC2 clone 2) were homozygous for the deletion at the LC1 cut site. The *ADA2* gene consists of ten exons, and the deletion occurred in the fifth exon, most likely causing a frameshift mutation, hence leading to defective mRNA. Yet the qPCR results showed that 1% mRNA expression of *ADA2* persisted in these clones compared to the control cells (Table 3). However, this difference could be linked to the inaccuracy of the primers (section 5.2.3). The KO effect must be determined at the protein level to conclude that the protein is no longer produced. The two remaining clones and the LC1/RC2 clone 2, which had an additional alteration created by the RC2 gRNA, were either heterozygous for at least one of the mutations or more than one cell was sorted into their wells during FACS. The latter explanation correlates with the varying KO efficiencies measured for the other selected clones (Appendix C Table A14).

5.2.3 Primer limitations

The PCR and qPCR primers used to validate the *ADA2* KO had several restrictions. Advancements in the primer pair specificity would be beneficial for further *ADA2* studies. In the current state, the PCR "LC1-RC2" primer pair is limited to observing whether an edit has occurred. By designing primers for ICE analysis, the Sanger sequencing results could be assessed with ICE Synthego. The advantage of this software is that it can assess the editing

efficiency in seconds. This would be of interest and could be a supplementary technique to qPCR. ICE Synthego cannot currently be used because the forward PCR primer is positioned too close to the LC1 cut site, and the PCR amplicon is too short. Another limitation of the PCR primer pair is the reverse primer. The Sanger sequencing results for the reverse primer were of such bad quality that no information could be attained. It is most likely due to the presence of a possible second binding site (Appendix B Figure A1). The primer pair produced a single band following PCR reaction with the optimal annealing temperature. This could imply that the binding was insufficient to the second site yet still occurred, interfering with the sequencing results. Optimally the gene edits observed in one sequence should be verified in the complementary strand.

The qPCR "exon 4-5" primer pair targeting *ADA2* also had limitations. As previously mentioned, the primers do not flank the complementary sequence of the RC2 guide, and the reverse primer overlaps with the complementary sequence of the LC1 guide. A primer pair should flank the target site to analyze the desired region accurately. The localization problem with the qPCR primer pair was known prior to the experiments. However, due to no other suitable primers, it was further used. Consequently, the KO efficiency calculated on the mRNA level was based on the LC1 cut site. The effect of the primer overlapping with the LC1 gRNA is unknown, and the uncertainty should be avoided. Designing a new primer pair flanking the two target sequences would allow comparison of the total KO efficiency when LC1 gRNA is used alone and in combination with RC2 gRNA. The other constraint that was not acknowledged until the end of the study was that primer pairs targeting *ADA2* and the reference gene *RNA18SN1* should produce quite similar C_q-values to enable reliable normalization. In this study the C_q difference was approximately 15, and it could potentially cause inaccurate normalization and quantification of the target gene expression even if the assumptions of the ΔΔCq method are sustained, as in this case given the reference gene was stably expressed and the target gene and reference gene were amplified with similar primer efficiencies. For further analysis, other endogenous controls should be tested and either replace *RNA18SN1* or be used alongside it to employ more than one control.

5.2.4 Antibody limitation

The immunoblotting analysis was intended to examine the loss of ADA2 protein. However, there is a lack of specific primary antibodies targeting ADA2. The three tested antibodies detected multiple bands on the membrane (Figure 22). Unspecific bands can be caused by antibodies binding to other proteins, a protein having different isoforms or post-translational modification, or protein aggregation. In this analysis, no difference in ADA2 expression level was observed between the non-edited and *ADA2*-edited cells, implying that ADA2 was equally expressed. This does not correlate with the qPCR and Sanger sequencing results obtained from the same samples. Alternatively, it could indicate that none of the observed bands represented the ADA2 protein.

The search for specific ADA2 antibodies has been ongoing in the Saarela group, and thus far, all the commercially available ADA2 antibodies tested have been unspecific. Currently, antibody protein detection in the group has been limited to human embryonic kidney (HEK) 293 cell models transfected by a plasmid with a Myc-tag to ADA2. Since ADA2 is an extracellular protein, it could be possible to extract the culture medium used to cultivate the THP-1 cells instead of the cell lysate. However, it has been tested in the research group previously, and more ADA2 was identified in the lysate. In the future, alternative methods for protein detection will be tested in the Saarela group. Unfortunately, multiple methods require specific antibodies. PICO assay could prove to be more accurate than immunoblotting due to utilizing two antibodies binding to different protein epitopes. To avoid the antibody-related complexities, mass spectroscopy could be employed instead to verify that the protein is no longer expressed.

5.3 Evaluation of the proliferation analysis

The effect of *ADA2* KO was evaluated in a proliferation analysis performed on electroporated bulk cells. The *ADA2*-edited cells measured significantly reduced cell proliferation rates compared to the non-edited control cells (Figure 25). There is limited literature directly investigating the proliferation of monocytic cells with a loss-of-function of *ADA2*. Yap et al. (2021) found that DADA2 patients have an imbalance in monocyte subtypes, with increased proportions of intermediate and non-classical subtypes and significantly reduced numbers of classical monocytes. This corresponds with Watanabe et al. (2021), which reported a decline in classical monocytes and a significant increase in intermediate monocytes in DADA2 patients compared to healthy donors. These findings could indicate that classical monocytes have a lower proliferation rate in DADA2 patients and could be an explanation for the proliferation decline found in the *ADA2*-edited THP-1 cells. In support of this, the THP-1 cell line is, in fact, characterized by the expression of CD14 and the absence of CD16, which resembles a classical monocytic subtype (Forrester et al., 2018). The cells edited with the LC1 gRNA had a lower proliferation rate than the LC1/RC2 cells. This could be explained by the higher KO efficiencies measured for the LC1 cells and that ADA2 is so crucial for viability that the consequence was greater. However, due to the "exon 4-5" primer pair not flanking the RC2 gRNA, we do not have knowledge of the overall KO efficiencies for the LC1/RC2 cells.

PLO, a synthetic amino acid chain, promotes cell attachment (Lindsey, 2003). It was used to adhere THP-1 cells to culture plates to enable proliferation assessment with Incucyte S3. PLO is commonly used for coating, yet it also facilitates the differentiation of multiple cell types (Hippman et al., 2023; Jafary et al., 2008). The effect of PLO on the differentiation of monocytes to macrophages is unclear, and no morphology changes were observed during the proliferation analysis. In addition, ADA2 deficiency is linked to increased macrophage proliferation (Zavialov et al., 2010), and in this experiment, *ADA2*-edited cells were associated with reduced proliferation. However, in future work the experiment could be performed with flow cytometry instead of an Incucyte where the cells would not need to adhere to the culture plates, eliminating the chance of macrophage differentiation.

Despite the significant difference between CRISPR/Cas9 *ADA2*-edited and non-edited cells found in the proliferation analysis, the experiment suffered two major limitations affecting the accuracy of the data. Prior to starting the analysis, the manufacturer sterilized the instrument

due to a previous contamination. Upon completion, it was the Institute's understanding that the incubator the Incucyte was placed in should not contain a tray of autoclaved water in order to avoid future contaminations. When the proliferation analysis was complete, it was conveyed by a representative of the manufacturer that this was a misunderstanding, and that water is vital for cell proliferation in the Incucyte as well. In general, the added water preserves a high humidity level, preventing excessive evaporation of the culture medium. Evaporation can result in a concentration imbalance of minerals, salt, and other components. Lack of autoclaved water could also lead to an increased "edge effect," where the medium in outer wells in a multi-well plate evaporates more quickly (Esser et al., 2011). Fortunately, in this analysis, the first and last columns in the 24-well plates were filled with culture medium without cells, and the same was applied to the two first and last rows, reducing the "edge effect".

The second limitation was the number of cells seeded into the 24-well plates. Due to recommendations by a fellow researcher, the plan was to normalize cell confluency in each well to the time point where the wells were 20% confluent to make sure the cells were in growth phase. Likely, on account of both a low input number and lack of a water tray, it took precisely 3 days to reach approximately 15% confluency. It was decided to normalize the cell confluency to this specific time point to start the analysis and avoid further confluency differences. Normalization facilitates accurate and consistent comparison between experimental conditions by minimizing differences in initial seeding densities. However, the initial input differences will increase after three cultivation days and affect the calculated proliferation rates. Optimally, the confluency differences should be as minimal as possible prior to normalization.

In light of the new knowledge and observations, the experiment will be repeated using sorted cells. Due to time constraints, it was not plausible to do it within this thesis.

5.4 Evaluation of the macrophage polarization experiment

Prior to studying the effect of *ADA2* KO on macrophage polarization, the conditions for differentiation and polarization from monocytes into M1 and M2a macrophages were examined in the THP-1 cells. The optimal conditions were evaluated based on light microscopy and cell morphology which corresponded with previously reported observations (Baxter et al., 2020). It would be beneficial to study the variable conditions in an Incucyte instrument to enable well imaging at the exact same place each time. Unfortunately, the Incucyte was not available. Furthermore, microscopy should be used in conjunction with other validation techniques. However, macrophage polarization has been studied numerous times using the THP-1 cell line, so the tested conditions were well documented in advance. Nevertheless, to draw significant conclusions, the optimization must be performed with more cells and a measurable validation method.

Sorted clones were differentiated into macrophages and further polarized according to the optimized protocol. qPCR primers were used to assess the relative mRNA expression of M1 and M2a markers. The data showed that cells with edited *ADA2* gene tended to polarize toward M1 macrophages. The only significant difference was measured for LC1/RC2 clones in the expression of M1 markers compared to non-edited M1 cells. Yet the mean value for all the *ADA2*-edited clones measured a fold change above 1 for M1 markers and below 1 for M2 markers, indicating that the polarization was skewed. This correlated with the results reported in the literature, which associates DADA2 with impaired macrophage polarization (Kaljas et al., 2017; Van Eyck et al., 2015). Zhou et al. (2014) found that patients with ADA2 deficiency showed poor polarization to M2 and increased proinflammatory cytokines produced by M1. The impact of this imbalance can be illustrated with the TNF inhibition treatment, which effectively restores the M1 and M2 ratio and controls most of the inflammatory manifestations of DADA2. However, as mentioned, the treatment is not efficient in managing the hematological features of the disorder (Deuitch et al., 2022).

The relatively low RNA yield obtained from the monocyte-derived macrophages may have contributed to the less significant difference between *ADA2*-edited and non-edited cells than we anticipated. When the RNA quantity is low, even minor differences in the obtained RNA amounts across samples could interfere with the analysis and lead to biased representation. However, the reference gene employed to normalize the qPCR product was unchanged between

ADA2 CRISPR/Cas9-edited cells and non-edited cells and should, therefore, help to adjust different amounts of RNA yield.

The reason for the low RNA yield was most likely due to the incorrect use of the cell detachment solution accutase. Microscopy was used to assess the detachment of cells, and it was observed that not all cells had detached from the culture plate following accutase incubation. Afterward, it was realized that the accutase had been thawed for two and a half months and stored at 4°C prior to use instead of being stored at -20°C as recommended by the supplier. In addition, the cell detachment method could affect the macrophage phenotype. Chen et al. (2015) differentiated primary monocytes and observed that enzymatic reagents such as accutase reduced the protein expression of MRC1, one of the M2 macrophage markers utilized in this study. Therefore, it would be interesting to compare the use of other detachment solutions not only on the RNA yield but also on the expression of macrophage markers, in order to conduct a more accurate gene expression analysis in the future. In addition, the experimental setup should also be upscaled to analyze a higher cell number.

6 Concluding remarks

Biallelic mutations in *ADA2* cause a rare genetic immunodeficiency disorder, DADA2. As KO models are indispensable tools in the realm of rare disease research, the primary goal of this thesis was to create a DADA2 cell model by knocking out the *ADA2* gene in a monocytic cell line, THP-1, using the CRISPR/Cas9 system. Several aspects of optimization were performed prior to studying the impact of *ADA2* KO on proliferation and polarization abilities. The most optimal conditions for THP-1 cell proliferation and transfection rates were to 1) include 2-ME and MEM NEAA in the culture medium, 2) use the SG cell line electroporation buffer, and 3) apply DV-100 over FF-100 as electroporation pulse code. To assess the KO efficiency, it was sufficient to incubate the electroporated cells for four days and set the PCR annealing temperature for the "LC1-RC2" primer pair to 66°C.

By sorting and cultivating CRISPR/Cas9-edited cells for a month, four cell clones were established as homozygous for the LC1 gRNA-induced mutation in *ADA2.* The homozygous deletion is expected to cause a frameshift mutation resulting in DADA2 cell models. In addition, one of the clones had an extra gene alteration created by the RC2 gRNA. The proliferation analysis implied that knocking out *ADA2* led to a lower proliferation rate compared to non-edited control cells. Furthermore, in a differentiation and polarization experiment, *ADA2*-edited clones indicated a higher ability to polarize to M1 macrophages than M2 macrophages, suggesting that ADA2 plays a role in the polarization process.

The current work lays the foundation for optimizing a cellular KO model for DADA2, which can be used to better understand the cellular abnormalities associated with this disease. However, due to multiple limitations encountered and a low sample size, confirmatory studies must be conducted to make the results reliable and significant.

7 Future perspectives

The work conducted in relation to this master´s thesis represents an advancement toward greater DADA2 understanding and lays the groundwork for further studies of ADA2 in immune cells. The most pivotal part of the thesis was the development of cell models homozygous for an *ADA2* mutation, expected to result in a frameshift mutation leading to a KO model of *ADA2* in a monocytic cell line. Prior to the study being completed, new electroporated cells were single-cell sorted and eventually handed over to other researchers. With multiple cell populations consisting of edited *ADA2*, the functional analysis can be repeated and give conclusive results.

The main goal is to enhance the current knowledge to eventually achieve more precise diagnosis and targeted treatment methods, improving the lives of patients suffering from ADA2 deficiency. Cell models are valuable tools that can contribute to this goal. However, to gain a more comprehensive understanding of DADA2's complexity, induced pluripotent stem cell (iPSC) disease modeling can be utilized. This can involve reprogramming somatic cells from patients or using the CRISPR/Cas9 tool to KO *ADA2* in healthy cells prior to reprogramming. Organoids such as bone marrow and thymus can be created through iPSC disease modeling and could offer a more complete perspective of DADA2's effects. The lack of an orthologous mice model has affected the research field. However, zebrafish have been utilized, and research indicates that loss-of-function zebrafish models could be an efficient tool for studying DADA2 (Brix et al., 2022).

There is currently no cure for DADA2. The CRISPR/Cas9 method shows immense potential as a gene therapy technique for treating monogenic PIDs. It can be used to restore gene functions by correcting the disease-causing mutations in patient cells. Since monogenic diseases are caused by a single gene defect, targeted editing is possible. Further improvements and research are needed to ensure patient safety and long-term and stable expression of the desired gene. However, it can revolutionize the treatment methods for rare diseases such as DADA2.

8 References

Aderem, A. (2003). Phagocytosis and the inflammatory response. *J Infect Dis*, *187 Suppl 2*, S340-345. https://doi.org/10.1086/374747

Akira, S., Uematsu, S., & Takeuchi, O. (2006). Pathogen recognition and innate immunity. *Cell*, *124*(4), 783-801. https://doi.org/10.1016/j.cell.2006.02.015

Aristizábal, B., & González, Á. (2013). Innate immune system. In *Autoimmunity: From Bench to Bedside* El Rosario University Press. https://www.ncbi.nlm.nih.gov/books/NBK459455/

Aschan, J. (2007). Risk assessment in haematopoietic stem cell transplantation: conditioning. *Best Pract Res Clin Haematol*, *20*(2), 295-310. https://doi.org/10.1016/j.beha.2006.09.004

Ashina, K., Tsubosaka, Y., Nakamura, T., Omori, K., Kobayashi, K., Hori, M., Ozaki, H., & Murata, T. (2015). Histamine Induces Vascular Hyperpermeability by Increasing Blood Flow and Endothelial Barrier Disruption In Vivo. *Plos One*, *10*(7), e0132367. https://doi.org/10.1371/journal.pone.0132367

Asmamaw, M., & Zawdie, B. (2021). Mechanism and Applications of CRISPR/Cas-9-Mediated Genome Editing. *Biologics*, *15*, 353-361. https://doi.org/10.2147/BTT.S326422

Auwerx, J. (1991). The human leukemia cell line, THP-1: a multifacetted model for the study of monocyte-macrophage differentiation. *Experientia*, *47*(1), 22-31. https://doi.org/10.1007/BF02041244

Barrangou, R., Fremaux, C., Deveau, H., Richards, M., Boyaval, P., Moineau, S., Romero, D. A., & Horvath, P. (2007). CRISPR provides acquired resistance against viruses in prokaryotes. *Science*, *315*(5819), 1709-1712. https://doi.org/10.1126/science.1138140

Barron, K. S., Aksentijevich, I., Deuitch, N. T., Stone, D. L., Hoffmann, P., Videgar-Laird, R., Soldatos, A., Bergerson, J., Toro, C., Cudrici, C., Nehrebecky, M., Romeo, T., Jones, A., Boehm, M., Kanakry, J. A., Dimitrova, D., Calvo, K. R., Alao, H., Kapuria, D., . . . Ombrello, A. K. (2021). The Spectrum of the Deficiency of Adenosine Deaminase 2: An Observational Analysis of a 60 Patient Cohort. *Front Immunol*, *12*, 811473. https://doi.org/10.3389/fimmu.2021.811473

Baxter, E. W., Graham, A. E., Re, N. A., Carr, I. M., Robinson, J. I., Mackie, S. L., & Morgan, A. W. (2020). Standardized protocols for differentiation of THP-1 cells to macrophages with distinct M(IFNgamma+LPS), M(IL-4) and M(IL-10) phenotypes. *Journal of Immunological Methods*, *478*, 112721. https://doi.org/10.1016/j.jim.2019.112721

Boyette, L. B., Macedo, C., Hadi, K., Elinoff, B. D., Walters, J. T., Ramaswamil, B., Chalasani, G., Taboas, J. M., Lakkis, F. G., & Metes, D. M. (2017). Phenotype, function, and differentiation potential of human monocyte subsets. *Plos One*, *12*(4). https://doi.org/ARTN e017646010.1371/journal.pone.0176460

Brix, A., Pettinato, E., Belleri, L., Zoccolillo, M., Mazzola, M., Del Bene, F., Mortellaro, A., & Pistocchi, A. (2022). A promising ada2 loss-of-function zebrafish model to study the pathogenesis and efficiently correct the Deficiency of Adenosine Deaminase 2 (DADA2) phenotype. https://air.unimi.it/handle/2434/1042231

Broere, F., & Van Eden, W. (2019). T Cell Subsets and T Cell-Mediated Immunity. In (pp. 23-35). Springer International Publishing. https://doi.org/10.1007/978-3-030-10811-3_3

Brouns, S. J., Jore, M. M., Lundgren, M., Westra, E. R., Slijkhuis, R. J., Snijders, A. P., Dickman, M. J., Makarova, K. S., Koonin, E. V., & van der Oost, J. (2008). Small CRISPR RNAs

guide antiviral defense in prokaryotes. *Science*, *321*(5891), 960-964. https://doi.org/10.1126/science.1159689

Caorsi, R., Penco, F., Schena, F., & Gattorno, M. (2016). Monogenic polyarteritis: the lesson of ADA2 deficiency. *Pediatr Rheumatol Online J*, *14*(1), 51. https://doi.org/10.1186/s12969-016-0111-7

Chen, S., So, E. C., Strome, S. E., & Zhang, X. (2015). Impact of Detachment Methods on M2 Macrophage Phenotype and Function. *Journal of Immunological Methods*, *426*, 56-61. https://doi.org/10.1016/j.jim.2015.08.001

Cong, L., Ran, F. A., Cox, D., Lin, S., Barretto, R., Habib, N., Hsu, P. D., Wu, X., Jiang, W., Marraffini, L. A., & Zhang, F. (2013). Multiplex genome engineering using CRISPR/Cas systems. *Science*, *339*(6121), 819-823. https://doi.org/10.1126/science.1231143

Davies, L. C., Jenkins, S. J., Allen, J. E., & Taylor, P. R. (2013). Tissue-resident macrophages. *Nat Immunol*, *14*(10), 986-995. https://doi.org/10.1038/ni.2705

Delves, P. J., & Roitt, I. M. (2000). The Immune System. *New England Journal of Medicine*, *343*(1), 37-49. https://doi.org/10.1056/nejm200007063430107

Deuitch, N. T., Yang, D., Lee, P. Y., Yu, X., Moura, N. S., Schnappauf, O., Ombrello, A. K., Stone, D., Kuehn, H. S., Rosenzweig, S. D., Hoffmann, P., Cudrici, C., Levy, D. M., Kessler, E., Soep, J. B., Hay, A. D., Dalrymple, A., Zhang, Y., Sun, L., . . . Zhou, Q. (2022). TNF inhibition in vasculitis management in adenosine deaminase 2 deficiency (DADA2). *J Allergy Clin Immunol*, *149*(5), 1812-1816 e1816. https://doi.org/10.1016/j.jaci.2021.10.030

Doudna, J. A., & Charpentier, E. (2014). Genome editing. The new frontier of genome engineering with CRISPR-Cas9. *Science*, *346*(6213), 1258096. https://doi.org/10.1126/science.1258096

Fayand, A., Chasset, F., Boutboul, D., Queyrel, V., Tieulie, N., Guichard, I., Dupin, N., Franck, N., Cohen, P., Bessis, D., Guenno, G. L., Kone-Paut, I., Belot, A., Bonhomme, A., Ducharme-Benard, S., Grateau, G., Sarrabay, G., Touitou, I., Boursier, G., & Georgin-Lavialle, S. (2021). DADA2 diagnosed in adulthood versus childhood: A comparative study on 306 patients including a systematic literature review and 12 French cases. *Semin Arthritis Rheum*, *51*(6), 1170-1179. https://doi.org/10.1016/j.semarthrit.2021.09.001

Footz, T. K., Brinkman-Mills, P., Banting, G. S., Maier, S. A., Riazi, M. A., Bridgland, L., Hu, S., Birren, B., Minoshima, S., Shimizu, N., Pan, H., Nguyen, T., Fang, F., Fu, Y., Ray, L., Wu, H., Shaull, S., Phan, S., Yao, Z., . . . McDermid, H. E. (2001). Analysis of the Cat Eye Syndrome Critical Region in Humans and the Region of Conserved Synteny in Mice: A Search for Candidate Genes at or near the Human Chromosome 22 Pericentromere. *Genome Research*, *11*(6), 1053-1070. https://doi.org/10.1101/gr.154901

Forrester, M. A., Wassall, H. J., Hall, L. S., Cao, H., Wilson, H. M., Barker, R. N., & Vickers, M. A. (2018). Similarities and differences in surface receptor expression by THP-1 monocytes and differentiated macrophages polarized using seven different conditioning regimens. *Cell Immunol*, *332*, 58-76. https://doi.org/10.1016/j.cellimm.2018.07.008

Gakis, C. (1996). Adenosine deaminase (ADA) isoenzymes ADA1 and ADA2: diagnostic and biological role. *Eur Respir J*, *9*(4), 632-633. https://doi.org/10.1183/09031936.96.09040632

Gao, Z. W., Yang, L., Liu, C., Wang, X., Guo, W. T., Zhang, H. Z., & Dong, K. (2022). Distinct Roles of Adenosine Deaminase Isoenzymes ADA1 and ADA2: A Pan-Cancer Analysis. *Front Immunol*, *13*, 903461. https://doi.org/10.3389/fimmu.2022.903461

Gehl, J. (2003). Electroporation: theory and methods, perspectives for drug delivery, gene therapy and research. *Acta Physiol Scand*, *177*(4), 437-447. https://doi.org/10.1046/j.1365-201X.2003.01093.x

Gharavi, A. T., Hanjani, N. A., Movahed, E., & Doroudian, M. (2022). The role of macrophage subtypes and exosomes in immunomodulation. *Cell Mol Biol Lett*, *27*(1), 83. https://doi.org/10.1186/s11658-022-00384-y

Gibas, Z., Becher, R., Kawinski, E., Horoszewicz, J., & Sandberg, A. A. (1984). A high-resolution study of chromosome changes in a human prostatic carcinoma cell line (LNCaP). *Cancer Genet Cytogenet*, *11*(4), 399-404. https://doi.org/10.1016/0165-4608(84)90020-7

Guilliams, M., Mildner, A., & Yona, S. (2018). Developmental and Functional Heterogeneity of Monocytes. *Immunity*, *49*(4), 595-613. https://doi.org/10.1016/j.immuni.2018.10.005

Hashem, H., Bucciol, G., Ozen, S., Unal, S., Bozkaya, I. O., Akarsu, N., Taskinen, M., Koskenvuo, M., Saarela, J., Dimitrova, D., Hickstein, D. D., Hsu, A. P., Holland, S. M., Krance, R., Sasa, G., Kumar, A. R., Muller, I., de Sousa, M. A., Delafontaine, S., . . . Meyts, I. (2021). Hematopoietic Cell Transplantation Cures Adenosine Deaminase 2 Deficiency: Report on 30 Patients. *J Clin Immunol*, *41*(7), 1633-1647. https://doi.org/10.1007/s10875-021-01098-0

Hasko, G., & Cronstein, B. N. (2004). Adenosine: an endogenous regulator of innate immunity. *Trends Immunol*, *25*(1), 33-39. https://doi.org/10.1016/j.it.2003.11.003

Hasko, G., Linden, J., Cronstein, B., & Pacher, P. (2008). Adenosine receptors: therapeutic aspects for inflammatory and immune diseases. *Nat Rev Drug Discov*, *7*(9), 759-770. https://doi.org/10.1038/nrd2638

Hettinger, J., Richards, D. M., Hansson, J., Barra, M. M., Joschko, A. C., Krijgsveld, J., & Feuerer, M. (2013). Origin of monocytes and macrophages in a committed progenitor. *Nat Immunol*, *14*(8), 821-830. https://doi.org/10.1038/ni.2638

Hille, F., & Charpentier, E. (2016). CRISPR-Cas: biology, mechanisms and relevance. *Philosophical Transactions of the Royal Society B-Biological Sciences*, *371*(1707). https://doi.org/ARTN2015049610.1098/rstb.2015.0496

Hippman, R. S., Snead, A. M., Petros, Z. A., Korkmaz-Vaisys, M. A., Patel, S., Sotelo, D., Dobria, A., Salkovski, M., Nguyen, T. T. A., Linares, R., Cologna, S. M., Gowrishankar, S., & Aldrich, L. N. (2023). Discovery of a Small-Molecule Modulator of the Autophagy-Lysosome Pathway That Targets Lamin A/C and LAMP1, Induces Autophagic Flux, and Affects Lysosome Positioning in Neurons. *Acs Chemical Neuroscience*, *14*(24), 4363-4382. https://doi.org/10.1021/acschemneuro.3c00573

Hoffman, W., Lakkis, F. G., & Chalasani, G. (2016). B Cells, Antibodies, and More. *Clin J Am Soc Nephrol*, *11*(1), 137-154. https://doi.org/10.2215/CJN.09430915

Hourani, T., Perez-Gonzalez, A., Khoshmanesh, K., Luwor, R., Achuthan, A. A., Baratchi, S., O'Brien-Simpson, N. M., & Al-Hourani, A. (2023). Label-free macrophage phenotype classification using machine learning methods. *Sci Rep*, *13*(1), 5202. https://doi.org/10.1038/s41598-023-32158-7

Hoy, S. M. (2024). Exagamglogene Autotemcel: First Approval. *Mol Diagn Ther*, *28*(2), 133-139. https://doi.org/10.1007/s40291-024-00696-z

Ishino, Y., Shinagawa, H., Makino, K., Amemura, M., & Nakata, A. (1987). Nucleotide sequence of the iap gene, responsible for alkaline phosphatase isozyme conversion in Escherichia coli, and identification of the gene product. *J Bacteriol*, *169*(12), 5429-5433. https://doi.org/10.1128/jb.169.12.5429-5433.1987

Italiani, P., & Boraschi, D. (2014). From Monocytes to M1/M2 Macrophages: Phenotypical vs. Functional Differentiation. *Front Immunol*, *5*, 514. https://doi.org/10.3389/fimmu.2014.00514

Jacobson, K. A., & Gao, Z. G. (2006). Adenosine receptors as therapeutic targets. *Nature Reviews Drug Discovery*, *5*(3), 247-264. https://doi.org/10.1038/nrd1983

Jafary, H., Larijani, B., Farrokhi, A., Pirouz, M., Mollamohammadi, S., & Baharvand, H. (2008). Differential effect of activin on mouse embryonic stem cell differentiation in insulin-secreting cells under nestin-positive selection and spontaneous differentiation protocols. *Cell Biology International*, *32*(2), 278-286. https://doi.org/10.1016/j.cellbi.2007.10.001

Jakubzick, C., Gautier, E. L., Gibbings, S. L., Sojka, D. K., Schlitzer, A., Johnson, T. E., Ivanov, S., Duan, Q., Bala, S., & Condon, T. (2013). Minimal differentiation of classical monocytes as they survey steady-state tissues and transport antigen to lymph nodes. *Immunity*, *39*(3), 599-610. https://doi.org/10.1016/j.immuni.2013.08.007.

Jee, H., Huang, Z., Baxter, S., Huang, Y., Taylor, M. L., Henderson, L. A., Rosenzweig, S., Sharma, A., Chambers, E. P., Hershfield, M. S., Zhou, Q., Dedeoglu, F., Aksentijevich, I., Nigrovic, P. A., O'Donnell-Luria, A., & Lee, P. Y. (2022). Comprehensive analysis of ADA2 genetic variants and estimation of carrier frequency driven by a function-based approach. *J Allergy Clin Immunol*, *149*(1), 379-387. https://doi.org/10.1016/j.jaci.2021.04.034

Jinek, M., Chylinski, K., Fonfara, I., Hauer, M., Doudna, J. A., & Charpentier, E. (2012). A programmable dual-RNA-guided DNA endonuclease in adaptive bacterial immunity. *Science*, *337*(6096), 816-821. https://doi.org/10.1126/science.1225829

Jinek, M., East, A., Cheng, A., Lin, S., Ma, E., & Doudna, J. (2013). RNA-programmed genome editing in human cells. *Elife*, *2*, e00471. https://doi.org/10.7554/eLife.00471

Kaljas, Y., Liu, C., Skaldin, M., Wu, C., Zhou, Q., Lu, Y., Aksentijevich, I., & Zavialov, A. V. (2017). Human adenosine deaminases ADA1 and ADA2 bind to different subsets of immune cells. *Cell Mol Life Sci*, *74*(3), 555-570. https://doi.org/10.1007/s00018-016-2357-0

Le Rhun, A., Escalera-Maurer, A., Bratovic, M., & Charpentier, E. (2019). CRISPR-Cas in Streptococcus pyogenes. *RNA Biol*, *16*(4), 380-389. https://doi.org/10.1080/15476286.2019.1582974

Lee, S. J., Yoon, B. R., Kim, H. Y., Yoo, S. J., Kang, S. W., & Lee, W. W. (2020). Activated Platelets Convert CD14(+)CD16(-) Into CD14(+)CD16(+) Monocytes With Enhanced FcgammaR-Mediated Phagocytosis and Skewed M2 Polarization. *Front Immunol*, *11*, 611133. https://doi.org/10.3389/fimmu.2020.611133

Liang, X., Potter, J., Kumar, S., Zou, Y., Quintanilla, R., Sridharan, M., Carte, J., Chen, W., Roark, N., Ranganathan, S., Ravinder, N., & Chesnut, J. D. (2015). Rapid and highly efficient mammalian cell engineering via Cas9 protein transfection. *J Biotechnol*, *208*, 44-53. https://doi.org/10.1016/j.jbiotec.2015.04.024

Lindsey, J. D. (2003). Culture of Retinal Neurons. *Ocular Neuroprotection*, 1. https://doi.org/10.1201/b14822

Lu, Y., Xue, J., Deng, T., Zhou, X., Yu, K., Deng, L., Huang, M., Yi, X., Liang, M., Wang, Y., Shen, H., Tong, R., Wang, W., Li, L., Song, J., Li, J., Su, X., Ding, Z., Gong, Y., . . . Mok, T. (2020). Safety and feasibility of CRISPR-edited T cells in patients with refractory non-small-cell lung cancer. *Nat Med*, *26*(5), 732-740. https://doi.org/10.1038/s41591-020-0840-5

Makarova, K. S., Grishin, N. V., Shabalina, S. A., Wolf, Y. I., & Koonin, E. V. (2006). A putative RNA-interference-based immune system in prokaryotes: computational analysis of the predicted enzymatic machinery, functional analogies with eukaryotic RNAi, and hypothetical mechanisms of action. *Biol Direct*, *1*, 7. https://doi.org/10.1186/1745-6150-1-7

Mali, P., Yang, L., Esvelt, K. M., Aach, J., Guell, M., DiCarlo, J. E., Norville, J. E., & Church, G. M. (2013). RNA-guided human genome engineering via Cas9. *Science*, *339*(6121), 823-826. https://doi.org/10.1126/science.1232033

Marshall, J. S., Warrington, R., Watson, W., & Kim, H. L. (2018). An introduction to immunology and immunopathology. *Allergy Asthma Clin Immunol*, *14*(Suppl 2), 49. https://doi.org/10.1186/s13223-018-0278-1

Martin, F. J., Amode, M. R., Aneja, A., Austine-Orimoloye, O., Azov, A. G., Barnes, I., Becker, A., Bennett, R., Berry, A., Bhai, J., Bhurji, S. K., Bignell, A., Boddu, S., Branco Lins, P. R., Brooks, L., Ramaraju, S. B., Charkhchi, M., Cockburn, A., Da Rin Fiorretto, L., . . . Flicek, P. (2023). Ensembl 2023. *Nucleic Acids Res*, *51*(D1), D933-D941. https://doi.org/10.1093/nar/gkac958

Martinet, W., Martinet, W., Schrijvers, D. M., & Kockx, M. M. (2003). Nucleofection as an efficient nonviral transfection method for humanmonocytic cells. *Biotechnology Letters*, *25*(13), 1025-1029. https://doi.org/10.1023/a:1024157508492

Martinez, F. O., Sica, A., Mantovani, A., & Locati, M. (2008). Macrophage activation and polarization. *Front Biosci*, *13*, 453-461. https://doi.org/10.2741/2692

McKinnon, K. M. (2018). Flow Cytometry: An Overview. *Curr Protoc Immunol*, *120*, 5 1 1-5 1 11. https://doi.org/10.1002/cpim.40

Meyts, I., & Aksentijevich, I. (2018). Deficiency of Adenosine Deaminase 2 (DADA2): Updates on the Phenotype, Genetics, Pathogenesis, and Treatment. *J Clin Immunol*, *38*(5), 569-578. https://doi.org/10.1007/s10875-018-0525-8

Mojica, F. J. M., Juez, G., & Rodriguezvalera, F. (1993). Transcription at Different Salinities of Haloferax-Mediterranei Sequences Adjacent to Partially Modified Psti Sites. *Molecular Microbiology*, *9*(3), 613-621. https://doi.org/DOI10.1111/j.1365-2958.1993.tb01721.x

Mojica, F. J. M., & Montoliu, L. (2016). On the Origin of CRISPR-Cas Technology: From Prokaryotes to Mammals. *Trends Microbiol*, *24*(10), 811-820. https://doi.org/10.1016/j.tim.2016.06.005

Maasho, K., Marusina, A., Reynolds, N. M., Coligan, J. E., & Borrego, F. (2004). Efficient gene transfer into the human natural killer cell line, NKL, using the Amaxa nucleofection system™. *Journal of Immunological Methods*, *284*(1-2), 133-140. https://doi.org/10.1016/j.jim.2003.10.010

Nanthapisal, S., Murphy, C., Omoyinmi, E., Hong, Y., Standing, A., Berg, S., Ekelund, M., Jolles, S., Harper, L., Youngstein, T., Gilmour, K., Klein, N. J., Eleftheriou, D., & Brogan, P. A. (2016). Deficiency of Adenosine Deaminase Type 2: A Description of Phenotype and Genotype in Fifteen Cases. *Arthritis Rheumatol*, *68*(9), 2314-2322. https://doi.org/10.1002/art.39699

Navon Elkan, P., Pierce, S. B., Segel, R., Walsh, T., Barash, J., Padeh, S., Zlotogorski, A., Berkun, Y., Press, J. J., Mukamel, M., Voth, I., Hashkes, P. J., Harel, L., Hoffer, V., Ling, E., Yalcinkaya, F., Kasapcopur, O., Lee, M. K., Klevit, R. E., . . . Levy-Lahad, E. (2014). Mutant adenosine deaminase 2 in a polyarteritis nodosa vasculopathy. *N Engl J Med*, *370*(10), 921-931. https://doi.org/10.1056/NEJMoa1307362

Nicol, F., Wong, M., MacLaughlin, F. C., Perrard, J., Wilson, E., Nordstrom, J. L., & Smith, L. C. (2002). Poly-L-glutamate, an anionic polymer, enhances transgene expression for plasmids delivered by intramuscular injection with in vivo electroporation. *Gene Ther*, *9*(20), 1351-1358. https://doi.org/10.1038/sj.gt.3301806

Orekhov, A. N., Orekhova, V. A., Nikiforov, N. G., Myasoedova, V. A., Grechko, A. V., Romanenko, E. B., Zhang, D., & Chistiakov, D. A. (2019). Monocyte differentiation and macrophage polarization. *Vessel Plus*, *2019*. https://doi.org/10.20517/2574-1209.2019.04

Parkin, J., & Cohen, B. (2001). An overview of the immune system. *Lancet*, *357*(9270), 1777-1789. https://doi.org/10.1016/S0140-6736(00)04904-7

Passlick, B., Flieger, D., & Ziegler-Heitbrock, H. W. (1989). Identification and characterization of a novel monocyte subpopulation in human peripheral blood. *Blood*, *74*(7), 2527-2534. https://www.ncbi.nlm.nih.gov/pubmed/2478233

Picard, C., Al-Herz, W., Bousfiha, A., Casanova, J. L., Chatila, T., Conley, M. E., Cunningham-Rundles, C., Etzioni, A., Holland, S. M., Klein, C., Nonoyama, S., Ochs, H. D., Oksenhendler, E., Puck, J. M., Sullivan, K. E., Tang, M. L., Franco, J. L., & Gaspar, H. B. (2015). Primary Immunodeficiency Diseases: an Update on the Classification from the International Union of Immunological Societies Expert Committee for Primary Immunodeficiency 2015. *J Clin Immunol*, *35*(8), 696-726. https://doi.org/10.1007/s10875-015-0201-1

Potter, H. (1988). Electroporation in biology: methods, applications, and instrumentation. *Anal Biochem*, *174*(2), 361-373. https://doi.org/10.1016/0003-2697(88)90035-8

Qin, Z. (2012). The use of THP-1 cells as a model for mimicking the function and regulation of monocytes and macrophages in the vasculature. *Atherosclerosis*, *221*(1), 2-11. https://doi.org/10.1016/j.atherosclerosis.2011.09.003

Raza, Y., Salman, H., & Luberto, C. (2021). Sphingolipids in Hematopoiesis: Exploring Their Role in Lineage Commitment. *Cells*, *10*(10). https://doi.org/ARTN 250710.3390/cells10102507

Rezaei, N., Aghamohammadi, A., & Notarangelo, D. (2017). *Primary Immunodeficiency Diseases*. Springer Berlin Heidelberg. https://doi.org/10.1007/978-3-662-52909-6

Richards, D. M., & Endres, R. G. (2014). The Mechanism of Phagocytosis: Two Stages of Engulfment. *Biophysical Journal*, *107*(7), 1542-1553. https://doi.org/10.1016/j.bpj.2014.07.070

Sahin, S., Adrovic, A., & Kasapcopur, O. (2020). A monogenic autoinflammatory disease with fatal vasculitis: deficiency of adenosine deaminase 2. *Curr Opin Rheumatol*, *32*(1), 3-14. https://doi.org/10.1097/BOR.0000000000000669

Sanger, F., & Coulson, A. R. (1975). A rapid method for determining sequences in DNA by primed synthesis with DNA polymerase. *J Mol Biol*, *94*(3), 441-448. https://doi.org/10.1016/0022-2836(75)90213-2

Savina, A., & Amigorena, S. (2007). Phagocytosis and antigen presentation in dendritic cells. *Immunological Reviews*, *219*, 143-156. https://doi.org/DOI 10.1111/j.1600-065X.2007.00552.x

Shaikh, R. A., Zhong, J. H., Lyu, M. J., Lin, S., Keskin, D., Zhang, G. L., Chitkushev, L., & Brusic, V. (2019). Classification of Five Cell Types from PBMC Samples using Single Cell Transcriptomics and Artificial Neural Networks. *2019 Ieee International Conference on Bioinformatics and Biomedicine (Bibm)*, 2207-2213. https://doi.org/10.1109/BIBM47256.2019.8983387

Shi, C., & Pamer, E. G. (2011). Monocyte recruitment during infection and inflammation. *Nature Reviews Immunology*, *11*(11), 762-774. https://doi.org/10.1038/nri3070

Skinner, B. M., & Johnson, E. E. (2017). Nuclear morphologies: their diversity and functional relevance. *Chromosoma*, *126*(2), 195-212. https://doi.org/10.1007/s00412-016-0614-5

Stone, K. D., Prussin, C., & Metcalfe, D. D. (2010). IgE, mast cells, basophils, and eosinophils. *J Allergy Clin Immunol*, *125*(2 Suppl 2), S73-80. https://doi.org/10.1016/j.jaci.2009.11.017

Staal, F. J. T., Aiuti, A., & Cavazzana, M. (2019). Autologous Stem-Cell-Based Gene Therapy for Inherited Disorders: State of the Art and Perspectives. *Front Pediatr*, *7*, 443. https://doi.org/10.3389/fped.2019.00443

THP-1. (2024). Knowledge Center from Lonza Bioscience. https://knowledge.lonza.com/cell?id=134

Tsuchiya, S., Yamabe, M., Yamaguchi, Y., Kobayashi, Y., Konno, T., & Tada, K. (1980). Establishment and characterization of a human acute monocytic leukemia cell line (THP-1). *Int J Cancer*, *26*(2), 171-176. https://doi.org/10.1002/ijc.2910260208

Turvey, S. E., & Broide, D. H. (2010). Innate immunity. *Journal of Allergy and Clinical Immunology*, *125*(2), S24-S32. https://doi.org/10.1016/j.jaci.2009.07.016

Uhlen, M., Fagerberg, L., Hallstrom, B. M., Lindskog, C., Oksvold, P., Mardinoglu, A., Sivertsson, A., Kampf, C., Sjostedt, E., Asplund, A., Olsson, I., Edlund, K., Lundberg, E., Navani, S., Szigyarto, C. A., Odeberg, J., Djureinovic, D., Takanen, J. O., Hober, S., . . . Ponten, F. (2015). Proteomics. Tissue-based map of the human proteome. *Science*, *347*(6220), 1260419. https://doi.org/10.1126/science.1260419

Van Eyck, L., Hershfield, M. S., Pombal, D., Kelly, S. J., Ganson, N. J., Moens, L., Frans, G., Schaballie, H., De Hertogh, G., Dooley, J., Bossuyt, X., Wouters, C., Liston, A., & Meyts, I. (2015). Hematopoietic stem cell transplantation rescues the immunologic phenotype and prevents vasculopathy in patients with adenosine deaminase 2 deficiency. *Journal of Allergy and Clinical Immunology*, *135*(1), 283-+. https://doi.org/10.1016/j.jaci.2014.10.010

van Montfrans, J., Zavialov, A., & Zhou, Q. (2014). Mutant ADA2 in vasculopathies. *N Engl J Med*, *371*(5), 478. https://doi.org/10.1056/NEJMc1405506

van Montfrans, J. M., Hartman, E. A. R., Braun, K. P. J., Hennekam, E. A. M., Hak, E. A., Nederkoorn, P. J., Westendorp, W. F., Bredius, R. G. M., Kollen, W. J. W., Schölvinck, E. H., Legger, G. E., Meyts, I., Liston, A., Lichtenbelt, K. D., Giltay, J. C., Van Haaften, G., De Vries Simons, G. M., Leavis, H., Sanders, C. J. G., . . . Van Gijn, M. E. (2016). Phenotypic variability in patients with ADA2 deficiency due to identical homozygous R169Q mutations. *Rheumatology*, *55*(5), 902-910. https://doi.org/10.1093/rheumatology/kev439

van Steenbrugge, G. J., van Uffelen, C. J., Bolt, J., & Schroder, F. H. (1991). The human prostatic cancer cell line LNCaP and its derived sublines: an in vitro model for the study of androgen sensitivity. *J Steroid Biochem Mol Biol*, *40*(1-3), 207-214. https://doi.org/10.1016/0960-0760(91)90184-7

Verhoeckx, K., Cotter, P., López-Expósito, I., Kleiveland, C., Lea, T., Mackie, A., Requena, T., Swiatecka, D., & Wichers, H. (2015). *The Impact of Food Bioactives on Health*. Springer International Publishing. https://doi.org/10.1007/978-3-319-16104-4

Wang, W., Yu, Z., Gou, L., Zhong, L., Li, J., Ma, M., Wang, C., Zhou, Y., Ru, Y., Sun, Z., Wei, Q., Dong, Y., & Song, H. (2020). Single-Center Overview of Pediatric Monogenic Autoinflammatory Diseases in the Past Decade: A Summary and Beyond. *Front Immunol*, *11*, 565099. https://doi.org/10.3389/fimmu.2020.565099

Whitelaw, D. M. (1972). Observations on human monocyte kinetics after pulse labeling. *Cell Tissue Kinet*, *5*(4), 311-317. https://doi.org/10.1111/j.1365-2184.1972.tb00369.x

Wu, Z., Zhang, Z., Lei, Z., & Lei, P. (2019). CD14: Biology and role in the pathogenesis of disease. *Cytokine Growth Factor Rev*, *48*, 24-31. https://doi.org/10.1016/j.cytogfr.2019.06.003

Yamauchi, T., & Moroishi, T. (2019). Hippo Pathway in Mammalian Adaptive Immune System. *Cells*, *8*(5). https://doi.org/10.3390/cells8050398

Yona, S., & Jung, S. (2010). Monocytes: subsets, origins, fates and functions. *Curr Opin Hematol*, *17*(1), 53-59. https://doi.org/10.1097/MOH.0b013e3283324f80

Zavialov, A. V., & Engstrom, A. (2005). Human ADA2 belongs to a new family of growth factors with adenosine deaminase activity. *Biochem J*, *391*(Pt 1), 51-57. https://doi.org/10.1042/BJ20050683

Zavialov, A. V., Yu, X., Spillmann, D., Lauvau, G., & Zavialov, A. V. (2010). Structural basis for the growth factor activity of human adenosine deaminase ADA2. *J Biol Chem*, *285*(16), 12367-12377. https://doi.org/10.1074/jbc.M109.083527

Zhou, Q., Yang, D., Ombrello, A. K., Zavialov, A. V., Toro, C., Zavialov, A. V., Stone, D. L., Chae, J. J., Rosenzweig, S. D., Bishop, K., Barron, K. S., Kuehn, H. S., Hoffmann, P., Negro, A., Tsai, W. L., Cowen, E. W., Pei, W., Milner, J. D., Silvin, C., . . . Aksentijevich, I. (2014). Early-onset stroke and vasculopathy associated with mutations in ADA2. *N Engl J Med*, *370*(10), 911-920. https://doi.org/10.1056/NEJMoa1307361

9 Appendix

9.1 Appendix A

Appendix A contains information about the software, kits, materials, equipment, disposables, and instruments used in this thesis. In addition, it included details about the gRNAs, antibodies, and composition of the "homemade" electroporation buffer.

Table A1. Software and web applications. The employed software and online tools are listed with the corresponding supplier.

Software and web applications	Supplier
BioRender	Science Suite
CFX Maestro	Bio-Rad
EndMemo	EndMemo
GeneTools	Certus Technology & EMQN
gnomAD v4.1.0	Broad Institute
GraphPad Prism 10.2.2	GraphPad
GXCapture	GT Vision
NCBI Primer BLAST	NCBI
Sequencher	Gene Codes Corporation
SnapGene® 5.3.2	GSL Biotech

Abbreviations: BLAST, Basic local alignment search tool; EMQN, European Molecular Genetics Quality Network; NCBI, National Center for Biotechnology Information.

Table A2. List of kits. The kits used in this study are listed, including manufacturer and cat. number.

Kits	Manufacturer	Cat. number
AllPrep DNA/RNA Mini Kit	Qiagen	80204
ExoSAP-IT™ *Express* PCR Product Cleanup Reagent	Applied Biosystems	75001.1.ML
iScript™ Advanced cDNA Synthesis Kit	Bio-Rad	1725038
Monarch® DNA Gel Extraction Kit	New England Biolabs	T1020S
Phusion™ Plus PCR Master Mix	Thermo Scientific	F631S
Pierce™ BCA Protein Assay Kit	Thermo Scientific	23227
PowerTrack™ SYBR Green Master Mix for qPCR	Applied Biosystems	A46110
QIAshredder	Qiagen	79656
Qubit™ dsDNA Quantification, High Sensitivity, Assay Kits	Invitrogen	Q32854
RNase-Free DNase I Kit	Norgen Biotek	25720
RNase-Free DNase Set	Qiagen	79254
SG Cell Line 4D-Nucleofector™ X Kit L	Lonza	V4XC-3024
SG Cell Line 4D-Nucleofector™ X Kit S	Lonza	V4XC-3032
Total RNA Purification Kit	Norgen Biotek	17250
Trans-Blot Turbo Mini 0.45 µm LF PVDF Transfer Kit	Bio-Rad	1704274
ZipRuler Express DNA Ladder Set, ready-to-use	Thermo Scientific	SM1373

Abbreviations: BCA, bicinchoninic acid; cat, catalog; cDNA, complementary DNA; DNA, deoxyribonucleic acid; DNase, deoxyribonuclease; dsDNA, double stranded DNA; LF, Low fluorescence; PCR, polymerase chain reaction; PVDF, polyvinylidene difluoride; qPCR, quantitative PCR; RNA, ribonucleic acid; RNase, ribonuclease.

Table A3. List of materials. The materials utilized throughout the study are listed with the corresponding manufacturer and cat. number.

Chemicals	Manufacturer	Cat. number
Absolutt alkohol prima 99,9% 1 liter	Antibac	600068
Accutase - Enzyme Cell Detachment Medium	Thermo Scientific	00-4555-56
Blotting Grade Blocker Nonfat Dry Milk	Bio-Rad	1706404
Cas9 protein (construct ID: psfCAS9TH24-c023)	Karolinska Institutet	N/A
Dimethyl Sulfoxide	Merck	276855
Nuclease-Free Duplex Buffer	Integrated DNA Technologies	11-01-03-01
eBioscience™ Fixable Viability Dye eFluor™ 520	Invitrogen	65-0867-14
UltraPure™ 0.5M EDTA, pH 8.0	Invitrogen	15575020
Fetal Bovine Serum, qualified, heat inactivated, United States	Gibco	16140071
Halt™ Protease Inhibitor Cocktail (100X)	Thermo Scientific	78430
"Homemade" electroporation buffer	NCMM	N/A
Human IFN-gamma Recombinant Protein, PeproTech®	Gibco	300-02
Human IL-4 Recombinant Protein, PeproTech®	Gibco	200-04
ImmunoCult™-SF Macrophage Medium	StemCell Technologies	10961

2x Laemmli Sample Buffer	Bio-Rad	1610737
eBioscience™ Lipopolysaccharide (LPS) Solution (500X)	Invitrogen	00-4976-93
MEM Non-Essential Amino Acids Solution (100X)	Gibco	11140050
2-Mercaptoethanol	Bio-Rad	1610710
2-Mercaptoethanol	Thermo Scientific	21985023
Methanol	Merck	34860
4–20% Mini-PROTEAN® TGX™ Precast Protein Gels	Bio-Rad	4561093
Milli Q water	NCMM	N/A
No-Stain™ Protein Labeling Reagent	Invitrogen	A44449
Nuclease-Free Water (not DEPC-Treated)	Invitrogen	AM9937
Opti-MEM Reduced Serum Medium	Gibco	31985062
Orange DNA Loading Dye (6X)	Thermo Scientific	00-4976-93
Phosphate Buffered Saline	NCMM	N/A
Penicillin-Streptomycin (10,000 U/mL)	Gibco	15140122
Phorbol-12-Myristate-13-Acetate	Merck	P1585
Poly-L-Ornithine Solution	Merck	P4957
Precision Plus Protein™ All Blue Prestained Protein Standards	Bio-Rad	1610373
RIPA Lysis and Extraction Buffer	Thermo Scientific	89901
RNase AWAY™ Surface Decontaminant	Thermo Scientific	7002PK
RPMI 1640 Medium (ATCC modification)	Gibco	A1049101
10X SDS-electrophoresis buffer	NCMM	N/A
SuperSignal™ West Dura Extended Duration Substrate	Thermo Scientific	34075
SYBR™ Safe DNA Gel Stain	Invitrogen	S33102
THP-1	ATCC	TIB-202
Trans-Blot Turbo 5x Transfer Buffer	Bio-Rad	10026938
Tris Buffered Saline with Tween 20 pH 7.6	Medicago	09-7510-100
Trypan Blue Stain (0.4%)	Invitrogen	T10282
TWEEN® 20	Merck	P1379
UltraPure™ Agarose	Invitrogen	16500500

Abbreviations: ATCC, American type culture collection; Cas9, CRISPR-associated protein 9; cat, catalog; CRISPR, clustered regulatory interspaced short palindromic repeats; DEPC, diethyl pyrocarbonate; DNA, deoxyribonucleic acid; EDTA, ethylenediamine tetraacetic acid; IFN, interferon; IL, interleukin; MEM, minimum essential medium; N/A, non applicable; NCMM, Centre for Molecular Medicine Norway; RIPA, radio-immunoprecipitation assay; RNase, ribonuclease; RPMI, Roswell Park Memorial Institute; SDS, sodium dodecyl sulfate; SF, serum-free.

Table A4. List of common equipment and disposables. Routine equipment and disposables utilized are listed with the corresponding manufacturer and cat. number.

Products	Manufacturer	Cat. number
Armadillo PCR plate, 96-well, orange, clear well	Thermo Scientific	AB2396O
Axyspin Mini Plate Spinner Centrifuge	Axygen	PLATESPINNER-230EU
Basic BA110 Analytical Balance	Sartorius	N/A
10 mL BD Luer-Lok™ Syringe only	BD	302995
BD Microlance™ 3 Needles Green	BD	301156
CoolCell® LX, Cell Freezing Container	Corning	432002
Countess™ Cell Counting Chamber Slides	Invitrogen	C10312
CryoPure tubes, 2 ml, QuickSeal screw cap, white	Sarstedt	72.379
Digital Dry Baths/Block Heaters	Thermo Scientific	88870005
DURAN® Original 45 Laboratory Bottle	DWK Life Sciences	218013651
Gel Releasers	Bio-Rad	1653320
LSE™ Mini Microcentrifuge, AC100-240V	Corning	6770
50 mL High Clarity PP Centrifuge Tube, Conical Bottom, Sterile	Falcon	352070
15 mL High Clarity PP Centrifuge Tube, Conical Bottom, Sterile	Falcon	352096
Nunc Non-treated T25 EasYFlask, Filter Cap	Thermo Scientific	169900
Nunc Non-treated T75 EasyFlask, Filter Cap	Thermo Scientific	156800
Nunc Non-treated T175 EasYFlask, Filter Cap	Thermo Scientific	159926
Nunc™ Non-Treated 6-well dish	Thermo Scientific	150239
Nunc™ Non-Treated 12-well dish	Thermo Scientific	150200
PCR plate full skirt, 96 well, white, Low Profile, 100 µl,	Sarstedt	72.1980.010
PCR strip of 8, 200 µl	Sarstedt	72.985.002
Picus® 2 Electronic 12-Channel Pipette	Sartorius	LH-747441
Picus® 2 Electronic Single Channel Pipette	Sartorius	LH-747021
qPCR film, free from DNase/RNase, material: PO, highly transparent	Sarstedt	95.1999
Qubit™ Assay Tubes	Invitrogen	Q32856
SafeSeal reaction tube, 1.5 ml	Sarstedt	72.706.400
Safetyspace® Filtered Pipette Tips 10	Sartorius	790011F
Safetyspace® Filtered Pipette Tips 120	Sartorius	790101F
Safetyspace® Filtered Pipette Tips 200	Sartorius	790201F
Safetyspace® Filtered Pipette Tips 1000	Sartorius	791001F
Serological pipette, with tip, plugged, 5 ml, sterile	Sarstedt	86.1253.001
Serological pipette, with tip, plugged, 10 ml, sterile	Sarstedt	86.1254.001
Serological pipette, with tip, plugged, 25 ml, sterile	Sarstedt	86.1685.001
Serological pipette, with tip, plugged, 50 ml, sterile	Sarstedt	86.1256.001

S1 Pipet Filler	Thermo Scientific	9501
Sterile Cell Strainers	Thermo Scientific	11587522
Stuart™ See-Saw Rocker SSL4	Cole-Parmer	51900-32
SUB Aqua 26 Plus	Grant	N/A
Tacta® Mechanical Pipette, 12 Channel	Sartorius	LH-729220
Tacta® Mechanical Pipette, Single Channel, 0.5-10	Sartorius	LH-729020
Tacta® Mechanical Pipette, Single Channel, 10-100	Sartorius	LH-729050
Tacta® Mechanical Pipette, Single Channel, 20-200	Sartorius	LH-729060
Tacta® Mechanical Pipette, Single Channel, 100-1000	Sartorius	LH-729070
VACUSAFE Aspiration System	Integra Biosciences	158300
96-well Clear Flat Bottom Polystyrene TC-treated Microplate	Corning	3595
24-well Clear Flat Bottom TC-treated Multiwell Cell Culture Plate	Falcon	353047
96-well Clear Round Bottom Not Treated Microplate	Falcon	351177
96-well Microplate Aluminum Sealing Tape, Nonsterile	Corning	6570
96-well Plate, Non-Treated Surface	Thermo Scientific	266120
Vortex genie 2	Scientific Industries	SI-0236

Abbreviations: cat, catalog; DNase, deoxyribonuclease; N/A, non applicable; PCR, polymerase chain reaction; PO, polyolefin; PP, polypropylene; qPCR, quantitative PCR; RNase, ribonuclease; TC, tissue culture.

Table A5. List of instruments. Utilized instruments are listed with the corresponding manufacturer and cat. number.

Instruments	Manufacturer	Cat. number
Autoflow Infrared direct heat CO2 Incubator	Nuaire	N/A
Axiovert 40 CFL Microscopy	ZEISS	Z-AXIO40C
Centrifuge 5910 R	Eppendorf	5943000516
CFX Opus 96 Real-Time PCR System	Bio-Rad	17007992
ChemiDoc™ Imaging System	Bio-Rad	12003153
GXCAM	GT Vision	N/A
Countess™ 2 Automated Cell Counter	Invitrogen	N/A
4D-Nucleofector® Core Unit	Lonza	AAF-1003B
4D-Nucleofector® X Unit	Lonza	AAF-1003X
Infinite® M Nano, single-mode microplate reader, monochromator optics	Tecan	30190086
Live-Cell Imaging and Analysis System: Incucyte® S3	Sartorius	4647
Mini-PROTEAN® Tetra Vertical Electrophoresis Cell	Bio-Rad	1658004
NanoDrop™ 2000 Spectrophotometer	Thermo Scientific	ND-2000
Nuaire NU-437-400E Biological Safety Cabinet	Nuaire	N/A
PowerPac™ High-Current Power Supply	Bio-Rad	1645052
Qubit™ 4 Fluorometer	Invitrogen	Q33226
SH800S Cell Sorter	Sony	N/A
Trans-Blot® Turbo™ Transfer System	Bio-Rad	1704150
T100 Thermal Cycler	Bio-Rad	1861096
Micro Star 21/21R Microcentrifuges, Ventilated/Refrigerated	VWR	521-2656
Wide Mini-Sub Cell Horizontal Electrophoresis System	Bio-Rad	1704469

Abbreviations: cat, catalog; N/A, non applicable; PCR, polymerase chain reaction.

Table A6. List of gRNAs. The LC1 and RC2 gRNAs utilized to edit *ADA2* in THP-1 cells. The guides were gifted by Judith Staerk.

Gene	gRNA ID	Sequence (5´ ➡ 3´)	Reference
ADA2	LC1	GAGAGCACCATGACGAAGAG	Judith Staerk
ADA2	RC2	TATTGCTGAAAAGCTCGGGT	Judith Staerk

Abbreviations: ADA2, adenosine deaminase 2; gRNA, guide RNA; RNA, ribonucleic acid.

Table A7. Primary and secondary antibodies used for immunoblotting. The primary antibodies used to assess the ADA2 protein level in *ADA2*-edited THP-1 cells. The Anti-rabbit IgG secondary antibody was used together with the polyclonal antibodies, and the Anti-mouse IgG antibody with the monoclonal antibody.

Antibody name	Antibody type	Specification	Species reactivity	Host	Dilution	Manufacturer	Cat. number
ADA2 TH	Primary	Polyclonal	Human	Rabbit	1:1000	Invitrogen	PA5-43014
ADA2 AN	Primary	Polyclonal	Human	Rabbit	1:500	Abnova	H00051816-W01P
ADA2 LB	Primary	Monoclonal	Human	Mouse	1:1000	Lifespan Biosciences	LS-B11847-50
Anti-rabbit IgG	Secondary	HRP-linked	Rabbit	Goat	1:5000	Cell Signaling Technology	7074
Anti-mouse IgG	Secondary	HRP-linked	Mouse	Horse	1:3000	Cell Signaling Technology	7076

Abbreviations: ADA2, adenosine deaminase 2; cat, catalog; IgG, immunoglobulin G.

Table A8. "Homemade" buffer recipe. The chemicals used to create the "homemade" electroporation buffer and their final concentrations.

Chemical	Final concentration
KCl	5 mM
$MgCl_2$ x $6H_2O$	15 mM
Na_2HPO_4 x $7H_2O$	80 mM
NaH_2PO_4 x $2H_2O$	40 mM
D-mannitol	50 mM

9.2 Appendix B

Appendix B consist of the primers and PCR cycling parameters utilized.

Table A9. PCR primers targeting *ADA2*. The PCR and sequencing primers used to assess *ADA2*-edited cells on the genomic level.

Gene	Sequence (5´ ➡ 3´)	Orientation	Reference
ADA2	GGCGTCTCTCACTGCTCACCTGAC	FWD	Judith Staerk
ADA2	CAGGCAGAGCTACTAGGCTGGG	REV	Judith Staerk

Abbreviations: ADA2, adenosine deaminase 2; FWD, forward; PCR, polymerase chain reaction; REV, reverse.

Table A10. Tested qPCR primers. All the tested qPCR primers and corresponding information, including target gene and sequence. The primers used in this study are highlighted grey.

Gene	Reference	ID	Orientation	Sequence (5´ ➡ 3´)
ADA2	Sanne Iversen Lurås	Primer pair 1	FWD	GTGGAGAGCACCATGACGAA
			REV	GCTCCGAATCAAGTTCCCCA
ADA2	Sanne Iversen Lurås	Primer pair 2	FWD	CCGGTGTATGAGCTCAGTGG
			REV	AAGATGTGGCTGTCATCGCA
ADA2	Sanne Iversen Lurås	Primer pair 3	FWD	AGCACCATGACGAAGAGTGG
			REV	CACGGTGGTGGCAGGGTTTG
ADA2	Yasaman Pakdaman	Primer pair 4	FWD	GGTGCTGAAACTGGTGTCTG
			REV	CAAACAGCTGGCCATGAACT
ADA2	Yasaman Pakdaman	Exon 4-5	FWD	CGCACCAGTGTTCAGAGACT
			REV	GTGGAGAGCACCATGACGAA
RNA18SN1	Yasaman Pakdaman	Primer pair 1	FWD	CTCAACACGGGAAACCTCAC
			REV	CGTTCTTAGTTGGTGGAGCG
ALOX15	Sanne Iversen Lurås	Primer pair 1	FWD	GCCTAAGGCTGTGCTGAAGA
			REV	CACTGTTTTCCACCACGCTG
ALOX15	Sanne Iversen Lurås	Primer pair 2	FWD	TGTGAAAGACGACCCAGAGC
			REV	GCACCCAAGAGTACCAGTCC
IL10	Sanne Iversen Lurås	Primer pair 1	FWD	GCAACCTGCCTAACATGCTTC
			REV	GGTTCTCAGCTTGGGGCAT
IL10	Sanne Iversen Lurås	Primer pair 2	FWD	CCTGCCTAACATGCTTCGAG
			REV	GGTTCTCAGCTTGGGGCATC
MRC1	Sanne Iversen Lurås	Primer pair 1	FWD	CCAAACGCCTTCATTTGCCA
			REV	ACCTTCCTTGCACCCTGATG

MRC1	Sanne Iversen Lurås	Primer pair 2	FWD	ACTCCACTTTCAGTGCCTGG
			REV	TCCATCCGTCCAAAGGAACG
CXCL9	Sanne Iversen Lurås	Primer pair 1	FWD	AGAAAGGGTCGCTGTTCCTG
			REV	TTTCTCGCAGGAAGGGCTTG
CXCL9	Sanne Iversen Lurås	Primer pair 2	FWD	GAGAAAGGGTCGCTGTTCCT
			REV	TTCTCGCAGGAAGGGCTTG
CXCL10	Sanne Iversen Lurås	Primer pair 1	FWD	TCCTGCAAGCCAATTTTGTCC
			REV	TTGATGGCCTTCGATTCTGG
CXCL10	Sanne Iversen Lurås	Primer pair 2	FWD	CCTGCAAGCCAATTTTGTCCA
			REV	AGACCTTTCCTTGCTAACTGCT
TNF-α	Sanne Iversen Lurås	Primer pair 1	FWD	ATCAGAGGGCCTGTACCTCA
			REV	GAGGTTGACCTTGGTCTGGT
TNF-α	Sanne Iversen Lurås	Primer pair 2	FWD	TGGCGTGGAGCTGAGAGATA
			REV	CTTGGTCTGGTAGGAGACGG
RPL37A	Sanne Iversen Lurås	Primer pair 1	FWD	AAGAGACGAGCTGTGGGGAT
			REV	TTACCGTGACAGCGGAAGTG
RPL37A	Sanne Iversen Lurås	Primer pair 2	FWD	TCGTCGGTAAATACGGGACC
			REV	CCCACAGCTCGTCTCTTCAT

Abbreviations: ADA2, adenosine deaminase 2; ALOX15, arachidonate 15-lipoxygenase; CXCL9, CXC motif chemokine ligand 9; CXCL10, CXC motif chemokine ligand 10; FWD, forward; IL10, interleukin-10; MRC1, mannose receptor C-type 1; PCR, polymerase chain reaction; qPCR, quantitative PCR; REV, reverse; RPL37A, ribosomal protein L37a; RNA, ribonucleic acid; RNA18SN1, RNA 18S ribosomal N1; TNF, tumor necrosis factor.

Table A11. PCR parameters for amplifying gDNA. The thermal cycler settings used to amplify target DNA. The Phusion Plus PCR Master Mix provided the 3-step protocol.

Cycle step	**Temperature**	**Duration**	**Cycles**
Initial Denaturation	98°C	30 s	1
Denaturation	98°C	10 s	35
Annealing	66°C	10 s	
Extension	72°C	20 s	
Final extension	72°C	5 min	1
	4°C	Infinity	Infinity

Abbreviations: DNA, deoxyribonucleic acid; gDNA, genomic DNA; PCR, polymerase chain reaction.

Table A12. RT-PCR parameters for cDNA synthesis. The settings used to synthesize cDNA from extracted RNA. The parameters were provided by iScript Advanced cDNA Synthesis Kit for RT-PCR.

Cycle step	Temperature	Duration	Cycles
Revers transcription	42°C	30 min	1
Revers transcription inactivation	95°C	1 min	1
	4°C	Infinity	Infinity

Abbreviations: cDNA, complementary DNA; DNA, deoxyribonucleic acid; PCR, polymerase chain reaction; RNA, ribonucleic acid; RT-PCR, real-time PCR.

Table A13. qPCR settings. The 3-step qPCR program provided by the PowerTrack SYBR Green Master Mix was followed to assess the mRNA level of various genes.

Cycle step	Temperature	Duration	Cycles
Enzyme activation	95°C	2 min	1
Denaturation	95°C	5 s	40
Annealing/extension	60°C	30 s	
Dissociation step	95°C	15 s	1
	60°C	1 min	
	95°C	15 s	

Abbreviations: mRNA, messenger RNA; PCR, polymerase chain reaction; qPCR, quantitative PCR; RNA, ribonucleic acid.

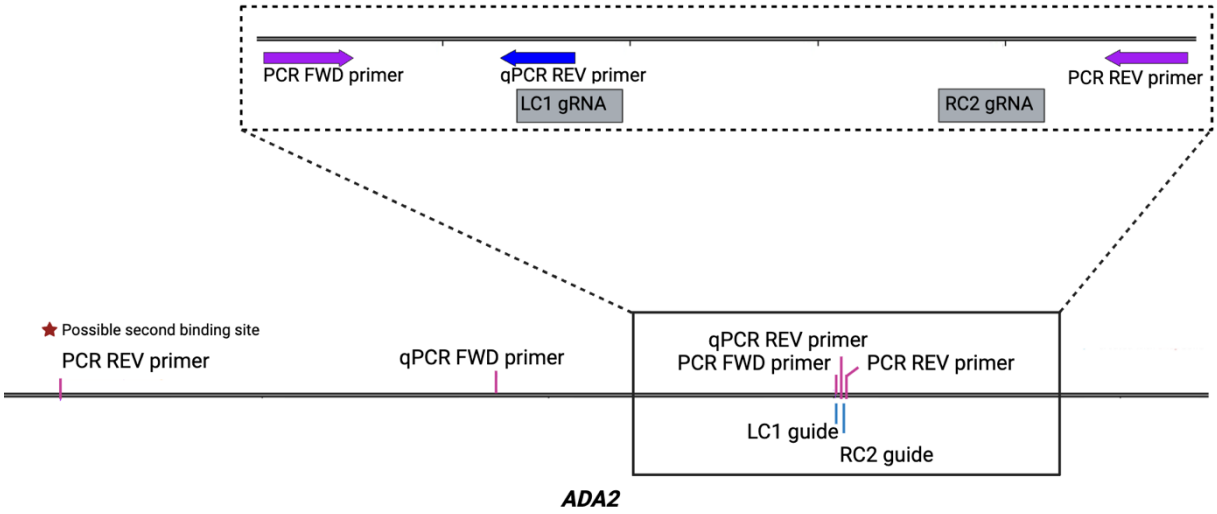

Figure A1. The localizations of the primer pairs and gRNAs in *ADA2*. The localization of the PCR "LC1-RC2" primer pair, qPCR "exon 4-5" primer pair, LC1 gRNA, and RC2 gRNA in the genomic sequence of *ADA2*. Abbreviations: ADA2, adenosine deaminase 2; gRNA, guide RNA; PCR, polymerase chain reaction; qPCR, quantitative PCR; RNA, ribonucleic acid. The figure was created with BioRender.com.

9.3 Appendix C

Appendix C contains supplementary data obtained from the sorted *ADA2* CRISPR/Cas9-edited THP-1 cells.

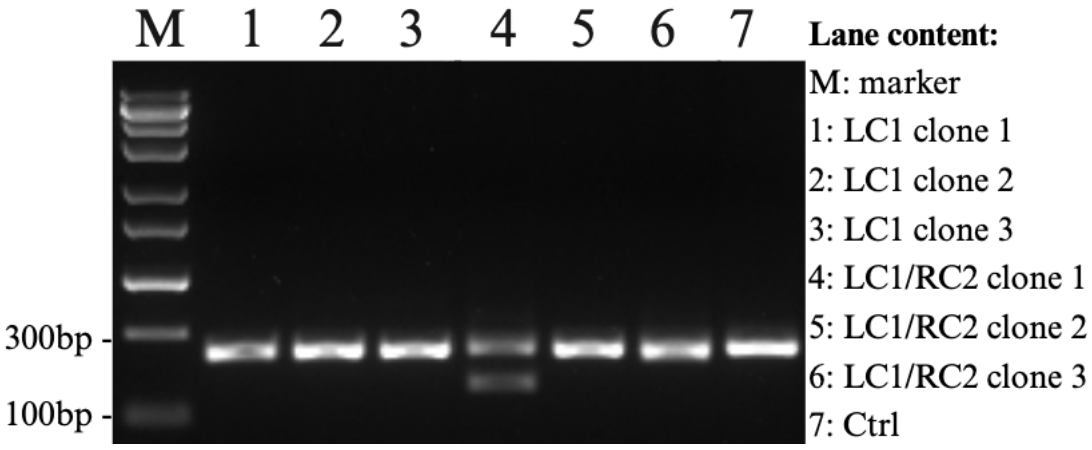

Figure A2. Gel electrophoresis of sorted *ADA2*-edited cells. The "LC1-RC2" primer pair targeting *ADA2* was utilized to amplify the target gDNA in sorted cells electroporated with LC1 gRNA (lane 1-3), LC1/RC2 gRNAs (lane 4-6) and non-edited cells (lane 7). The marker used was ZipRulerExpress DNA 1. Abbreviations: ADA2, adenosine deaminase 2; DNA, deoxyribonucleic acid; gDNA, genomic DNA; gRNA, guide RNA; RNA, ribonucleic acid.

Table A14. Reduced expression of *ADA2* in sorted THP-1 cells. The relative mRNA expression ($\Delta\Delta C_q$) and KO efficiency of *ADA2* in the remaining 14 clones. *RNA18SN1* was used as the reference gene to normalize *ADA2* expression.

Sample	$\Delta\Delta C_q$	KO efficiency
LC1 4	0.03	97 %
LC1 5	0.04	96 %
LC1 6	0.26	74 %
LC1 7	0.14	86 %
LC1 8	0.04	96 %
LC1 9	0.07	93 %
LC1 10	0.03	97 %
LC1/RC2 4	0.05	95 %
LC1/RC2 5	0.03	97 %
LC1/RC2 6	0.13	87 %
LC1/RC2 7	0.15	85 %
LC1/RC2 8	0.05	95 %
LC1/RC2 9	0.03	97 %
LC1/RC2 10	N/A	100%

Abbreviations: ADA2, adenosine deaminase 2; KO, knockout; mRNA, messenger RNA; N/A, non applicable; RNA, ribonucleic acid; RNA18SN1, RNA 18S ribosomal N1.

9.4 Appendix D

Appendix D contains analyzed flow cytometry data of THP-1 cells electroporated with a GFP vector and the gating used to sort *ADA2*-edited cells.

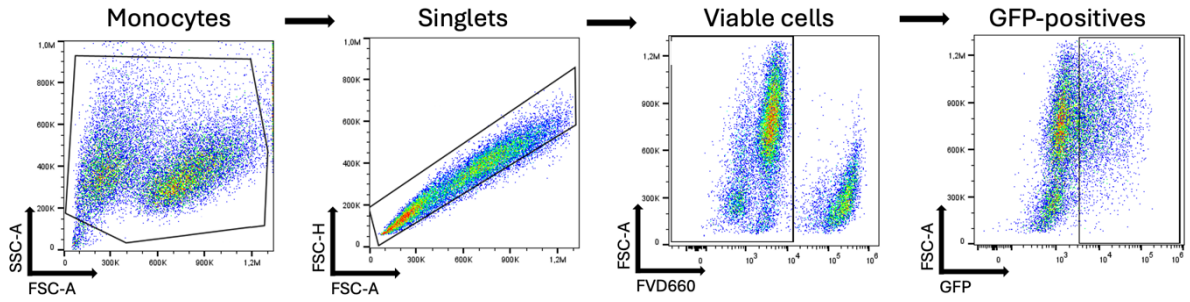

Figure A3. General gating strategy. The general gating strategy for detecting GFP expression in viable electroporated THP-1 cells. Abbreviations: GFP, green fluorescent protein.

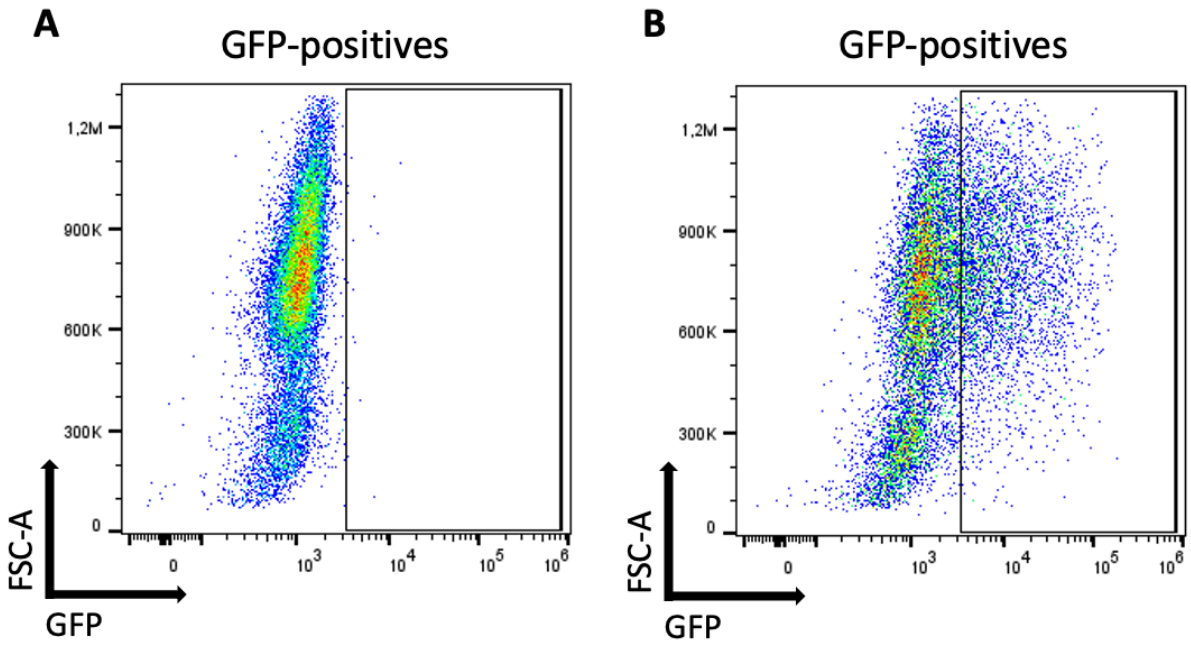

Figure A4. Comparison of GFP expression. The GFP expression shown in A) a negative control, which consisted of THP-1 cells electroporated without a GFP vector, and B) a THP-1 sample electroporated with a GFP vector. The data is gated from viable single cells according to the gating strategy in Appendix D Figure A3. Abbreviations: GFP, green fluorescent protein.

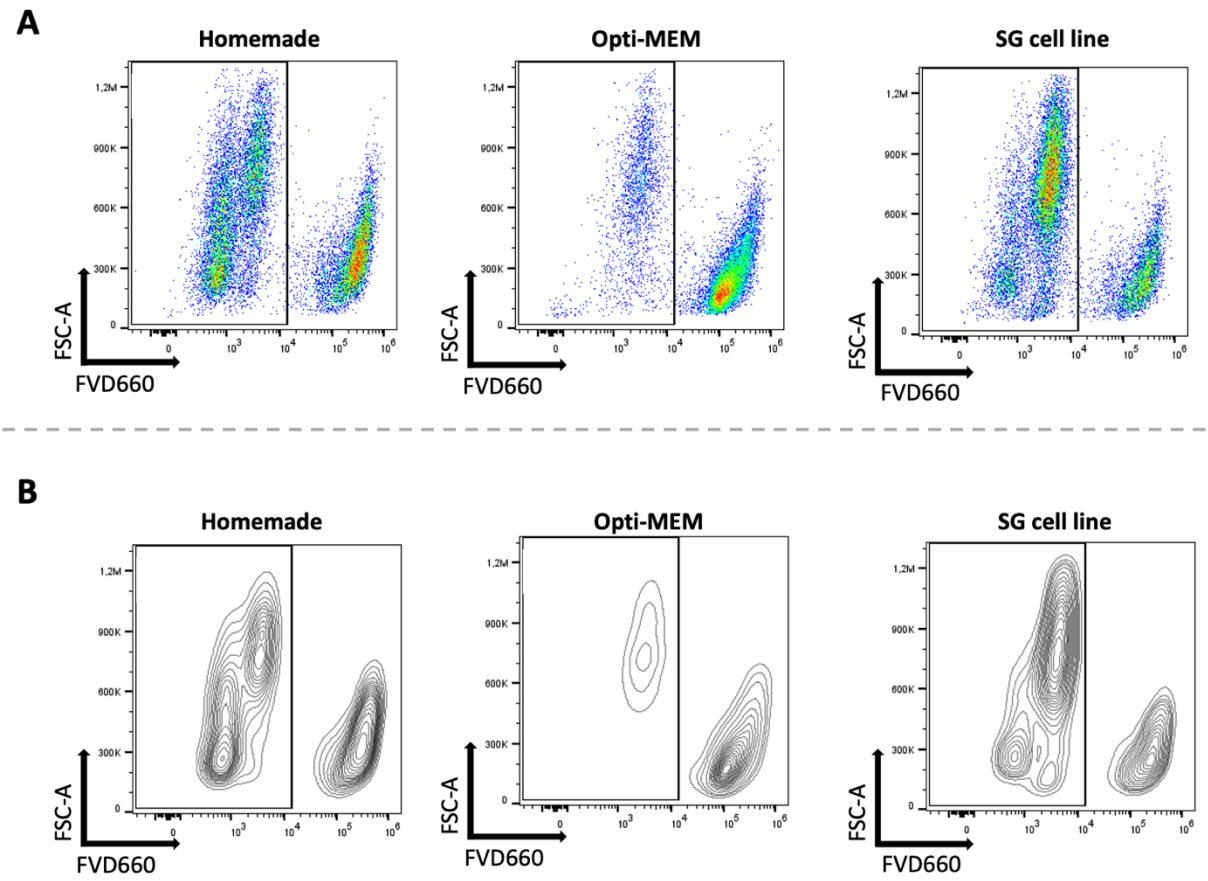

Figure A5. Detection of live THP-1 cells following electroporation of a GFP vector. The proportion of viable cells is visualized after electroporation in the "homemade" buffer, Opti-MEM, and lastly, the SG cell line buffer. The results are given in A) dot and B) contour plots. The data represents one out of three technical replicates for each electroporation condition presented in Figure 16 A, and it is gated from single cells according to the gating strategy in Appendix D Figure A3. Abbreviations: GFP, green fluorescent protein; MEM, minimal essential medium.

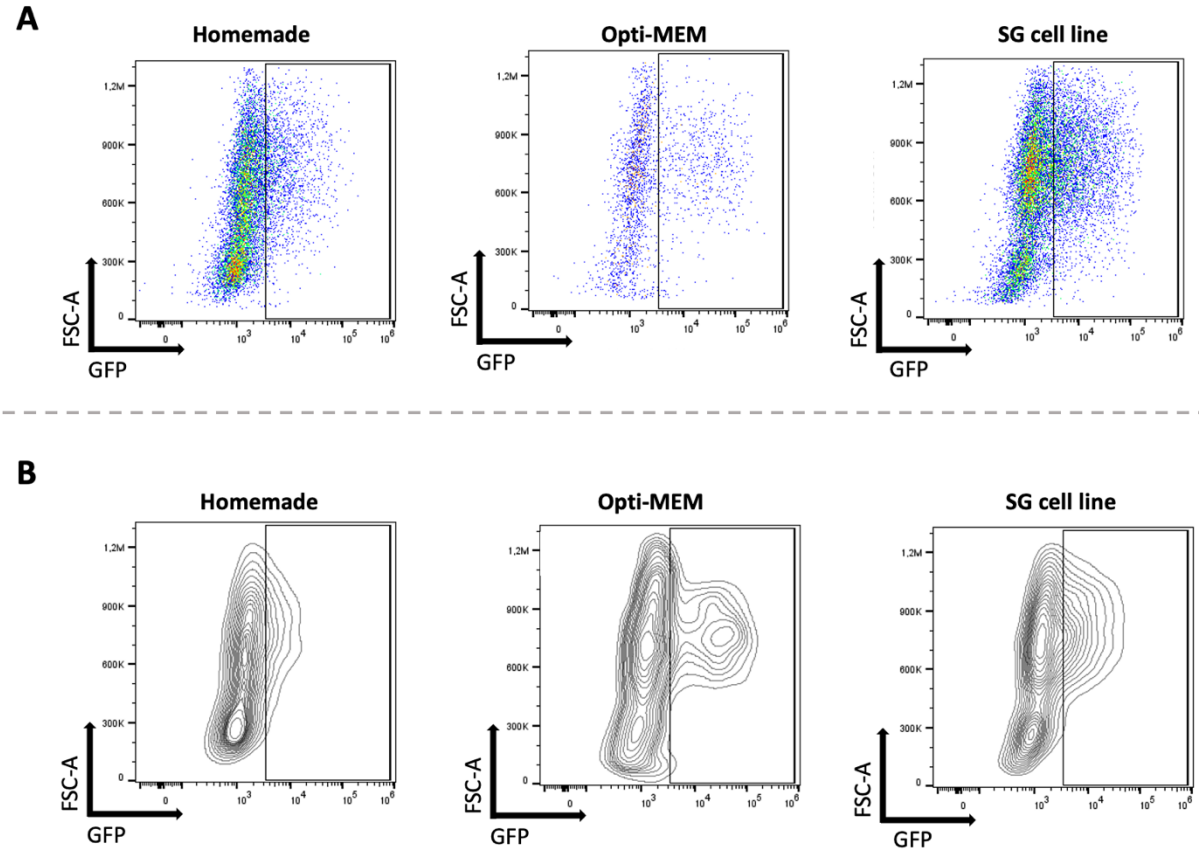

Figure A6. Detection of viable GFP-positive THP-1 cells following electroporation of a GFP vector. The proportion of live GFP-positive cells is visualized after electroporation conducted in the "homemade" buffer, Opti-MEM, and lastly, the SG cell line buffer. The results are given in A) dot and B) contour plots. The data represents one out of three technical replicates for each electroporation condition presented in Figure 16 B, and it is gated from viable single cells according to the gating strategy in Appendix D Figure A3. Abbreviations: GFP, green fluorescent protein; MEM, minimal essential medium.

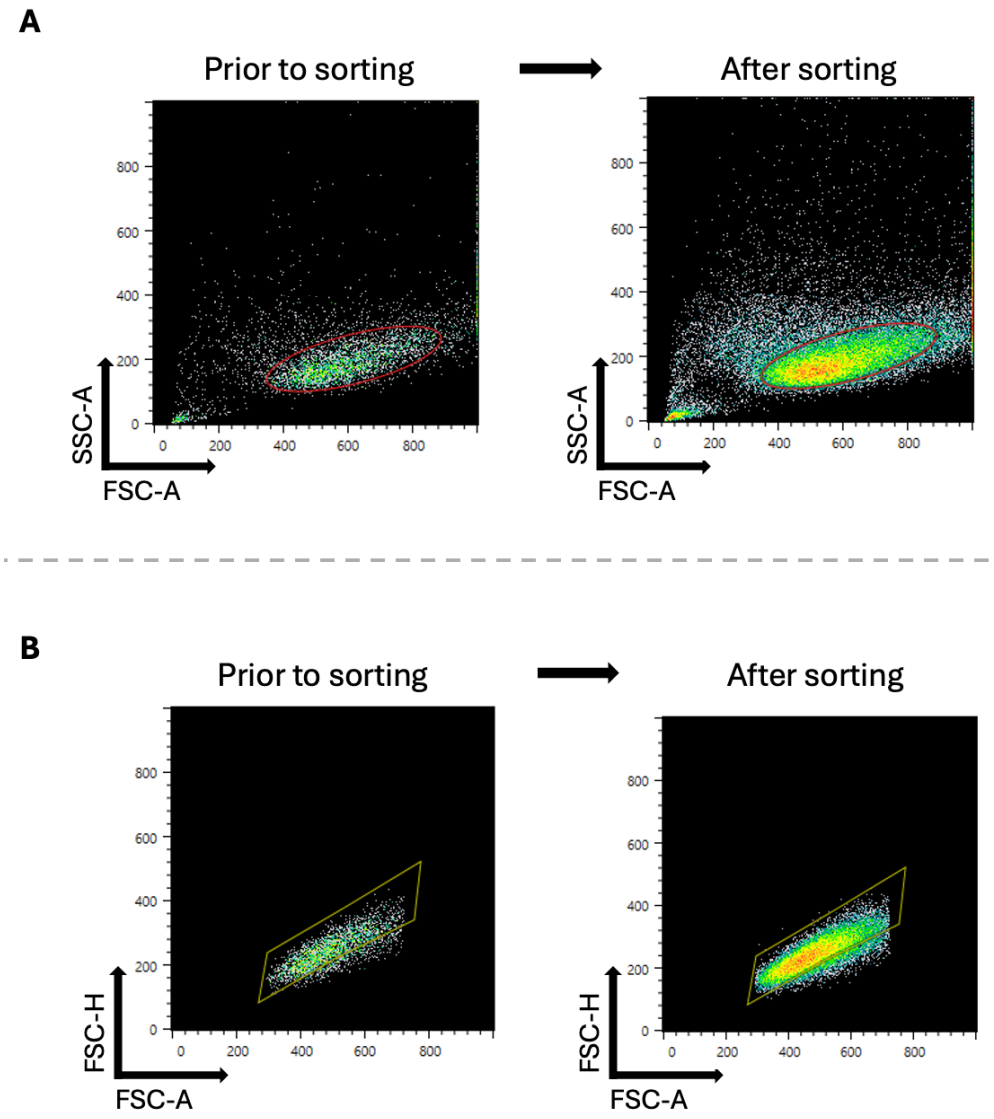

Figure A7. General gating for single-cell sorting. The general gating strategy used to single-cell sort *ADA2*-edited THP-1 cells. The progression from before sorting to after sorting for A) the monocyte gating, and B) the single-cell gating. Abbreviations: ADA2, adenosine deaminase 2.

9.5 Appendix E

Appendix E illustrates the total protein staining of the membranes employed in the immunoblot experiment (section 4.1.8.1).

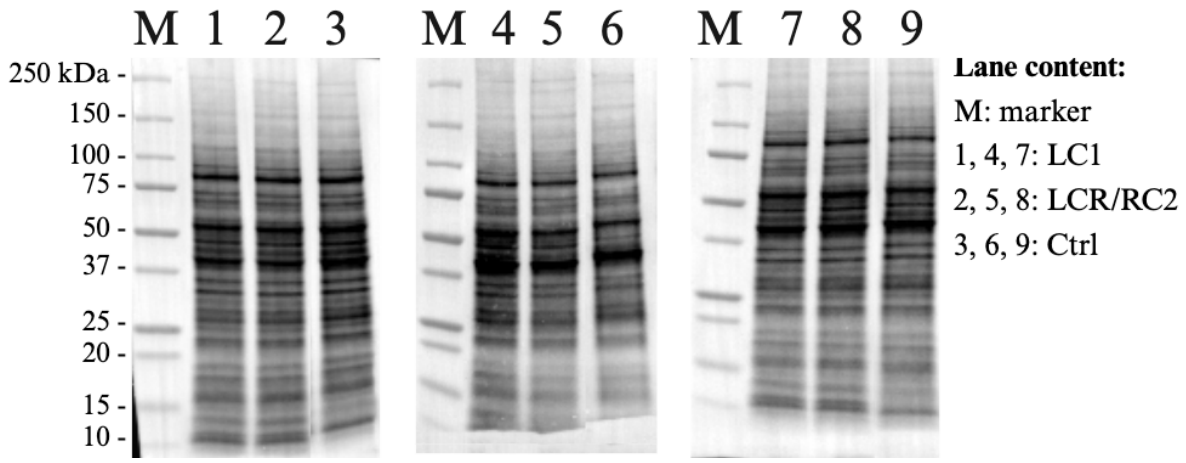

Figure A8. Total protein staining images. The total protein staining of THP-1 cells electroporated with LC1 (lane 1, 4, 7), LC1/RC2 (lane 2, 5, 8), and non-edited control cells (lane 3, 6, 9). The primary antibodies tested were ADA2 TH (lane 1-3), ADA2 AN (lane 4-6), and ADA2 LB (lane 7-9). The marker used was Precision Plus Protein™ All Blue Prestained Protein Standards. Abbreviations: ADA2, adenosine deaminase 2.

9.6 Appendix F

Appendix F contains supplementary data for the proliferation analysis performed on *ADA2* CRISPR/Cas9-edited bulk cells, more specifically, illustrations of the used confluency mask parameters and the outlier removed from the analysis (section 4.2.1).

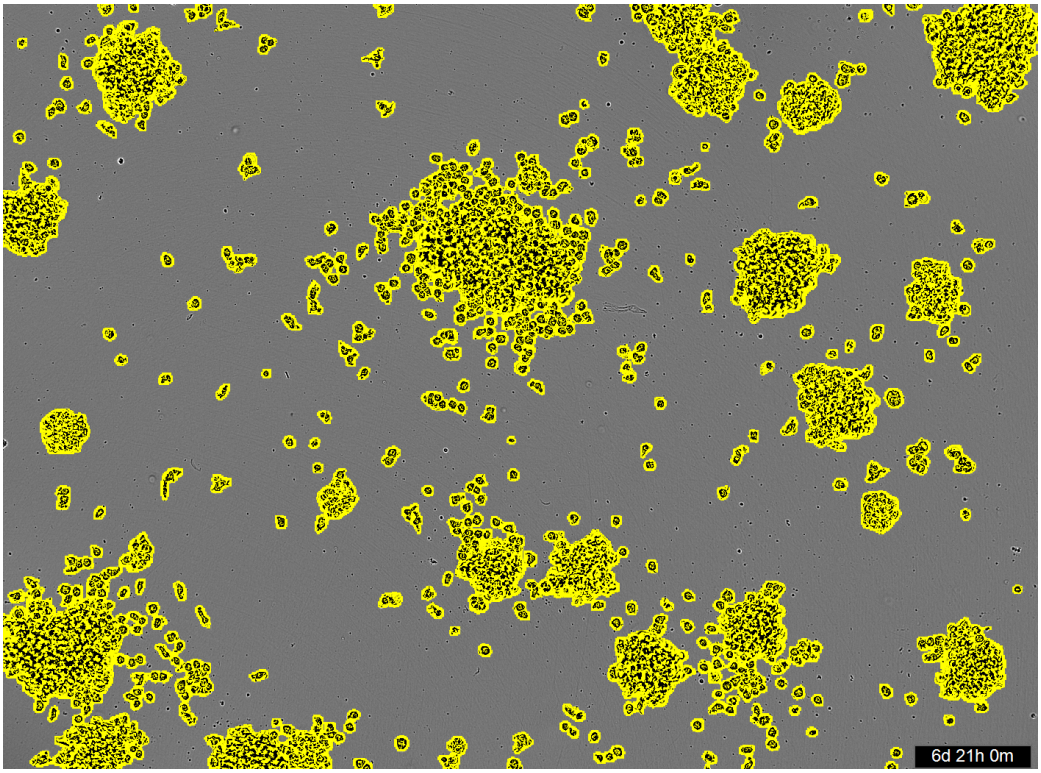

Figure A9. Confluence mask parameters. The confluence mask settings used in the proliferation analysis (Figure 25) were set to 200 μm^2 as the minimum area and 0.955 as the maximum eccentricity. The masking is visualized in one random well, which was analyzed in the proliferation analysis.

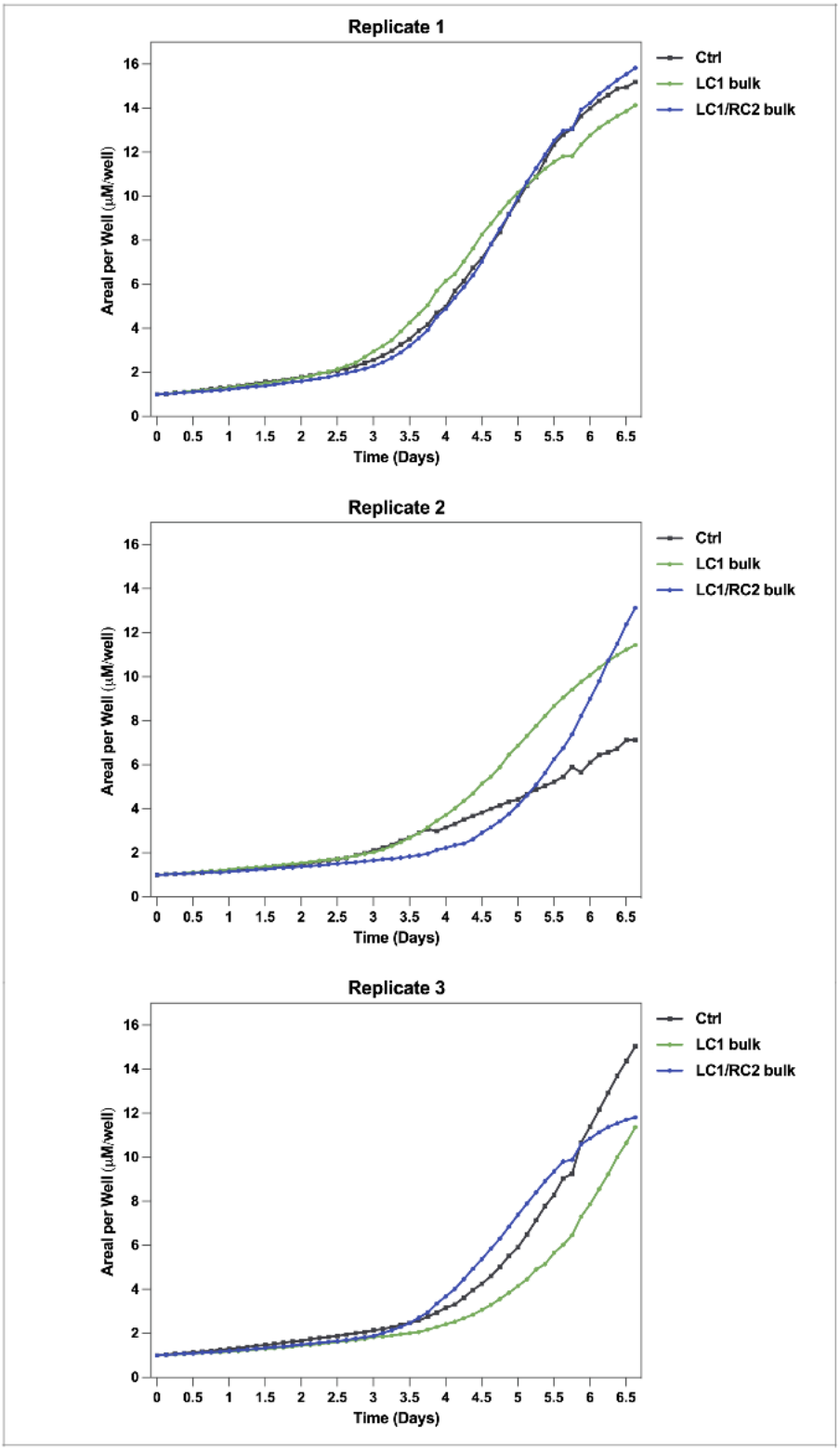

Figure A10. Proliferation of individual biological replicates of *ADA2*-edited bulk cells. THP-1 cells electroporated with LC1 or LC1/RC2 gRNAs were incubated in Incucyte S3, where their proliferation rates were assessed and compared to non-edited control cells (Ctrl). Three biological replicates are individually shown. The time is shown along the x-axis and the areal per well ratio along the y-axis. The Ctrl in replicate 2 was an outlier removed from the proliferation analysis (Figure 25). The graphs represent the mean (n=8) of technical replicates. Abbreviations: ADA2, adenosine deaminase 2; gRNA, guide RNA; RNA, ribonucleic acid.

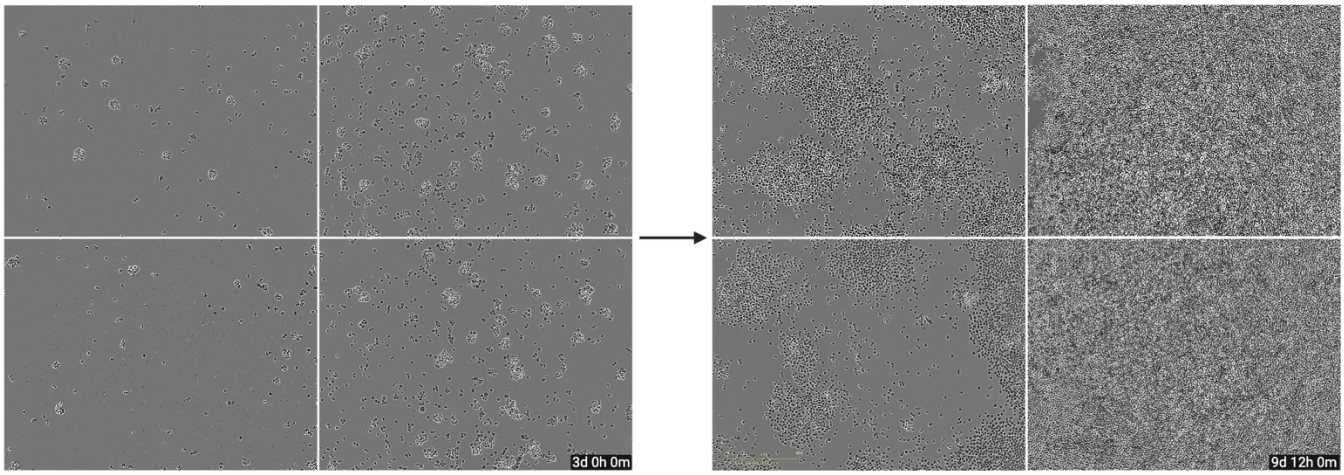

Figure A11. Cell movement of the proliferation analysis outlier. The resulting cell movement in the control outlier (Appendix F Figure A10, Replicate 2, Ctrl), which was removed from the proliferation analysis (Figure 25), directly after medium transfer (3d 0b 0m) to the last timepoint analyzed (9d 12h 0m). The data shown represents one out of eight technical replicates.

Norges miljø- og biovitenskapelige universitet
Noregs miljø- og biovitskapelege universitet
Norwegian University of Life Sciences

Postboks 5003
NO-1432 Ås
Norway